La investigación reportada en esta tesis es parte de los programas de investigación del CICESE (Centro de Investigación Científica y de Educación Superior de Ensenada, Baja California).

La investigación fue financiada por el SECIHTI (Secretaría de Ciencia, Humanidades, Tecnología e Innovación).

Centro de Investigación Científica y de Educación Superior de Ensenada, Baja California

Doctor of Science
in Marine Ecology

Organic carbon concentrations, fluxes and accumulation rates in the Gulf of Mexico

A dissertation
submitted in partial satisfaction of the requirements for the degree
Doctor in Science

By:

Yéssica Vanessa Contreras Pacheco

Ensenada, Baja California, México
2025

A Dissertation Presented by

Yéssica Vanessa Contreras Pacheco

And approved by the following Committee

Dr. Juan Carlos Herguera García
Thesis Director

Dr. Helmut Maske Rubach

Dra. María Asunción Lago Lestón

Dr. Patrick Rafter

Dr. Misael Díaz Asencio

Dr. Rafael Andrés Cabral Tena
Coordinator of the Postgraduate Program in Marine Ecology

Dra. Ana Denise Re Araujo
Director of Graduate Studies

Resumen de la tesis que presenta **Yéssica Vanessa Contreras Pacheco** como requisito parcial para la obtención del grado de Doctor en Ciencias en Ecología Marina.

Concentraciones, flujos y tasas de acumulación de carbono orgánico en el Golfo de México

Resumen aprobado por:

Dr. Juan Carlos Herguera García
Director de tesis

Este trabajo estudia la dinámica del carbono orgánico particulado (COP) en la columna de agua, sus flujos y acumulación en la región profunda del golfo de México (GoM), analizando las variables que regulan su concentración, su transporte hacia el fondo y su almacenamiento en sedimentos. Los procesos oceánicos de mesoescala, especialmente los remolinos ciclónicos y anticiclónicos, influyen sobre su distribución y concentración. Los remolinos ciclónicos promueven el ascenso de nutrientes, impulsando la productividad primaria aumentando las concentraciones de COP, mientras que los remolinos anticiclónicos generan condiciones pobres en nutrientes, disminuyendo las concentraciones de COP. En las regiones de Perdido y Coatzacoalcos, los flujos de carbono orgánico reflejan patrones estacionales y pulsos de alta concentración, asociados tanto a procesos locales como a interacciones entre fuentes continentales y oceanográficas regionales. En particular, se observó como la llegada de los remolinos a la plataforma continental, generan un transporte costa afuera de aguas ricas en nutrientes y clorofila, lo que intensifica la exportación de carbono orgánico en estas regiones. El análisis de los núcleos de sedimento revela una variabilidad espacial en las tasas de acumulación de carbono orgánico en áreas con ciertas características geomorfológicas como los montes submarinos y cañones de Campeche. Las tasas de consumo de carbono orgánico en sedimentos son mayores en áreas de mayor flujo, lo que indica que las comunidades bentónicas y la bioturbación juegan un papel importante en la modulación del almacenamiento de carbono en estos ambientes profundos. Este estudio destaca la importancia de la interacción entre los procesos físicos y biológicos en la dinámica del carbono en el GoM, donde los remolinos de mesoescala, aportes continentales y de características geomorfológicas del fondo regulan la distribución, el flujo, el almacenamiento y el secuestro de carbono orgánico en los sedimentos. Los hallazgos contribuyen a comprender mejor los mecanismos de secuestro de carbono en ambientes profundos y ofrecen información que puede ayudar a anticipar como el ciclo del carbono podría responder a futuros cambios ambientales y climáticos en el GoM.

Palabras clave: Golfo de México, carbono orgánico, concentraciones, isótopos, flujos

Abstract of the thesis presented **by Yéssica Vanessa Contreras Pacheco** as a partial requirement to obtain the Doctor of Science degree in Marine Ecology.

Organic carbon concentrations, fluxes and accumulation rates in the Gulf of Mexico

Abstract approved by:

Dr. Juan Carlos Herguera García
Thesis Director

In this work, we present evidence of the interaction between the dynamics of particulate organic carbon in the water column, their fluxes, and accumulation in the deep region of the Gulf of Mexico and analyze the variables that control their concentration in the water column, its transport to the bottom, and its storage in sediments. Mesoscale oceanic processes, especially cyclonic and anticyclonic eddies, influence the distribution and concentration of organic carbon in the water column. Cyclonic eddies promote the ascent of nutrients at their center, boosting primary productivity and increasing POC concentrations, while anticyclonic eddies generate nutrient-poor conditions at their core and decrease POC concentrations. In the Perdido and Coatzacoalcos regions, organic carbon fluxes reflect seasonal patterns and pulses associated with both local processes and interactions between continental and local oceanographic sources. We present observations on the role of the interaction between eddies and the continental shelf currents generating an offshore transport of nutrient and chlorophyll-rich waters, which intensify the export of organic carbon in these regions. Sediment core analysis reveals a spatial variability in organic carbon accumulation rates in areas with characteristic geomorphological features, such as Campeche seamounts and canyons. Sediment organic carbon consumption rates are higher in areas of higher fluxes, indicating that benthic communities and bioturbation play an important role in modulating carbon storage in these deep-sea environments. This study highlights the importance of the interaction between physical and biological processes in the GoM carbon dynamics, where mesoscale eddies, continental inputs, and geomorphological features regulate organic carbon distribution, flux, and final storage. The findings contribute to a better understanding of carbon sequestration mechanisms in deep-sea environments and offer information that can help anticipate how the carbon cycle might respond to future environmental and climatic changes in the GoM.

Keywords: Gulf of México, organic carbon, concentrations, isotopes, fluxes

Dedication

To my parents, there are no words to describe the admiration, love, and gratitude I feel for you.

To my sisters, brothers, and the new members of the crew, I love you all.

To my uncle Enrique and Marivel, Sarita, Cami, Andrea, and Papoy, love you. I will always be grateful for your unconditional love and support.

To my chosen family, Naye (Quetims), Cris and Juls, Mally (Pinwi and Javi), Mimi, Hope and Jaime, Dore, Eliana (Gael), Pablito, Rafa, Fer, Tono and Pao, Angel, Angello, Jose and Gaby, Bertha, Pily and Alma, as well as my basketball teammates and all those friends who accompanied me on this path and shared an experience. Your friendship has enriched this process and influenced my life. Thank you.

To my Gerard, for being you, for being here, for being with me all the time, for your constant love and support, thank you always and forever. From all the me's who have loved all the you's.

Acknowledgments

I am grateful to the Centro de Investigación Científica y de Educación Superior de Ensenada, Baja California (CICESE) for providing the opportunity to pursue my doctoral degree in the Marine Ecology program for the stipend during the final months of my studies and for their continuous support throughout this journey. I would like to thank the coordinator, Dr. Rafael, and the staff of the graduate program for their assistance throughout my studies.

I also thank the Secretaría de Ciencia, Humanidades, Tecnología e Innovación (SECIHTI) for the doctoral fellowship that made this research possible.

My sincere appreciation goes to the CiGOM project, and everyone involved, as well as to the members of the LIEP3 laboratory, especially Bertha Acosta, Jose Abella, Dore Bobadilla, Felipe García, Gerardo Quintanilla, Cinthya Nava, Axel Rosas, Aidé Egremy.

I extend special thanks to POGO for supporting my training in particulate fluxes. I want to thank especially Marika Takeuchi, Sari Giering, Andy Rees, Will Major, Jack Williams, Eloise, Sarah Breimann, Philippa, Rosseana, Prima, Gavin and Motjaba and all the scientific group and the crew or AMT30 RRS Discovery for making this opportunity such a life experience.

I am profoundly grateful to my thesis committee members, Dr. Helmut Maske, Dr. María Asunción Lago Lestón, Dr. Misael Días Asencio, and Dr. Patrick Rafter, for their guidance, insightful feedback, and dedication to my project. I am also grateful to Sharon Herzka for her invaluable support.

I am deeply thankful to my thesis supervisor, Juan Carlos Herguera; thank you for everything, everything, everything.

Table of Contents

Page

List of Figures

List of Tables

Chapter 1. Introduction

The increasing importance of anthropogenic activities has altered the climate, oceans, and global carbon cycle since the beginning of the Industrial Revolution, with recent decades seeing an acceleration due to the global rise in fossil fuel combustion (P. Falkowski et al., 2000). The global carbon cycle is a critical component of Earth's climate system, regulating the atmospheric concentration of CO_2 and influencing global temperatures (Houghton, 2007). Over the last two hundred years, approximately 400 petagrams (Pg) of carbon (C) have been released into the atmosphere as carbon dioxide (Sabine et al., 2004).

Despite CO_2 constituting only about 0.040% of atmospheric gases, it significantly contributes to the anthropogenic greenhouse effect, with a relative contribution of 60% compared to other gases like CH_4, N_2O, O_3, CFC-11, and CFC-12 (Rodhe, 1990). The ocean is the largest sink of anthropogenic CO_2, capturing approximately 118 ± 18 Pg C between 1800 and 1994. From 1980 to 1999, the ocean captured, on average, ~1.9 Pg C a^{-1} and about 27% of the total anthropogenic emissions that reached 7.1 Pg C a^{-1} (Sarmiento, 2006).

Within the marine environment, the carbon cycle plays a pivotal role in sequestering atmospheric CO_2, thereby partially mitigating the impacts of climate change (P. G. Falkowski et al., 1998). An array of complex processes involving various pathways and mechanisms, including the production, transformation, and transport of carbon through the water column, its storage in the intermediate and deep ocean waters, and its eventual deposition and storage in marine sediments (Houghton, 2007).

The solubility pump and biological pump are key processes in the ocean's role as a carbon sink (Volk & Hoffert, 1985). The higher solubility of CO_2 in seawater, due to its reaction with water forming carbonic acid, results in dissolved inorganic carbon in the form of bicarbonate and carbonate ions (Libes, 2011). The solubility pump involves the enrichment of the oceanic carbon pool due to the high solubility of inorganic carbon in seawater and the ocean's capacity to store carbon for extended periods (Volk, 1989; Longhurst & Harrison, 1989; Longhurst, 1991 and Ducklow et al., 2001). The biological pump, regulated by primary production, converts inorganic carbon into organic carbon at the ocean's surface, influenced by temperature, solar irradiance, ocean circulation, and nutrient supply (Turner, 2015).

Organic carbon in the water column primarily originates from phytoplankton and zooplankton, terrestrial vegetation decomposition, and aquatic organism metabolism, including bacterial loops (Kharbush et al.,

2020). The fluxes of organic carbon are closely linked to processes in the upper ocean, with a portion of synthesized organic carbon exported to the subsurface ocean through particle aggregation and transport by marine organisms (Turner, 2015). The export intensity varies with the coupling between primary production and remineralization processes by zooplankton and bacteria in the upper ocean (Henson et al., 2019).

The transfer of organic carbon to the sea floor primarily occurs through the deposition of fecal waste, driven by gravity. The quantity varies in response to trophic environmental conditions. The amount of sediment, predominantly biogenic, is dependent on production rates and the physical, chemical, and biological characteristics of the environment (Heinze et al., 1991).

A fraction of this organic carbon settles on the ocean floor, supporting benthic organisms and resident microbiota (Figure 1). The biological pump is estimated to remove over 10 billion tons of carbon from epipelagic ocean waters (Buesseler & Boyd, 2009), but only about 10% of this carbon flux reaches the mesopelagic zone (Martin et al., 1987). Passow and Carlson (2012) approximated that roughly two-thirds of the vertical carbon gradient in the ocean is attributed to the biological pump, with the remainder linked to the solubility pump.

However, only a small fraction of the organic carbon produced at the surface by phytoplankton ultimately reaches the sediments. An even smaller portion is accumulated in the geological record, implying a long-term carbon sequestration process spanning tens to hundreds of millions of years (Figure 1).

The burial efficiency of organic carbon in sediments is influenced by factors such as sedimentation rate, bottom-water oxygen levels, microbial activity (Arndt et al., 2013) and organic matter degradation (Kharbush et al., 2020 and Emerson et al., 1985). The interaction between the water column and sedimentary processes thus plays a crucial role in determining the long-term sequestration of carbon in the ocean (Hedges & Keil, 1995).

Given the ocean's critical role in the carbon cycle and its implications for climate change, numerous studies have been conducted to understand the processes influencing carbon distribution, storage, and sequestration in sea floor sediments (Canfield, 1993; Goñi et al., 1997; Schwing et al., 2018 and Anwar et al., 2018). Evidence shows significant changes in ocean biogeochemistry and ecology since the mid-20th century, but the lack of pre-Industrial Revolution data limits the evaluation of the current changes'

magnitude and direction (Poloczanska et al., 2013; Beaugrand et al., 2013; Rosenzweig et al., 2008 and Hillebrand et al., 2020).

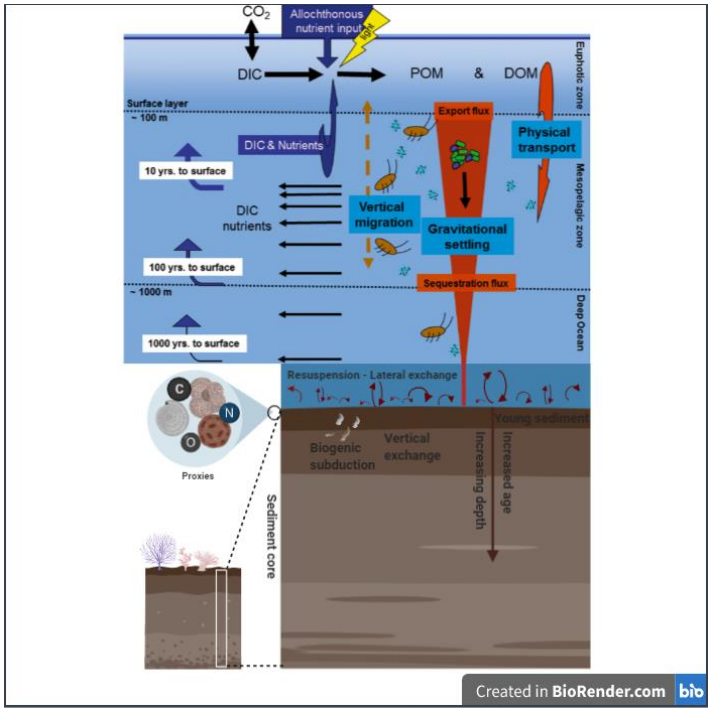

Figure 1. Conceptual model of the transfer of organic carbon to deep-waters until its sequestration in sediments. Modified from De La Rocha y Passow (2007).

This study aims to investigate the dynamics of particulate organic carbon in the abyssal plain of the Gulf of Mexico by examining the role of mesoscale eddies on organic carbon transport, calculating particle fluxes using sediment trap data, and assessing carbon storage in the sediments. By linking these processes across different temporal and spatial scales, this research will contribute to a more comprehensive understanding of the marine carbon cycle and its implications for global carbon sequestration in this land-enclosed small ocean basin.

1.1 Related work

Carbon in the ocean is found in several forms, including dissolved inorganic carbon (DIC), dissolved organic carbon (DOC), and particulate organic carbon (POC), typically in a ratio of approximately 2000:38:1, respectively (Denman, 2007). The ocean contains an estimated 37,000 gigatons (Gt) of DIC (Falkowski et al., 2000 and Sarmiento & Gruber, 2013), 685 Gt of DOC (Hansell & Carlson, 1998), and between 13 to 23

Gt of POC (Eglinton & Repeta, 2004). DOC and POC are distinguished by size, with particles larger than 0.45 µm classified as POC, while those smaller are considered DOC (Sharp, 1973).

Although the pool of POC in the ocean is small relative to DIC and DOC, it plays an important role in keeping DIC concentrations low in surface waters and transferring them to deep-waters by gravity in an amount equivalent to the injection of subsurface nutrients into the photic zone (Denman, 2007). The transfer of POC to deep-waters decreases the partial pressure of CO_2 in surface waters, which, when rebalanced with the atmosphere, functions as a sink for atmospheric CO_2 (Yamanaka & Tajika, 1996).

Carbon has two stable isotopes: carbon-12 (^{12}C) and carbon-13 (^{13}C). The isotopic composition of a substance is determined with respect to a reference or standard using the δ notation, in units per thousand (‰); the isotopic ratio $^{13}C / {}^{12}C$ is always expressed with the heavier isotope over the lighter one (Fry, 2008). The isotopic composition of organic carbon in phytoplankton is determined by its metabolic processes and carbon synthesis pathways. During photosynthesis, carbon assimilation introduces the most significant isotopic fractionation in the surface ocean. Primary producers fix inorganic carbon from their environment and convert it into organic carbon through photosynthetic processes, preferentially incorporating lighter isotopes (Goericke & Fry, 1994; Laws et al., 1995 and O'Leary & Langton, 1989). This fractionation is mediated by the metabolic system of phytoplankton, particularly by the enzyme Ribulose-1,5-bisphosphate carboxylase oxygenase (RUBISCO), which catalyzes CO_2 fixation during photosynthesis (Tcherkez, 2006).

The carbon isotopic composition can be influenced by many other factors, such as the assimilation of isotopically heavier species (HCO_3^-) (Burkhardt et al., 1999 and Sharkey et al., 1985), temperature effects on the enzyme (Tcherkez, 2006) and intracellular conversion processes to lipids, carbohydrates, and proteins further fractionate and alter the $\delta^{13}C$ of POC (Degens et al., 1968).

The variability of $\delta^{13}C$ in phytoplankton can also be attributed to the cell size and geometry, influencing carbon uptake by diffusion or enzymatic transport, which can fractionate the $\delta^{13}C$ and mask environmental effects. The importance of knowing these processes lies in the fact that the fractionation during the assimilation of $CO_{2\,(aq)}$ determines the isotopic composition at the base of the food web (Rau et al., 2001; Young et al., 2013; Yamanaka & Tajika, 1996; Onstad et al., 2000 and Burkhardt et al., 1999).

Studies and compilations have been published on how the large ocean ecosystem and its biogeochemical cycles are being altered due to climate change (Stocker, 2013 and Abram et al., 2016). Emerging global

trends indicate changes in ocean color as an indicator of phytoplankton production, species phenology, and community composition in marine ecosystems (Poloczanska et al., 2013; Beaugrand et al., 2013 and Hoegh-Guldberg, 2010).

Despite global evidence of climate change, its effects on the GoM ecosystem, carbon distribution, storage, and subsequent sequestration in sediments remain understudied. Understanding these impacts is crucial for assessing the role of marine sediments in the GoM as a carbon sink and their significance in climate change. One pressing question is whether the GoM ecosystem has crossed the threshold of natural variability over decadal to centennial scales, transitioning into a new equilibrium state known as the Anthropocene (Waters et al., 2016).

A significant challenge is the lack of extended baseline data to evaluate trends in nutrient and carbon cycling in the photic zone. This study proposes using the sedimentary record to establish a baseline predating the last century (Figure 1). To assess the impact of anthropogenic climate change on the marine environment, modern data, and instrumental observations must be compared with the pre-Industrial Revolution baseline, as done in other ocean regions (Field et al., 2006).

Biogeochemistry and the broader ecosystem of the GoM have only been subject to scientific study since the mid-20th century. Unfortunately, there is a lack of continuous, long-term data that could provide insights into the historical stability or trends of this ecosystem (Poloczanska et al., 2013; Beaugrand et al., 2013; Rosenzweig et al., 2008 and Hillebrand et al., 2018). This lack of a pre-Industrial Revolution baseline hampers our ability to assess the extent and nature of the differences between current systems and those observed today. These limitations challenge predictions of climate change impacts on the GoM's ecosystem structure, functioning, and resources.

Understanding organic carbon concentrations in the water column requires examining the complex interplay of physical, chemical, and biological factors. These mechanisms are vital for comprehending the global ocean's carbon cycle, including processes governing carbon transfer through the water column and its accumulation in sediments. Simultaneously, organic matter accumulation in sediments responds to shifts in organic matter export due to nutrient changes in the photic zone (Sarmiento & Gruber, 2013). Reconstructing these variations offers valuable insights into the biological pump's fluctuations in the GoM's slope and abyssal plain.

1.2 Justification

Research in the GoM is vital due to its significant scientific, economic, environmental, and social relevance. This research helps to establish the basic characteristics of this region and its role in the global carbon cycle. This knowledge is essential for assessing the impact of environmental events, such as oil spills, and for guiding restoration efforts to return the ecosystem to its original state.

Additionally, this research fills a knowledge gap by providing valuable data on carbon deposits in the abyssal region of the GoM, a traditionally understudied area, due to the complexities and costs of data collection. The findings will have global applicability and illuminate the mechanisms that affect concentrations and fluxes of organic matter in the water column and their sequestration in the marine sediment. These insights are crucial to understanding environmental changes on a global scale.

1.3 Objectives

1.3.1 Main objective

Analyze the concentrations of organic matter and its fluxes in the water column until its sequestration in the sediments of the Gulf of Mexico.

1.3.2 Specific objectives

Characterize the spatial and temporal variations in particulate organic carbon concentrations within the water column during three research cruises in the abyssal plain.

Determine organic matter fluxes within the water column by using data from two sediment traps located in the northwestern and southern regions of the GoM.

Reconstruct the spatial and temporal variability in the accumulation, sequestration, and isotopic composition of organic carbon in the slope and abyssal plain marine sediments.

Chapter 2. Particulate organic carbon in the deep-water region of the Gulf of Mexico (Contreras- et al., 2023)

2.1 Introduction

The reservoir of particulate organic carbon (POC) in the ocean, while considerably smaller than the dissolved organic carbon (DOC) pool, with an approximate POC: DOC ratio of 1:38, (Denman, 2007), is an essential constituent of sequestered carbon, in addition to the dissolved and particulate inorganic carbon pools (Sarmiento & Gruber, 2013). POC sinks through the water column across isopycnals, scavenging other particles and transporting carbon and associated elements to deep-waters, where some of them are remineralized or resuspended, and a minor fraction is eventually sequestered in the sediments (Eppley & Peterson, 1979 and Stramska, 2009).

The POC in oceanic regions consists mainly of living organisms and marine snow, which is an aggregate of phytoplankton and small zooplankton fragments, fecal pellets, and other particles, also known as organic aggregates, which includes non-living material and uncharacterized components from biological, mineral, and anthropogenic sources (Hedges et al., 2000; Hedges & Keil, 1995; Kharbush et al., 2020; Knauer et al., 1979; Lutz et al., 2002; Riley, 1963 and Stramski et al., 2008). Near active natural oil seeps or oil spills, POC can incorporate “dead carbon” or hydrocarbon-derived carbon in a process that has been described as Marine Oil Snow Sedimentation and Flocculent Accumulation. This process has been shown to be an important pathway for the distribution and destination of spilled oil, which in the Gulf of Mexico accounts for up to 14% of the total oil released as a result of the Deepwater Horizon oil spill in 2010 (Daly et al., 2016).

Particulate organic carbon concentration in the euphotic layer is thought to reflect primary production, a process during which photosynthesis fuels the formation of organic carbon from dissolved inorganic carbon and nutrients, thereby decreasing the partial pressure of carbon dioxide in surface waters (Stramska, 2009). Many of these processes are sensitive to fluctuations in temperature, light availability, ocean circulation, vertical mixing, and nutrient inputs into the surface ocean’s euphotic layer (Dawson et al., 2018; Dobashi et al., 2022 and Frenger et al., 2018).

In oligotrophic regions, the mixed layer is generally considered as quasi-homogeneous with little to no variability in density and is usually depleted in nutrients due to uptake by primary producers (Falkowski et al., 1992 and Velásquez-Aristizábal et al., 2022). The deepening of this layer allows for subsurface mixing of nutrients toward the surface, fueling biological productivity and consequently increasing POC concentrations (Gardner et al., 1999). These changes can be further driven by vertical mixing from the isopycnal displacement by anticyclonic and cyclonic eddies, especially under strongly stratified upper ocean conditions during summer (Gaube et al., 2014, 2019).

Mesoscale processes are responsible for the mixing and transport of heat, salt, and biogeochemical tracers across the global oceans and may act as a moderating factor in global climate change (Faghmous et al., 2015). Thus, understanding ocean eddy dynamics and their role in influencing various oceanographic and biological phenomena is of keen scientific interest (Faghmous et al., 2015 and Falkowski et al., 1998). The productivity-enhancing effects of eddies are particularly important in low-nutrient environments, where mesoscale processes can regulate the net upward flux of limiting nutrients as a result of the undulation of nutrient isosurfaces: where the shoaling of isopycnal surfaces tends to bring nutrients into the euphotic zone thereby enhancing productivity, whereas their deepening leads to a lack of change or even a decrease in primary productivity (Gruber et al., 2011).

Remotely sensed Sea Surface Height (SSH) yields important information on the spatial distribution and intensity of ocean eddies and is strongly related to circulation patterns in the ocean, lending insight into nutrient transport crucial to the understanding of the spatial variability of biological production (Gruber et al., 2011). The measurements performed with various *in-situ* and remote sensing platforms provide an effective tool for studying biogeochemical constituents of oceanic waters like chlorophyll-a, particulate inorganic carbon, and particulate organic carbon (Stramski et al., 2008); Ocean Biology Processing Group, G. M, 2022).

The GoM is a semi-enclosed sea linked to the Atlantic Ocean through the Florida Straits and to the Caribbean Sea through the Yucatan Channel (Oey et al., 2005). The deep-water region of the GoM is characteristic for its oligotrophic and nutrient-limited surface waters, which are relatively isolated from coastal eutrophic waters (Martínez-López & Zavala-Hidalgo, 2009 and Pasqueron De Fommervault et al., 2017). The Loop Current (LC) brings warm water into the GoM, which leads to high stratification in its area of influence, especially during the summer. Higher intrusion of the LC into the GoM is observed more frequently during the summer, which along with the upper ocean warming, influences the circulation in the interior of the gulf (Sturges & Leben, 2000). In the GoM, positive SSH anomalies are indicative of

anticyclonic eddies that are characterized by a deep, warm water layer (Dobashi et al., 2022 and Müller-Karger et al., 2015).

The LC and detached LC eddies transport Caribbean Subtropical Underwater into the GoM, which is clearly distinguishable from the GoM common water (Vidal et al., 1992). This common water is formed by vertical convective mixing during the winter season, or by the mixing induced by the collision of detached LC eddies against the western GoM boundary (Schmitz et al., 2013). These mesoscale features drive hydrodynamic processes throughout the central GoM that fuel mixing processes and affect biological productivity patterns (Cervantes-Díaz et al., 2022; Müller-Karger et al., 2015 and Pérez-Brunius et al., 2012).

The most energetic mesoscale events are the detachment of large anticyclonic eddies from the LC that drift to the west (Sturges & Leben, 2000), which are dynamically linked with cyclonic and anticyclonic eddies in the Gulf's interior (Jouanno et al., 2016). The periods between detachments are highly variable (ranging between 0.5 and 18.5 months), implying that there are some years with no eddy detachments from the LC, while during other years these can happen up to three times per year (Delgado et al., 2019; Leben, 2005; Sturges & Leben, 2000 and Vukovich, 2007, 2012). In addition to the quasi-periodic shedding of LC eddies, other processes, and structures influence the productivity in the southern Bay of Campeche, like the semi-permanent cyclonic eddy in the southern Gulf (Pérez-Brunius et al., 2012), the confluence of seasonal along-shelf currents (Martínez-López & Zavala-Hidalgo, 2009), and upwelling processes along the eastern margin of the Bay of Campeche and off the northeast shelf of the Yucatan Peninsula (Zavala-Hidalgo et al., 2006).

The mixed layer depth's (MLD) seasonal cycle is driven by the surface ocean cooling during winter months, fueled by northern winds that lead to the erosion of the stratification of its surface waters and a deepening of the mixed layer (Müller-Karger et al., 1991). This wintertime convection of the MLD due to strong winter winds or "nortes" ends during the late spring, when the warming cycle of the surface waters begins; the MLD becomes shallower throughout the summer into the early fall, when the stratification of the upper layers is strongest (Martínez-López & Zavala-Hidalgo, 2009 and Müller-Karger et al., 1991). These cycles of winter mixing, and summer stratification are thought to be the main controlling factors of the surface chlorophyll-a concentration in GoM (Müller-Karger et al., 2015).

Modeling efforts suggest the higher integrated content of chlorophyll-a (Chl_a) over the upper 350 m occurs in winter whereas lower ocean concentrations happen in summer, while April-May and October-November are transitional periods (Damien et al., 2018). In addition, float data show that mesoscale

activity is most likely the main source of variability for the Chl_a concentration in the deepwater region of the GoM, with higher concentrations observed in cyclones compared to anticyclones (Linacre et al., 2019 and Pasqueron De Fommervault et al., 2017).

Additionally, cyclonic and anticyclonic eddies drive vertical mixing through the modulation of nutrient transport to the euphotic zone, thereby exerting influence on Chl_a concentrations in the euphotic layer (M. C. Honda et al., 2018; McGillicuddy, 2016) as well as POC concentrations (McGillicuddy, 2016). Still, there are limited field observations available to characterize how mesoscale physical processes may affect the POC of the deep-water region of the GoM (Müller-Karger et al., 2015).

POC in the GoM has been mostly studied over the continental shelf, particularly in the north and northeast. The transport of freshwater plumes and filaments from the Mississippi and the Atchafalaya Rivers advect higher nutrient concentration waters to the northern shelf region, especially to the continental shelves of Louisiana and Texas (Bianchi et al., 1997; Goñi et al., 1997; Trefry et al., 1994 and Wang et al., 2004). However, the role of mesoscale structures on POC concentrations in the GOM's deepwater region, especially in the southern gulf and the Bay of Campeche, known for its relatively higher productivity within the gulf (Linacre et al., 2015 and Martínez-López & Zavala-Hidalgo, 2009), has yet to be examined. Hence, our study aims to understand the role of mesoscale eddies on POC concentrations in the upper layer of the southern GoM´s deep-water region.

2.2 Materials and methods

2.2.1 Sampling

For the sampling, 319 discrete seawater samples were collected during three cruises covering the deep-water region of the southern GoM on board the R/V Justo Sierra using Niskin bottles mounted on a rosette (Table 1). At each station, continuous profiles of temperature, pressure, conductivity, and chlorophyll fluorescence were measured with a Sea-Bird® 9 plus CTD and sensors.

In Figure 2, we present a map of the stations and the bathymetry of the deep-water region of GoM. All stations were > 1000 m depth; casts at some stations were done to 1000 m regardless of depth (hereafter referred to as shallow cast stations), and some to about 40 m off the bottom (deep cast stations).

Table 1. Oceanographic cruise sampling dates for particulate organic carbon (POC) in the oceanic Gulf of Mexico.

Cruises	Year	Months	Season	Stations sampled
XIXIMI 4	2015	August 27-September 16	Summer	46
XIXIMI 5	2016	June 10-June 25	Early Summer	32
XIXIMI 6	2017	August 15-September 8	Summer	30

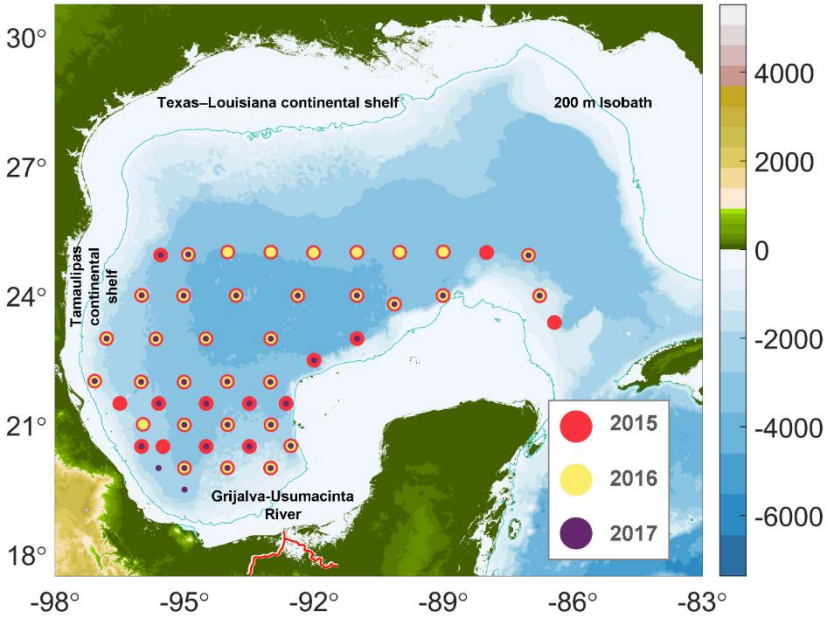

Figure 2. Stations covered in the 2015, 2016, and 2017 XIXIMI cruises. Red circles represent stations sampled in 2015, yellow circles stations sampled in 2016, and purple circles are the stations sampled in 2017. The blue line represents the 200m isobath, and the red line the Grijalva-Usumacinta River.

2.2.2 Sampling, processing and chemical analysis

Given the low concentration of POC in the oligotrophic waters of the GoM, it was necessary to pool water samples collected at different depths of the water column for analysis. At the shallow cast stations (<1000 m), the samples comprised depth filtrations of seawater from three discrete depths ranging from 10-50, 75-250, and 300- 1000 m (i.e., samples were pooled, and data were obtained for these three broad layers). For the deep cast stations, samples were pooled from 10 m to the depth of maximum fluorescence, between 150- 800 m, and from 1000 m to a few meters above the sea floor. The basic rationale behind the pooling of several depths was the need to filter large volumes of water to obtain the necessary amount of carbon for the analysis. Discrete sampling depths were generally consistent, except for the targeted

sampling during each cast of the chlorophyll maximum and oxygen minimum (identified based on the CTD profiles). For visualization purposes, POC values are plotted at the average depth of all the discrete samples collected within any given layer.

POC sampling and processing followed the Joint Global Ocean Flux Study methodology of knap et al. (1996) with some modifications. Specifically, the seawater was filtered through a pre-combusted (500°C for 4 hours) Whatman® glass microfiber filter (GF/F) with a diameter of 45 mm and 0.7 µm pore size. Typically, between 7.5 L and 60 L of water was filtered to get a minimum weight per determination of 100 mg for POC. Filtered samples were placed in ethanol-cleaned aluminum foil, stored frozen during the cruise, and transported to the laboratory for processing. In the laboratory, the samples were freeze-dried and then treated by acid fumigation with 1N hydrochloric acid in a desiccator for 24 hours to remove the particulate inorganic carbon. Filters were then scraped with an X-Act® knife to obtain the POC sample while minimizing the glass fiber from the filters and encapsulated in tin capsules.

The concentrations were determined on a Costech® CHN analyzer at the Stable Isotope Laboratory at CICESE and are reported as µmol/L. The international references used for POC were USGS 40 and IAEA-CH 6. POC concentrations were corrected for blanks (unused filters with the same treatment as the rest) and calibrated using different weighted samples of sulfanilamide. The detection limit of this method is 4.16 µmol C (50 µg C).

2.2.3 Data analysis

2.2.3.1 Satellite data

POC data were not generated for the surface layer during our cruises because water samples were used for other analyses. Hence, we used the satellite-derived surface concentrations to complement the POC station profiles (https://oceancolor.gsfc.nasa.gov/data/aqua/). We obtained daily estimates of POC concentration (mg m^{-3}) and Chl_a surface concentrations (mg m^{-3}) from the Moderate-Resolution Imaging Spectroradiometer (MODIS-Aqua Satellite) Level 3 mapped product with a spatial resolution of 0.04° (~ 4.4 Km) for 2015, 2016 and 2017 (NASA Ocean Biology Processing Group, 2018). Because of the lack of data at some station locations due to clouds, sun glint, low light levels, etc., we filled the gaps using the average value of the nearest data points by considering radial increments of 0.04° around the location, up

to a fourth iteration when needed (for a maximum radius of 0.16° around a station). If surface POC concentrations were unavailable within the maximum, the station was eliminated from further analysis.

The surface POC concentration is based on an empirical relationship between *in-situ* measurements of POC and blue-to-green band ratios of remote sensing reflectance. The algorithms have yielded good performance over vast areas of the oceans, including different hyper oligotrophic and oligotrophic provinces, with a determination coefficient between 0.7 and 0.9 (Stramski et al., 2008).

Daily SSH data were obtained from AVISO (https://www.aviso.altimetry.fr/en/home.html) using a gridded mesh with a spatial resolution of 0.25° (~ 27.8 Km) for 2015, 2016 and 2017. The non-steric SSH (SSH_{ns}) was calculated by subtracting the average SSH value for the GoM data (Domínguez-Guadarrama & Pérez-Brunius, 2017).

2.2.3.2 Hydrographic, data, and biogeochemical proxies

The *in-situ* density profiles were calculated from conservative temperature, absolute salinity, and pressure profiles using the GSW Oceanographic Toolbox from The International Thermodynamic Equation of Seawater (TEOS-10) (McDougall & Barker, 2011).

Apparent oxygen utilization (AOU) profiles were calculated as the difference between oxygen gas solubility and the measured oxygen concentration in water using TEOS-10 (McDougall & Barker, 2011). In the absence of direct turbulent dissipation measurements, the MLD is commonly derived from oceanic profile data using threshold, integral, least squares regression, or other proxies (Thomson & Fine, 2003). In our case, the MLD was defined as the depth of the maximum Brunt- Väisälä Frequency, calculated from absolute salinity, conservative temperature, pressure, and latitude using TEOS-10 (McDougall & Barker, 2011). The maximum fluorescence depth (MFD) was defined as the highest fluorescence value obtained from the vertical profile of each station.

2.2.3.3 POC data

Quantitative estimates of integrated POC in the surface layer vary depending on the choice of the depth to which the integration is made (Stramska, 2009). We used three different depths to estimate integrated

POC: (1) to a constant depth of 100 m (POC_{100}), (2) within the mixed layer at each station, with a boundary defined by the Brunt Väisällä frequency since it provides a link between the physical structure of the water column and the depth of mixing, and (3) to the depth of the fluorescence maximum, as indicative of the depth with the highest chlorophyll fluorescence.

This was done to evaluate which criteria better explained the spatial patterns of POC in terms of the physical and biological variables used in this study. To examine the main controls on the POC concentration in the upper layer of the GoM, POC data for each station were interpolated with a Piecewise Cubic Hermite Interpolating Polynomial method with a 1 m resolution, which preserves the shape of the data and respects monotonicity (Fritsch & Carlson, 1980).

2.2.3.4 SSH_{ns} data

To find out how the SSH_{ns} may influence the concentrations of POC in the water column, we correlated the surface POC concentrations against the SSH_{ns}. We generated two data sets of SSH_{ns}:

- Daily sea surface height, which corresponds to SSH_{ns} for the day when the samples were taken.
- Monthly sea surface height, which corresponds to the average of the SSH_{ns} during the period of the cruise.

Kelly et al. (2021) examined the contributions and mechanisms of the carbon budgets in the GoM. They concluded that lateral transport of organic matter is substantial in oligotrophic ocean regions of the northeastern Gulf near the LC and may be crucial to multiple trophic levels in the GoM.

To explore the possibility of lateral transport between the production and formation of POC, we also correlated POC concentrations with SSH_{ns} considered a radius of 0.25 degrees around the stations (daily and monthly SSH (0.25°)).

We also correlated the surface POC concentration of each cruise vs. the surface Chl_a concentrations, MFD, and MLD to evaluate whether there was a spatial relationship.

2.2.3.5 Identification and classification of mesoscale structures

Mesoscale structures are mainly generated by ocean large-scale circulation instabilities due to wind or topographic obstacles, creating variability around the ocean´s mean state. It helps us to understand the role of mesoscale structures on ocean dynamics (including POC production and export) and to discriminate the effect of eddies from other processes 2014 (Pegliasco et al., 2022).

To understand the relationship between mesoscale features and POC concentrations, we used "The altimetric Mesoscale Eddy Trajectories Atlas (META3.2 DT allsat) products, processed by CNES/CLS in the DUACS system and distributed by AVISO+ (https://aviso.altimetry.fr)". The algorithm used for these products is derived from Mason et al., (2014) and further described in (Pegliasco et al., 2022).This method follows four steps: filtering, detection, estimation of eddy characteristics, and tracking. For further algorithm descriptions, check the manual ¨Mesoscale Eddy Trajectory Atlas Product Handboook¨ (Aviso+ Altimetry, 2022).

After downloading the altimetric mesoscale eddy trajectories dataset, we filtered it by date, longitude, and latitude. We used this to identify daily mesoscale structures within the GoM during the three cruises, obtaining a map for each day; in total, 21, 15, and 25 maps were obtained for 2015, 2016, and 2017, respectively (Table 1).

Figure 3 presents an example of the approach to selecting centers and borders in cyclones and anticyclones. To aid in the understanding of the results obtained from eddy identification, we also examined geostrophic flows (downloaded from https://cds.climate.copernicus.eu/#!/home).

We classified eddies based on their rotational direction in the Northern Hemisphere as either cyclonic (counterclockwise) or anticyclonic (clockwise). The results from the Mesoscale Eddy Trajectories Atlas allow us to visually determine whether our sampling stations were located near the center of a structure or near the border (within a radius less than ~0.08° from the contour).

We classified stations based on whether they were located near the center of a cyclonic eddy (CCE), near the border of a cyclonic eddy (BCE), near the center of an anticyclonic eddy (CAE), or near the border of an anticyclonic eddy (BAE).

Stations outside these features were classified as no eddy (NE). We grouped the stations according to their categories and made composite vertical profiles of fluorescence, density, AOU, and POC using pooled data for the three cruises.

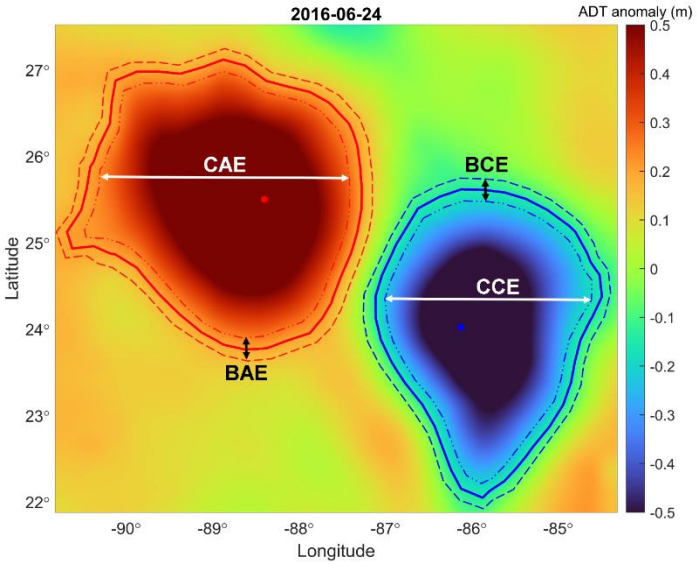

Figure 3. Absolute dynamic topography anomaly map depicting cyclonic and anticyclonic mesoscale structures observed on June 24, 2016. The blue/red line and dot represents the cyclone/anticyclone contour and center, data extracted from the altimetric Mesoscale Eddy Trajectories Atlas at AVISO+. The areas delimited by the dotted lines represent the border and center classification zone for the sampling stations that were in mesoscale structures.

2.2.3.6 Statistical analysis

A two-sided Wilcoxon rank sum test (equivalent to a Mann-Whitney U-test) was used to compare the medians of MLD and MFD between years.

A Kruskal-Wallis analysis was used to test differences in the MLD and MFD between cruises and in surface POC concentrations and integrated POC_{100} in each category of mesoscale feature ($\alpha = 0.05$).

Principal component analysis (PCA) was applied to examine associations between the oceanographic variables and the POC concentrations among the station's classifications. When two variables were highly correlated (Pearson's correlation $r>0.7$), one was removed prior to PCA.

The analysis included density at 10 m depth, MLD, MFD, SSH_{ns}, surface Chl_a, the fluorescence maximum, the depth at which the slope of the AOU changes towards positive values, surface salinity, sea surface temperature, the average temperature in the first 100 m and integrated POC_{100} concentration.

2.3 Results

2.3.1 Oceanographic conditions and POC concentrations

Figure 4 presents maps of non-steric SSH, sampled stations, and the geostrophic velocities mapped from the average period of each cruise (Table 1). During 2015 and 2016, there were stronger mesoscale circulation features in the central GoM than during 2017. During the 2015 cruise, two large anticyclones were observed between 24° and 28°N; Olympus (1), recently released from the LC, and the remnant of Nautilus (2) formed in May 2015 (www.horizonmarine.com; Figure 4). During this cruise we further observed the lowest SSHns values in the Bay of Campeche region. In 2016, a large anticyclone called Poseidon (3) had been recently detached from the LC, and the rest of the GoM presented higher SSHns values than during the 2015 cruise. In 2017, the LC showed a high level of intrusion into the GoM, but there were no large anticyclones within the gulf, and the SSHns were generally higher than during the 2016 cruise but lower than in 2015.

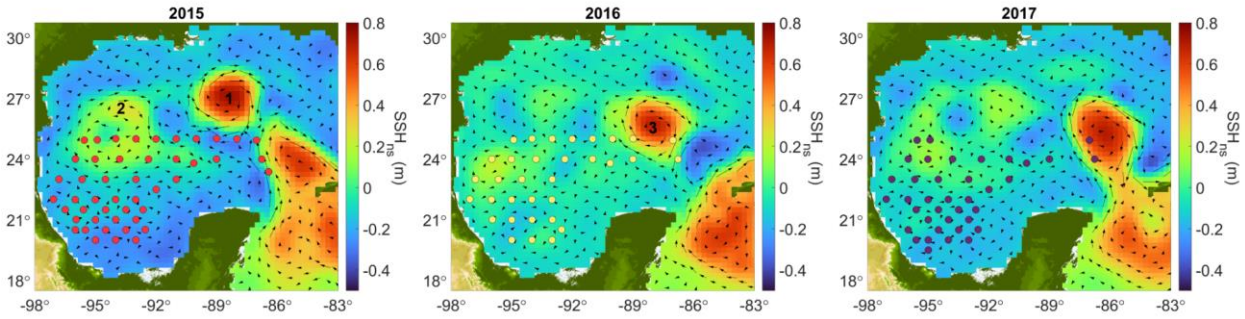

Figure 4. Mean non-steric sea surface height (SSHns) for the GoM during 2015, 2016, and 2017 cruises. Arrows represent geostrophic velocities. 1: Olympus. 2: Nautilus remnants. 3: Poseidon. Circles represent stations sampled during each cruise.

A Kruskal-Wallis test indicated that the median MLD differed between years ($p<<0.001$). The MLD maps presented in Figure 5 indicate that during 2015 the MLD was deeper in the northwestern part of the study area (~58 m), while the shallowest depths (~20 m) were in the east.

MLDs were markedly shallower during the 2016 cruise (Figure 5-middle panel) with an overall mean of 27 m. During that cruise, the Bay of Campeche showed the shallowest MLD, around ~15 m. During 2017, the MLD was deeper than in 2016 (Figure 5-right panel) with a mean of 35±9 m and with the deepest values toward the center of the GoM.

The median MFD differed significantly between years, as indicated by the Kruskal-Wallis test ($p = 0.012$). The MFD maps in Figure 5B (cruise´s average is in Table 2) show that the highest values were consistently located over the central gulf (abyssal region) during the three cruises, with a mean depth during 2015 of 73±24 m, 88±15 m during 2016, and 86±21 m during 2017.

Table 2. Mixed layer depth and maximum fluorescence depth during three cruises covering the southern Gulf of Mexico's deep-water region.

Year	MLD (m)				MFD (m)			
	Average	SD	Max	Min	Average	SD	Max	Min
2015	37	12	58	8	73	24	121	7
2016	27	9	51	15	88	15	122	63
2017	35	9	56	13	86	21	136	29

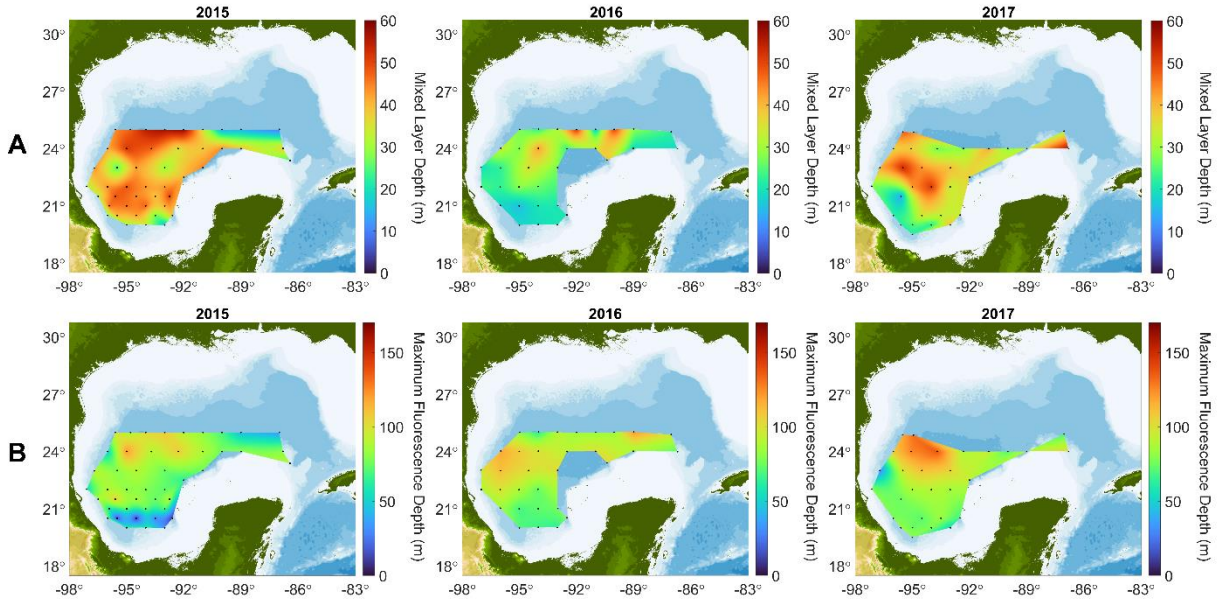

Figure 5. Mixed layer depth (MLD - A, top panels) and maximum fluorescence depth (MFD - B, bottom panels) in the GoM during 2015, 2016, and 2017 cruises.

2.3.2 Characterization of POC profiles and the integrated POC_{100}

In Figure 6, POC profiles showed a pattern consistent with the well-known exponential decay with depth in the water column (Suess, 1980), with higher concentrations at the surface (between 2 to 7 µmol L^{-1}) and decreasing with depth to values less than 1 µmol L^{-1} below 700m.

The sinking velocity of POC aggregates is mainly determined by their size, internal microstructure (porosity and heterogeneous composition), density, and the amounts of biogenic calcium carbonate and opal structures that act as ballast minerals (Iversen & Ploug, 2010; De La Rocha & Passow, 2007 and Armstrong et al., 2001). In addition, POC's sinking velocity and flux are hypothesized to be modulated by microbial remineralization and by zooplankton grazing (Guidi et al., 2009).

To understand the control of the surface ocean conditions on POC concentrations in the GoM, we considered different integrated depths sampled during the 2015, 2016, and 2017 cruises; the maps are shown in Figure 7, and the average, standard deviations and coefficients of variation are in Table 3.

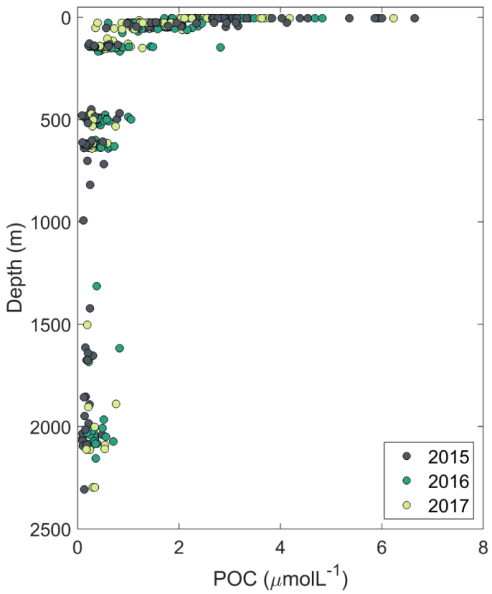

Figure 6. Surface and subsurface particulate organic carbon (POC) concentrations at different depths in the GoM for 2015, 2016, and 2017 cruises. POC concentrations at depths below the surface reflected the mean of the three discrete water sampling depths from which water samples were pooled.

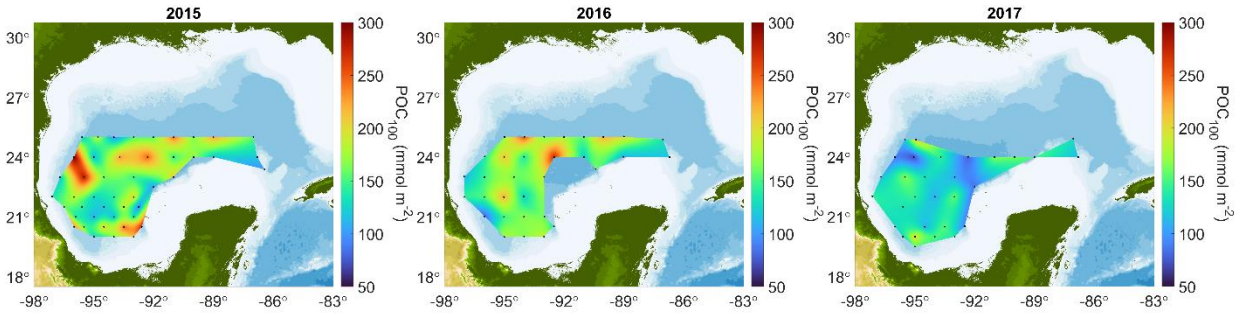

Figure 7. Integrated particulate organic carbon concentration for the first 100 m (POC_{100}).

In Figure 7, integrated POC_{100} showed mean values of 276 mmol m^{-2} during 2015 and 2016, and lower mean values during 2017 (207 mmol m^{-2}). The Kruskal-Wallis test indicated the medians in the integrated POC_{100}, between 2015, 2016 and 2017 were significantly different ($p = 0.003$).

The integrated POC_{100} during 2015 showed a spread of values between 125 – 200 mmol m^{-2} throughout the GoM, with highest values (300 mmol m^{-2}) at two stations located in the western region, and the lowest between 21º–22º N. During 2016, the spatial distribution of POC_{100} showed similar spatial patterns to 2015, with values between 150 - 250 mmol m^{-2} and the lowest values in the Bay of Campeche. In contrast, during 2017 all integrated measures of POC were mostly lower than during the previous two years. POC_{100} showed values between 60 and 150 mmol m^{-2} in the central GoM stations.

Table 3. Integrated POC_{100} during three cruises covering the southern Gulf of Mexico's deepwater region.

Year	Variable	Average (mmol m^{-2})	S. D	Variation coefficient
2015	POC_{100}	276	183	0.66
2016	POC_{100}	276	82	0.29
2017	POC_{100}	207	60	0.29

2.3.3 Influence of mesoscale structures on POC concentrations

The interpolated POC, density, fluorescence, and AOU profiles for the stations in each category (CCE, CAE, BCE, BAE, and NE) were pooled across years to examine the influence of mesoscale structures; means and standard deviations were calculated to provide a visual representation of the variability (Figure 8).

The CCE (yellow) density profile presented the shallowest MLD, with a shallow pycnocline at ~20 m (Figure 8A - top panel). The MFD was located close to 75 m, with increasing AOU's values below ~50 m. POC showed a mean concentration of ~3.6 µmol L^{-1} near the surface, decreasing to 0.7 µmol L^{-1} at 250 m depth.

Profiles from BCE stations (purple) showed well-stratified waters, with a relatively deeper mixed layer depth of ~35 m, and deeper MFD than stations near the center of cyclonic eddies (~75 m depth with a secondary peak at about 100m). The AOU profiles were similar at CCE and BCE stations, showing negative or close to 0 values from the surface to ~60 m. Below this depth, consumption and recycling of organic carbon was more important than production by primary productivity, as indicated by increasingly positive AOU values.

Mean POC concentrations were higher at stations near the center of cyclonic eddies (CCE) than near their borders (BCE). CCE stations showed the shallowest of the density profiles, which is consistent with the shallowest pycnocline near the core of cyclonic eddies.

The fluorescence profiles (CCE and BCE) showed a similar maximum fluorescence depth (~75 m), however, consistently higher fluorescence values were observed at all depths at stations near the CCE than in the BCE, suggesting higher chlorophyll concentrations throughout the water column. As for AOU, profiles from the CCE showed changes in the slope to positive values at shallower depths than stations in BCE (Figure 8A - top panel). The stations located near the core of anticyclones (CAE, blue) showed a weak pycnocline and a MFD between 80 m to 125 m. The AOU profiles showed changes towards positive values at ~100 m. In contrast, for BAE stations (orange), the pycnocline was located at ~25 m, while the MFD was found at ~80 m; the AOU profile showed a balance between consumption and production values for the first 50 m. The average POC average on the surface was ~2.8 µmol L^{-1}(Figure 8B - middle panel).

Near-surface POC concentrations at CAE stations were slightly lower (between ~1.9 and ~2.3 µmol L^{-1}) than stations near BAE (between ~2.1 and ~3 µmol L^{-1}) up to ~40 m depth (among ~0.8 and ~2.1 µmol L^{-1}); below that depth POC values were very similar (with values ranging between ~0.1 and ~1.7 µmol L^{-1}).

Comparison of CAE and BAE density profiles indicated a higher density at a given depth below ~30 m, indicative of a deepening of the isopycnals at the core of the anticyclonic eddies. CAE had lower fluorescence values down to 100 m, and a deeper fluorescence maximum than BAE stations. The AOU profiles for CAE show the change in slope to positive values almost 25 m deeper than BAE (Figure 8B - middle panel).

The mean profiles of density, fluorescence, AOU and POC for NE stations are in Figure 8C. The pycnocline is observed in the first upper ~25 m implying a relatively shallow mixed layer, and a relatively deep fluorescence maximum at ~80 m. The AOU profile indicates a close balance between production and

consumption for the first 50 m, below which respiration begins to dominate as AOU increases. The POC concentrations show an overall average value of ~3.7 µmol L^{-1}, although showing a high variability (Figure 8C - bottom panel).

A Kruskal-Wallis test was applied to the median integrated POC_{100} between the four different structures (CCE, BCE, CAE, and BAE), and there was no difference (p=0.131). Another Kruskal-Wallis test was applied for the medians of surface POC (5m) between the four different structures (CCE, BCE, CAE, and BAE) and results show that the means in the surface POC were different (p=0.023).

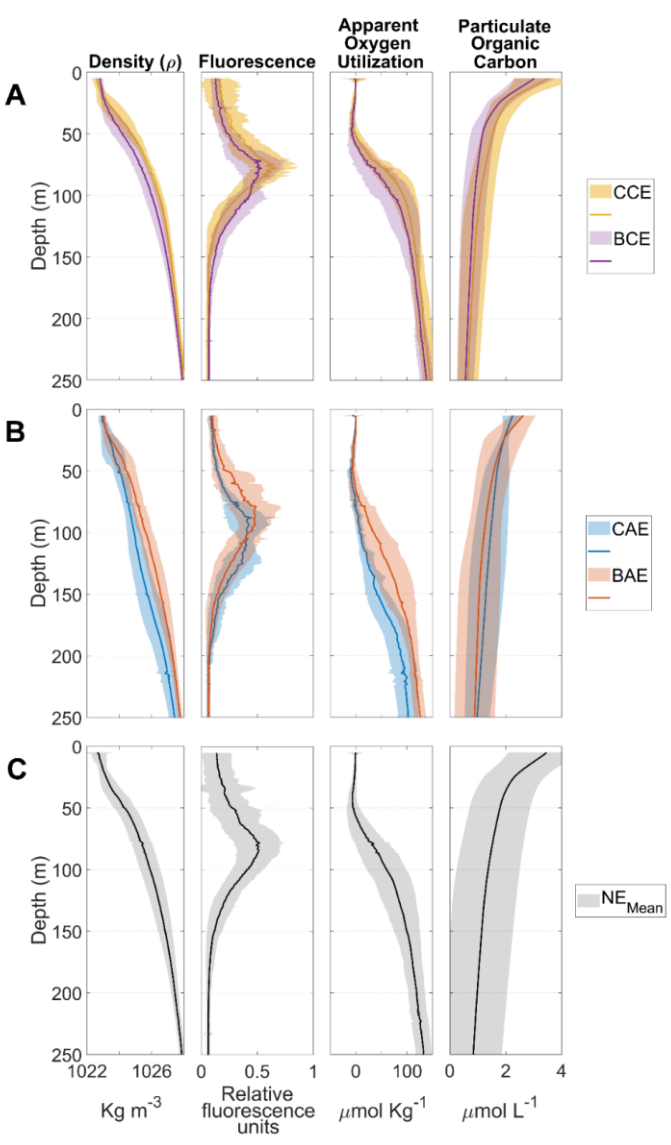

Figure 8. Mean and standard deviation profiles of density, fluorescence, apparent oxygen utilization, and particulate organic carbon for stations that fell near the center of a cyclonic eddy (CCE - yellow, A, top panel), near the border of a cyclonic eddy (BCE - purple, A, top panel), near the center of an anticyclonic eddy (CAE - blue, B, middle panel), near the border of an anticyclonic eddy (BAE - B, orange, middle panel) and the stations free of eddy influence (NE - black, C, bottom panel) during the 2015, 2016 and 2017 GoM cruises.

2.3.4 Correlations between POC and oceanographic variables

There were weak negative and non-significant Pearson correlation coefficients between integrated POC concentrations and SSH_{ns} (r= -0.10 to -0.22), even when SSH was estimated over a broader area around each station (daily SSH and daily SSH (0.25°) as well as monthly SSH and monthly SSH (0.25°)).

The correlation between integrated POC and the MLD, MFD, and Chl_a are shown in Table 4. Only the 2015 cruise showed significant correlations between the POC_{100} and MLD, MFD, and Chl_a.

The statistically significant negative correlations most likely result from higher (lower) POC integrated values associated with shallower (deeper) mixed layer depths and a shoaling (deepening) of the maximum fluorescence depth.

Table 4. Correlation analysis between POC_{100} vs. mixed layer depth, maximum fluorescence depth, and surface Chl_a concentrations. Significant correlations are in bold. N/A means not applicable.

Year	Variable	POC_{100}	
		r	p
2015	MLD	**-0.44**	**0.00**
	MFD	**-0.33**	**0.02**
	Chl_a	**0.63**	**0.00**
2016	MLD	0.22	0.23
	MFD	-0.05	0.77
	Chl_a	0.19	0.30
2017	MLD	-0.12	0.54
	MFD	-0.02	0.90
	Chl_a	0.32	0.09

The correlations between SSH_{ns} and MLD, MFD and Chl_a are shown in Table 5. Satellite-derived SSH_{ns} and MLD show statistically significant positive correlations during 2015 and 2017. There were also significant positive correlations between SSH_{ns} and MFD for 2015 and 2016; when SSH_{ns} was negative (positive), the maximum fluorescence depth was found at a shallower (deeper) depth. Negative SSH_{ns} values are associated with divergence in cyclonic structures, which leads to a shallower MLD and MFD, while positive SSH_{ns} values are associated with convergence and anticyclonic structures with the opposite pattern in the MLD and MFD.

Surface Chl_a vs. MFD and MLD consistently showed negative and statistically significant correlations for the three cruises. The negative correlation coefficients imply a deeper (shallower) maximum fluorescence depth associated with lower (higher) concentrations of a Chl_a (Table 5).

Table 5. Correlations between non-steric sea surface height, maximum fluorescence depth, mixed layer depth, and surface Chl_a concentrations. Significant correlations are in bold.

Year	SSH_{ns} - MLD		SSH_{ns} - MFD		MFD - MLD		MFD – Chl_a		MLD – Chl_a	
	r	p	r	p	r	p	r	p	r	p
2015	0.28	0.06	**0.59**	**0.00**	**0.48**	**0.00**	**-0.62**	**0.00**	**-0.51**	**0.00**
2016	0.13	0.47	**0.66**	**0.00**	**0.38**	**0.03**	**-0.8**	**0.00**	**-0.36**	**0.05**
2017	0.35	0.06	0.29	0.12	0.31	0.1	**-0.43**	**0.02**	-0.32	0.08

The PCA indicated that components 1 and 2 explained 52.1% of the variability (Component 1= 33.2% and Component 2=18.9%; Figure 9).

The PCA results grouped stations based on their locations at the centers and edges of mesoscale structures, showing the largest separation between stations at the CCE and CAE, and an overlap between BCE and BAE (Figure 9).

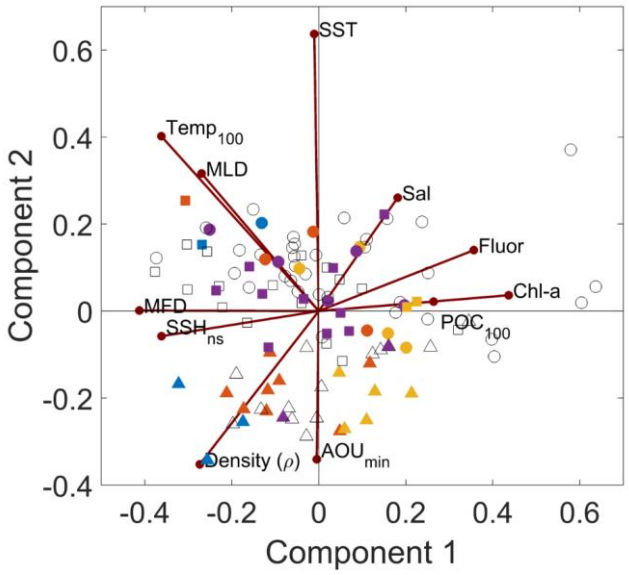

Figure 9. Principal component analysis of oceanographic variables and integrated POC_{100} estimates. The color indicates the classification of the mesoscale structures; stations near the center of cyclonic eddies are in yellow, near the border of cyclonic eddies in purple, near the center of anticyclonic eddies in blue, and near the border of anticyclonic eddies in orange. Colorless symbols indicate stations outside of eddies. The stations sampled in 2015 are indicated in circles, 2016 in triangles, and 2017 in squares.

The CCE stations (yellow) were positively correlated with Chl_a, Fluorescence, salinity and POC_{100}, and negatively correlated with the average temperature at 100m, MLD, MFD, SSH_{ns} and to a lesser extent the density. CAE stations (blue) were negatively correlated with Sal, Fluor, Chl_a and POC_{100}, and positively correlated with average temperature at 100m, MLD, MFD, SSH_{ns} and density.

Chl_a, fluorescence, integrated POC_{100} and salinity cluster in the positive region of component 1 while MFD, average temperature at 100m, SSH_{ns} density and MLD are grouped in the negative region. Most of the stations sampled during 2015 (circles) were correlated with sea surface temperature, MLD, salinity, and fluorescence.

In contrast, during 2016 (triangles), the stations were correlated with the average temperature at 100m, density and the depth where the AOU changes towards positive values. The stations sampled in 2017 (squares) fell all over the multivariate space.

2.4 Discussion

The mechanisms that control POC concentrations in the ocean differ depending on the region and the season (Dobashi et al., 2022). Sources of organic carbon in the GoM can include terrestrial and marine sources (Bianchi et al., 1997). The contribution of terrestrial organic carbon from terrestrial sources, including estuaries, is particularly important in coastal and shelf waters and constitutes an important component of global organic carbon (Hedges, 1992). Specifically, river inputs play a significant role in the distribution of POC (Meybeck, 1982). The Mississippi-Atchafalaya River and the Grijalva-Usumacinta River Systems are the largest sources of freshwater inflow to the northern and southern GoM, respectively (Kemp et al., 2016). The Mississippi- Atchafalaya River System has been shown to influence the distribution of POC and plays an important role in the organic carbon transport to the shelf and northern oceanic region (Trefry et al., 1994 and Rosenheim et al., 2013), while in the southern Gulf the Usumacinta-Grijalva River System is the main source of POC (Cuevas-Lara et al., 2021). In addition, POC fluxes are further influenced by mineral ballast, such as calcium carbonate, the concentrations of which are closely related to POC concentrations (Klaas & Archer, 2002).

The concentration profiles of POC in the GoM's deep-water region showed values that range between 2 and 7μM in the upper layer during the summer season. These concentrations are comparable with the values (4.48 ± 5.22 μM) previously reported for samples obtained under oligotrophic conditions in South and North Pacific Gyres in 2004 and 2012 (Stramski et al., 2022) in Table 6. Also, POC concentrations in the Equatorial Pacific Ocean collected between 30°N-15°S and 180-160°W in 2012 range between 0.75 and 8.8 μM; the smallest values were from oligotrophic regions, and the highest for the high-nutrient Equatorial Pacific region (Graff et al., 2015).

Stramski et al., (2022) sampled different oceanographic conditions ranging from oligotrophic environments like the South Atlantic Gyre to higher productivity regions of the Atlantic Ocean. They report concentrations of 4.77 ± 1.68 μM along north-to-south transects covered in 2005 and 2010. In another study, POC concentrations ranging between 1.67 and 6.33 μM were reported from samples collected in the North Atlantic Drift, North Atlantic Subtropical Gyre, North Atlantic Tropical Gyre, Western Tropical Atlantic, the South Atlantic Gyre, and the South Subtropical Convergence during 2014 (Strubinger Sandoval et al., 2022).

Reports from comparable oligotrophic regions like the Sargasso Sea showed POC concentrations between 1.18 and 2.96 μM from 1988 to 2004 (Duforêt-Gaurier et al., 2010), while the Hawaii Ocean time-series showed a range between 2 and 5 μM (Świrgoń & Stramska, 2015). In the southern deep-water region of the GoM, we found POC concentrations that are comparable with those reported for the northern open waters of GoM by Liu & Xue, (2020), who measured concentrations of 3±1 µM in May between 2010 and 2013 along the coast of Louisiana in the north GoM. However, they also reported much higher concentrations in the surface waters influenced by the plumes near the Mississippi River Delta (values around 14±6 µM). These high concentrations were attributed to the discharge of the Mississippi and Atchafalaya Rivers.

Table 6. Particulate organic carbon concentrations from different study areas.

Study	POC concentration (µM) [min-max] {Mean±SD}	Location	Sampling years
This study	[2-7]	Deep-water region of the GoM	[2015-2017]
Graff et al., 2015	[0.75-8.88]	Equatorial Pacific Ocean	2012
Duforêt-Gaurier et al., 2010	[1.18-2.96]	Sargasso Sea	[1988-2004]
Strubinger-Sandoval et al., 2022	[1.67-6.33]	Atlantic Ocean	2014
Świrgoń and Stramska 2015	[2-5]	Hawaiian Islands	[1997-2012]
Liu et al., 2020	{3±1}	Offshore Louisiana (Northern GoM)	[2010-2013]
Stramski et al., 2022	{4.48±5.22}	Pacific Ocean	[2004-2012]
Stramski et al., 2022	{4.77±1.68}	Atlantic Ocean	[2005 2010]
Liu et al., 2020	{14±6}	Mississippi River Delta (Northern GoM)	[2010-2013]

Hence, POC concentrations in the southern deep-water region of the GoM fall within the range observed in oligotrophic regions like the Sargasso Sea, and the subtropical gyres in the Atlantic and Pacific oceans during the summer season. An analysis of the global distribution of integrated POC_{100} from 1995 to 2012 showed a range of values from ~20 to ~900 mmol m^{-2} (Balch et al., 2018). The comparison of global estimates with our results is consistent with the oligotrophic nature of the southern deep-water region of GoM during the summer season.

POC concentrations in the water column showed the consistent well-known exponential decay with depth, with relatively high variability in the euphotic layer and decreasing concentrations below 700 m (<1 μM). To understand the mechanisms that could control this upper layer variability in the southern region of GoM, POC concentrations were integrated over different depths (100 m, MLD, MFD) and correlated with different variables. Integrated POC within the mixed layer depth and the fluorescence maximum depth did not show significant correlations with any of the oceanographic variables for any of the 3 years.

However, when integrating over the euphotic layer (with depths of ~100 m; (Linacre et al., 2019) our results showed a negative correlation with the MFD and the MLD and a positive one with the surface Chl_a concentration for the 2015 cruise. The POC_{100} showed similar average integrated concentrations of ~276 mmol m^{-2} for 2015 and 2016, although the variability was much higher in 2015 than in 2016. In contrast, during the 2017 cruise, POC_{100} was lower, with a mean value of 207 mmol m^{-2}. Differences in POC_{100} between years were significant due to the high variability between stations. These data suggest that MFD and MLD may occasionally play a role in modulating POC concentrations in the upper water column although it is not a consistent control over time and that there may be other mechanisms contributing to this intermittent relationship.

It is important to mention that although the three cruises took place during the summer season, the level of mesoscale activity differed. During 2015 and 2016 mesoscale activity was higher in central GoM than in 2017. The observed significant correlations between POC_{100} and the MLD, MFD and surface Chl_a concentrations for the 2015 cruise may be related to the two large anticyclones that were present in the central deep-water region; these were the remnants of Nautilus eddy and the recently released Olympus eddy. Thus, the higher variability in integrated POC concentrations found for 2015, may be attributed to an intensification of mixing processes associated with the edges of the anticyclonic eddies and consequently with the vertical transport of nutrients fueling the POC production in the euphotic layer. According to the results from the algorithm of AVISO, the average number of anticyclones during the cruise in 2015 was 6.7, in 2016 it was 5.4 and in 2017 was 4.7. Hence, the number of mesoscale structures may

be another contributing control to the variability of integrated $POC_{100,}$ especially during the summer season characteristic for strongly stratified upper ocean conditions.

Large and highly energetic mesoscale eddies exert a strong influence on the biogeochemical variables of the upper water column. Eddies are associated with vertical mixing, which affects nutrient transport and the Chl_a concentration in the euphotic layer (McGillicuddy, 2016), and our results in Figure 8 show that the POC upper layer concentrations may be modulated by their location within cyclonic and anticyclonic eddies. However, although we observed significant differences in the medians considering the first 5 m of the water column, we did not find significant differences in the integrated POC_{100} medians.

Higher POC concentrations, associated with the shoaling of density profiles and the deep fluorescence maximum are consistently observed at stations near the CCE than at stations near the BCE. These features are consistent with a shallowing (deepening) of the pycnocline near the core (border) of cyclonic eddies. Cyclonic eddies show an anti-clockwise flow of currents with negative SSH_{ns} at its center and counterclockwise geostrophic velocities, a shallower thermocline, and a conspicuous shoaling of isopycnals bringing colder, nutrient-rich subsurface waters closer to the euphotic zone at its center (Seki et al., 2001), all of them enhancing phytoplankton productivity, higher chlorophyll and POC concentrations in the euphotic layer (Bakun, 2006 and Bidigare et al., 2003).

The BCE shows consistently lower POC concentrations than stations in the CCE, with close to ~0.5 µmol L^{-1} difference in their mean values (Figure 7). The Chl_a concentrations at the center of a cyclonic eddy are consistently higher than at the borders, most likely as a result of the shoaling of the pycnocline allowing nutrients to reach the euphotic layer and thus fuel the phytoplankton productivity at depth (McGillicuddy, 2016). Honda et al., (2018) have shown how cyclonic eddies may affect the POC flux in the oligotrophic region of the subtropical North Pacific Ocean through the shoaling of the pycnocline driven by the passage of cyclonic eddies over the observation area, resulting in increased Chl_a in the subsurface layer and enhanced POC flux to the deep-sea region. This flux is positively related to the concentration of POC in the water column (Roca-Martí et al., 2021).

In contrast, anticyclonic eddies with clockwise geostrophic velocities (arrows) are convergence zones favoring the piling up of relatively warmer and lower-density water masses at their core, producing positive SSH_{ns}. Anticyclonic eddies are generally considered nutrient-depleted relative to cyclonic eddies (Seki et al., 2001). However, the POC fluxes observed in anticyclones in the eastern tropical North Atlantic show the opposite behavior, with larger fluxes comparable to those observed in mesotrophic or eutrophic

regions (Fiedler et al., 2016). Here, stations at the CAE mostly showed lower POC average concentrations by ~0.4 µmol L^{-1} (Figure 7) than those in the BAE. In addition, near the core of the anticyclones, there was a lower density gradient with depth, lower fluorescence, and a deeper MFD. A characteristic transect through an anticyclonic eddy shows a deepening (shallowing) of the pycnocline and MFD near the core (border) of these mesoscale features.

Previous work reported differences in cyclonic and anticyclonic eddies within the GoM. (Lee-Sánchez et al., 2022) analyzed vertical nutrient profiles for two cruises, one in the winter (February - March) of 2013 and the other in the beginning of summer (June) of 2016. Their results showed that mesoscale eddies play a strong modulating role in the vertical distribution of nitrate and nitrite, particularly in the first 250 m. In the cores of recently detached Loop Current eddies, the nitracline reached maximum depths, and there were lower nutrient concentrations in the euphotic layer. Data from ARGO measurements in the GoM showed that the depth and the magnitude of the DFM or deep chlorophyll maximum are also strongly controlled by the mesoscale variability, showing consistently lower chlorophyll concentration in anticyclones (Damien et al., 2018 and Pasqueron De Fommervault et al., 2017). Based on a biogeochemical model, primary productivity in the Loop Current Eddies is higher than the average rates in the surrounding open waters of the GoM. This anomalous behavior is explained by the mixed layer response during winter convective mixing, which reaches deeper into nutrient-rich waters due to the very low-density gradient with depth in the anticyclonic eddy. Although we didn't observe this process, since our data were always collected in the summer season, we coincide with their observation of the strong influence exerted by the mesoscale activity in the surface ocean chlorophyll concentration and, more specifically, within Loop Current Eddies (Damien et al., 2021).

All these observations show how mesoscale structures do exert some influence in the concentrations of POC in the upper layer. However, correlations of POC concentrations versus SSH_{ns}, which in principle is related to the mesoscale structures, didn't show a significant relationship. To explore this apparent lack of correlation, we calculated the Pearson correlation coefficient between satellite POC concentrations and SSHns in every coordinate of the data mesh of the GoM, considering the average of 8 days for the three summer months of 2015, 2016, and 2017 (Figure 10).

The relationship is presented in Figure 10, and a clear negative relationship between the POC concentrations in the surface ocean and SSH_{ns} was observed over a broad region in the central abyssal region, especially during 2015 and 2016. This is most likely related to the east-west trajectories of large, detached eddies from the LC. These negative correlations show lower POC concentrations associated with

higher SSH_{ns}, implying the importance of these mesoscale structures in controlling POC concentrations in the euphotic layer of the deep-water region of the GoM.

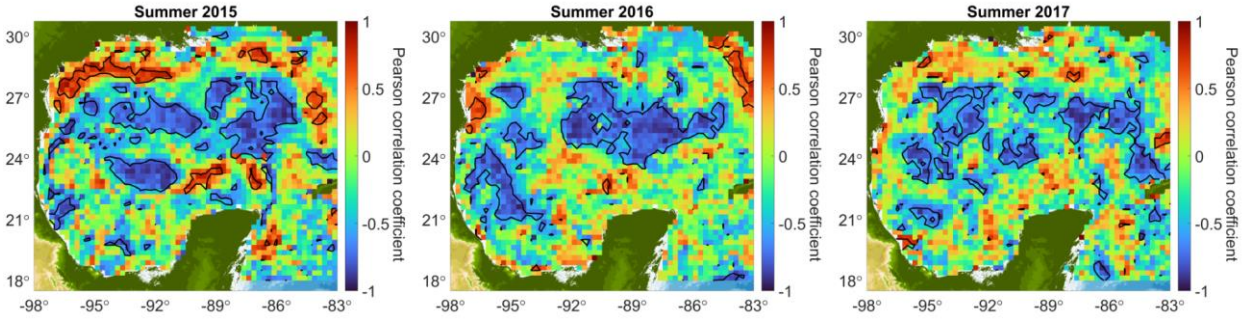

Figure 10. Spatial correlation maps for the summers of 2015, 2016, and 2017 between surface POC (https://oceancolor.gsfc.nasa.gov/data/aqua/) and SSH_{ns} (https://www.aviso.altimetry.fr/en/home.html), both derived from satellite data. Pearson's correlation coefficients are shown in colors, with hot colors indicating positive correlation and cold colors negative correlation. The black contours represent a confidence level of 95%.

Although our observations show how the POC concentrations may be modulated by mesoscale dynamics in the southern deep-water region of the GoM, it is important to mention that other processes deserve further studies to explain the observed variability. For instance, primary production is associated with seasonal high freshwater inputs, including those from the Tamaulipas shelf in the west, the Mississippi-Atchafalaya River System in the north, and the outflows of the Grijalva-Usumacinta River System in the south. In addition, further studies should be focused on the possible effects of increasing the stability of the upper water column due to rising sea surface temperatures in the interior of the GoM, and how this warming affects mixing in mesoscale features, and, consequently, primary production and upper layer POC concentrations to better understand the biological carbon pump in the GoM.

Chapter 3. Estimate the POM fluxes in the water column from two sediment traps in the northwest and south of the Gulf of Mexico

3.1 Introduction

Throughout Earth's history, the ocean has acted as a major reservoir of carbon, undergoing continuous cycles along with various other elements on a global scale, from the surface waters to the sea floor depths (Boyd et al., 2019).

Since the onset of industrialization in the mid-18th century, the ocean has sequestered a minimum of 25% of anthropogenic carbon dioxide (CO_2) emissions, thus playing a crucial role in mitigating the effects of climate change (Sabine et al., 2004).

Ocean ecosystems drive the biological pump, exporting organic carbon from the well-lit upper ocean through sinking biogenic particles into the stratified interior, where it's sequestered over varying time scales (Falkowski et al., 1998). The gravitational sinking of organic debris from ocean ecosystems is a dominant mechanism of biological carbon pump that regulates the global climate (Laurenceau-Cornec et al., 2023).

Sediment traps are indispensable tools for quantifying the vertical flux of particulate matter in marine environments on seasonal and annual timescales, playing a crucial role in biogeochemical studies. They enable researchers to capture sinking particles from various depths in the water column, thus providing insights into the processes governing the transport and deposition of organic and inorganic materials (Buesseler et al., 2007).

The GoM is a semi-enclosed basin characterized by its complex hydrography and dynamic circulation patterns, which are influenced by factors such as riverine inputs, seasonal stratification, and mesoscale circulation features like eddies and the Loop Current (Oey et al., 2005 and Sturges & Leben, 2000). These factors create a heterogeneous environment that affects the distribution and flux of particulate matter.

Sediment traps in the GoM have been used to study a variety of oceanographic processes, including the cycling of carbon and nutrients, the impact of mesoscale eddies, and the formation and transport of

marine snow, particularly in the northern region (Daly et al., 2016; Giering et al., 2018 and Hung et al., 2010). These studies have provided valuable insights into the dynamics of particulate matter and the biogeochemical processes that regulate the marine ecosystem.

Sediment traps also provide valuable data for understanding long-term changes in particulate fluxes and their responses to climatic and anthropogenic influences. For example, increased nutrient loading from rivers due to agricultural runoff has been linked to eutrophication and hypoxia in the northern GoM, affecting POM fluxes and sedimentation rates (Rabalais et al., 2002). By capturing temporal variations in particle fluxes, sediment traps help elucidate the interplay between natural processes and human activities in shaping the marine environment.

Rivers generally exhibit an isotopic signature ranging from approximately -24 ‰ to -28 ‰ (Kendall et al., 2001), while hydrocarbons typically display isotopic compositions around -25 ‰ or lighter (Freeman et al., 1990; Silverman & Epstein, 1958). These isotopic signatures are important for tracing the origin of organic carbon in marine environments, allowing for the identification of riverine and hydrocarbon inputs to the ocean.

Furthermore, sediment trap data contributes to the calibration and validation of biogeochemical models, enhancing our ability to predict the impacts of environmental changes on marine ecosystems. They provide measurements that complement remote sensing observations and improve the accuracy of carbon flux estimates in regional and global areas.

They offer insights into the complex interactions between physical and biological processes that govern particulate matter fluxes and their implications for carbon cycling and marine ecosystem health (Honjo et al., 2008).

3.2 Materials and methods

3.2.1 Sampling

Sediment trap moorings were deployed at two sites of the GoM: Perdido region (PR) (25.431° N, 96.072° W) and Coatzacoalcos (Coat) (19.386° N, 94.059° W, Figure 11).

The traps collected material at synchronous 18-day intervals from June 2016 to July 2017 (Table 7).

Both sites featured sediment traps at 1000 m depth, approximately 55 m above the sea floor.

The traps used were from McLane Research Labs Inc. model Parflux Mark78H-21 with a 0.5 m^2 collection opening and 21 collection bottles of 500 ml capacity filled with a formaldehyde solution at 37% prepared with filtered (0.2 µm) seawater.

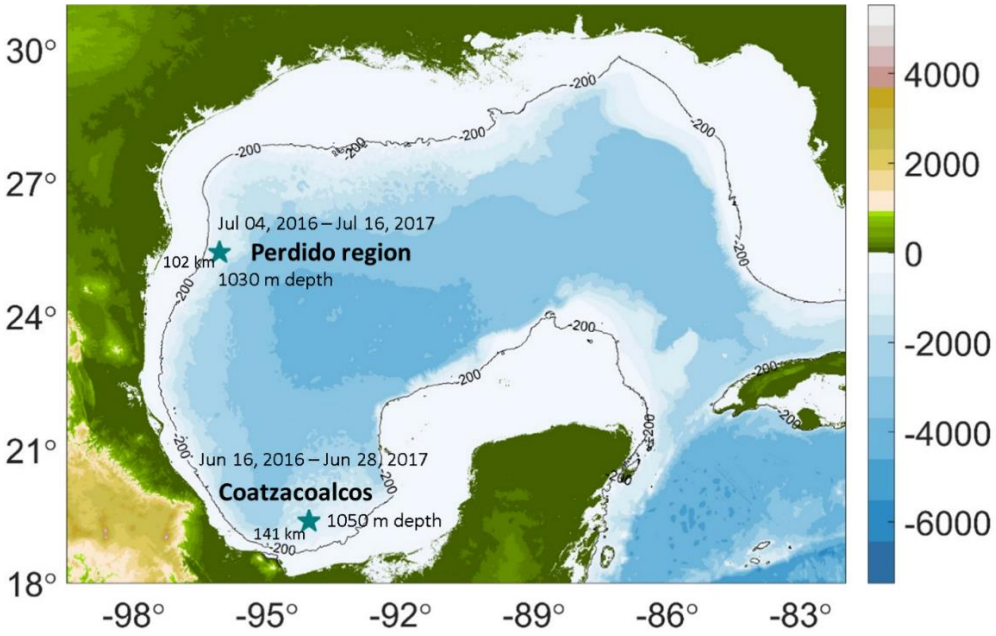

Figure 11. Location of Perdido region and Coatzacoalcos sediment traps in the Gulf of Mexico.

The design of each of the arrangements was anchored to the seabed through a 900 kg dead weight, had two acoustic releasers model 865-A from Teledyne Benthos, and included a series of buoys to maintain verticality and flotation.

3.2.2 Sampling processing, chemical analysis and measurement

Upon sediment trap recovery on board, forty-one samples were retrieved: twenty for PR and twenty-one for Coat. The sample cups were stored at 4°C in the dark until processed at the laboratory.

Table 7. Coatzacoalcos and Perdido region sediment trap sampling dates.

Perdido region				Coatzacoalcos			
Sample	Days	Start	End	Sample	Days	Start	End
1	-	-	-	1	18	16-Jun-16	3-Jul-16
2	18	4-Jul-16	21-Jul-16	2	18	4-Jul-16	21-Jul-16
3	18	22-Jul-16	8-Aug-16	3	18	22-Jul-16	8-Aug-16
4	18	9-Aug-16	26-Aug-16	4	18	9-Aug-16	26-Aug-16
5	18	27-Aug-16	13-Sep-16	5	18	27-Aug-16	13-Sep-16
6	18	14-Sep-16	1-Oct-16	6	18	14-Sep-16	1-Oct-16
7	18	2-Oct-16	19-Oct-16	7	18	2-Oct-16	19-Oct-16
8	18	20-Oct-16	6-Nov-16	8	18	20-Oct-16	6-Nov-16
9	18	7-Nov-16	24-Nov-16	9	18	7-Nov-16	24-Nov-16
10	18	25-Nov-16	12-Dec-16	10	18	25-Nov-16	12-Dec-16
11	18	13-Dec-16	30-Dec-16	11	18	13-Dec-16	30-Dec-16
12	18	31-Dec-16	17-Jan-17	12	18	31-Dec-16	17-Jan-17
13	18	18-Jan-17	4-Feb-17	13	18	18-Jan-17	4-Feb-17
14	18	5-Feb-17	22-Feb-17	14	18	5-Feb-17	22-Feb-17
15	18	23-Feb-17	12-Mar-17	15	18	23-Feb-17	12-Mar-17
16	18	13-Mar-17	30-Mar-17	16	18	13-Mar-17	30-Mar-17
17	18	31-Mar-17	17-Apr-17	17	18	31-Mar-17	17-Apr-17
18	18	18-Apr-17	5-May-17	18	18	18-Apr-17	5-May-17
19	18	6-May-17	23-May-17	19	18	6-May-17	23-May-17
20	18	24-May-17	10-Jun-17	20	18	24-May-17	10-Jun-17
21	18	11-Jun-17	28-Jun-17	21	18	11-Jun-17	28-Jun-17
22	18	29-Jun-17	16-Jul-17	22	-	-	-
Σ	378			Σ	378		

Once in the laboratory, samples were sieved through a 1 mm nylon mesh to remove swimmers and large aggregates. Subsequently, each sample was evenly divided into ten subsamples of 50 ml using a wet sampler divider (WSD-10 McLane Laboratory) with deviations between aliquots <5.0% and stored in 50 ml conical tubes. The aliquots were freeze-dried, grounded, and homogenized with an agate mortar. Total mass was determined by weighing two freeze-dried aliquots of each sample.

To determine organic carbon concentration, aliquots were treated with a hydrochloric acid solution (HCl, 1N) to dissolve carbonates. Deionized water was added, and after centrifugation to remove the supernatant, the remaining sediments were dried at 25 °C in an oven and encapsulated in tin capsules. To determine organic nitrogen concentration, aliquots were directly encapsulated in tin capsules after freeze-dried, without any preceding treatment.

Organic carbon and nitrogen concentrations, along with their isotopic compositions ($\delta^{13}C$ and $\delta^{15}N$), were determined on a Costech® CHN analyzer coupled to a Thermo Scientific DeltaV plus Advantage® isotope ratio mass spectrometer at the Stable Isotope Laboratory at CICESE. Organic carbon and nitrogen concentrations are reported as µg and isotope ratios were expressed in standard δ-notation relative to Pee Dee Belemnite (v PDB) for the $\delta^{13}C$ and atmospheric N_2 for the $\delta^{15}N$ via laboratory standards calibrated to internationally certified reference standards, USGS40 and Sucrose for carbon and nitrogen the IAEA-N2 and USGS40. The average precision from certified values was ±0.06‰. We did 2 or 3 replicates for each sample, depending on the availability and the reproducibility. The organic carbon concentrations were corrected for the carbonate dissolution prior to the analysis and reported as a percent of total sediment.

3.2.3 Data analysis

3.2.3.1 Buoy data

We obtained the wind speed (m/s) time series from the National Data Buoy Center (https://www.ndbc.noaa.gov/station_history.php?station=kywf1). We used data from two buoys, Station ID 42045 and Station ID 42055. The data reported represents the average over an eight-minute period; we compute the average over a period of 1 day.

3.2.3.2 Model-generated data

Daily net primary production surface data was obtained from the Vertically Generalized Production Model (VGOM) in Ocean Productivity (http://orca.science.oregonstate.edu/npp_products.php).

Daily geostrophic velocities were obtained from the Hybrid Coordinate Ocean Model (HYCOM) (https://www.hycom.org/data/goml0pt04/expt-32pt5). The GoM model has a 1/25° equatorial resolution and a latitudinal resolution of 1/25°. The data assimilation is performed using the Navy Coupled Ocean Data Assimilation (NCODA) system with a model forecast as the first guess. NCODA assimilates available satellite altimeter observations, satellite imaging, and *in-situ* sea surface temperature, as well as available *in-situ* vertical temperature and salinity profiles from XBTs, ARGO floats, and moored buoys.

3.2.3.3 Satellite data

We obtained daily surface concentrations estimates of Chl_a (mg m^{-3}), POC (mg m^{-3}), PIC (mol m^{-3}), and SST (°C) from the Moderate-Resolution Imaging Spectroradiometer (MODIS-Aqua Satellite) Level 3 (https://oceancolor.gsfc.nasa.gov/l3/) mapped product with a spatial resolution of 0.04° (~4.4 Km) for 2016 and 2017 (NASA Goddard Space Flight Center, et al., 2018).

Daily satellite surface salinity data, measured in parts per thousand ($1e^{-3}$), is obtained from NASA's Soil Moisture Active Passive (SMAP) mission (https://salinity.oceansciences.org/). This data is provided on a 0.25x0.25-degree grid and is averaged over an 8-day period.

Daily SSH data were obtained from AVISO (https://www.aviso.altimetry.fr/en/home.html) using a gridded mesh with a spatial resolution of 0.25° (~27.8 Km) for 2016 and 2017. The SSH_{ns} was calculated by subtracting the average SSH value for the GoM data (Domínguez-Guadarrama & Pérez-Brunius, 2017).

3.2.3.4 Statistical analysis

A Shapiro-Wilk test was applied to our data to assess whether they follow a normal distribution. We use the median and its quartiles to describe the central tendency and dispersion of the data set.

We conducted a multiple linear regression analysis to establish a model that captures the linear relationship between chlorophyll-a, sea surface temperature (SST), and their connections to the organic carbon fluxes captured by the sediment traps.

To evaluate multicollinearity, we calculated Pearson correlation coefficients. The normality of the residual distribution was examined using the Shapiro-Wilk test. We also investigated the autocorrelation among the residuals through the Durbin-Watson test and evaluated the homoscedasticity using the Breusch-Pagan test.

3.3 Results

The total mass fluxes (TMF) in mg $m^{-2}d^{-1}$ for both stations were calculated using the following equation:

$$TMF = \frac{M * N}{At * T} \quad (1)$$

Where *M* (mg) is the dry mass of the aliquot, *N* is the sample fraction, At is the trap opening area (m), and *T* (days) is the elapsed time. Organic carbon fluxes were determined by multiplying the TMF by organic carbon concentration.

3.3.1 Perdido region

The median value of organic carbon fluxes was 6.29 mg $m^{-2}d^{-1}$, which aligns with the Q2 line shown in Figure 12a. Two flux peaks stand out above the median: the first one during September and October 2016 and the second one during March and the first half of April 2017. Additionally, a smaller third pulse was observed in December 2016.

In the upper-right panel (Figure 12b), the $\delta^{13}C$ isotopic composition showed a median value of -23.67‰, with most values clustering around this central tendency, indicating negligible variability until the end of the record in June 2017. However, a small shift towards a lighter isotopic composition was observed in mid-September 2016, accompanied by increased data dispersion. Similar variations occurred in February of 2017. The summer of 2017 exhibits the most significant transition toward consistently heavier isotopic values -23‰ in the last three samples.

In the lower-right panel illustrating the C: N ratio (Figure 12d), the observed values exhibit significant variability, spanning from 5 to 11, with a median value of 8, closely resembling values typically found in marine environments. An elevated carbon-to-nitrogen ratio is often associated with continental influences

or refractory carbon, indicating continental inputs or the presence of refractory carbon. Elevated C: N ratios coincide with the timing of the initial organic carbon flux pulse and the period corresponding to the second significant peak. A notable contrast emerges in the lowest C: N values, aligning with the summer of 2017, a period characterized by the lowest organic carbon fluxes.

The $\delta^{15}N$ isotopic composition exhibited a median value of 3.65‰ (Figure 12c). From the summer of 2016 through the end of spring, the isotopic values displayed minimal fluctuations. However, a distinct shift becomes evident in the summer of 2017, with significantly heavier values reaching approximately 6‰. Subsequently, in the following month, the values declined, moving towards markedly lighter values and approaching 2.5‰ at the end of the sampling period.

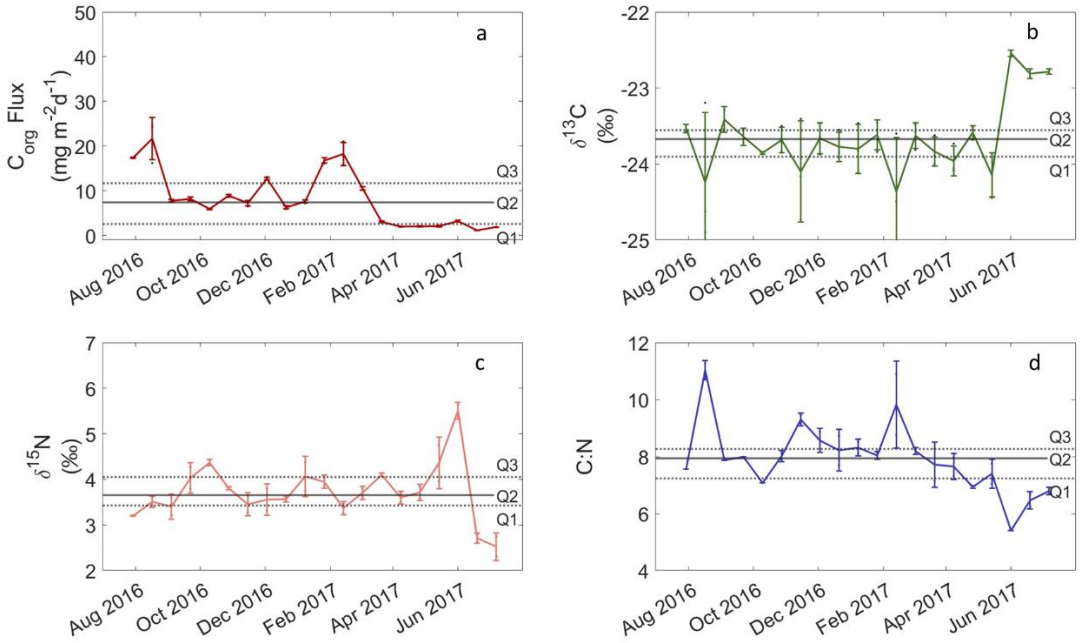

Figure 12. A comprehensive view of organic carbon and nitrogen-related parameters for the Perdido region during the period from July 2016 to June 2017. a) time series of organic carbon fluxes, b) isotopic organic carbon composition ($\delta^{13}C‰_{PDB}$), c) isotopic nitrogen composition ($\delta^{15}N‰_{AIR}$), and d) carbon-to-nitrogen ratio. In each panel, the Q2 line represents the median value, serving as a measure of central tendency. To assess the variability of these medians, we've added dashed lines, Q1 and Q3, which correspond to the lower and upper interquartile ranges, encompassing 25% of the observations each and aiding in identifying data points that fall outside the typical range.

In Figure 13, we present the time series data from satellites for the same time interval. The first panel (Figure 13a) shows the seasonality of the SSTs in the PR. Summer temperatures peak at 30 °C, while in winter, there is a decrease to around 25°C. Subsequently, the temperature experiences a gradual increase after spring, finally reaching levels like those recorded in the summer of 2016.

In the PR, SSH_{ns} (Figure 13b) showed the arrival of mesoscale features, negative anomalies showed the passage of cyclonic eddies, and positive anomalies to anticyclonic eddies. Negative anomalies during the summer of 2016 suggest the area is at the center of a cyclonic eddy or the edge of the anticyclonic eddy. There is a transition during mid-summer to values close to zero, probably due to the absence of eddies, lasting all winter. Subsequently, there is a modest elevation, probably the passage of an anticyclonic gyre during spring. In the third panel (Figure 13c), salinity data from June 2016 show abnormally low salinity values at the beginning of the sampling period. Showing an increase to approximately 36.5 units for the rest of the summer and fluctuating values during fall and winter, reaching higher values during summer.

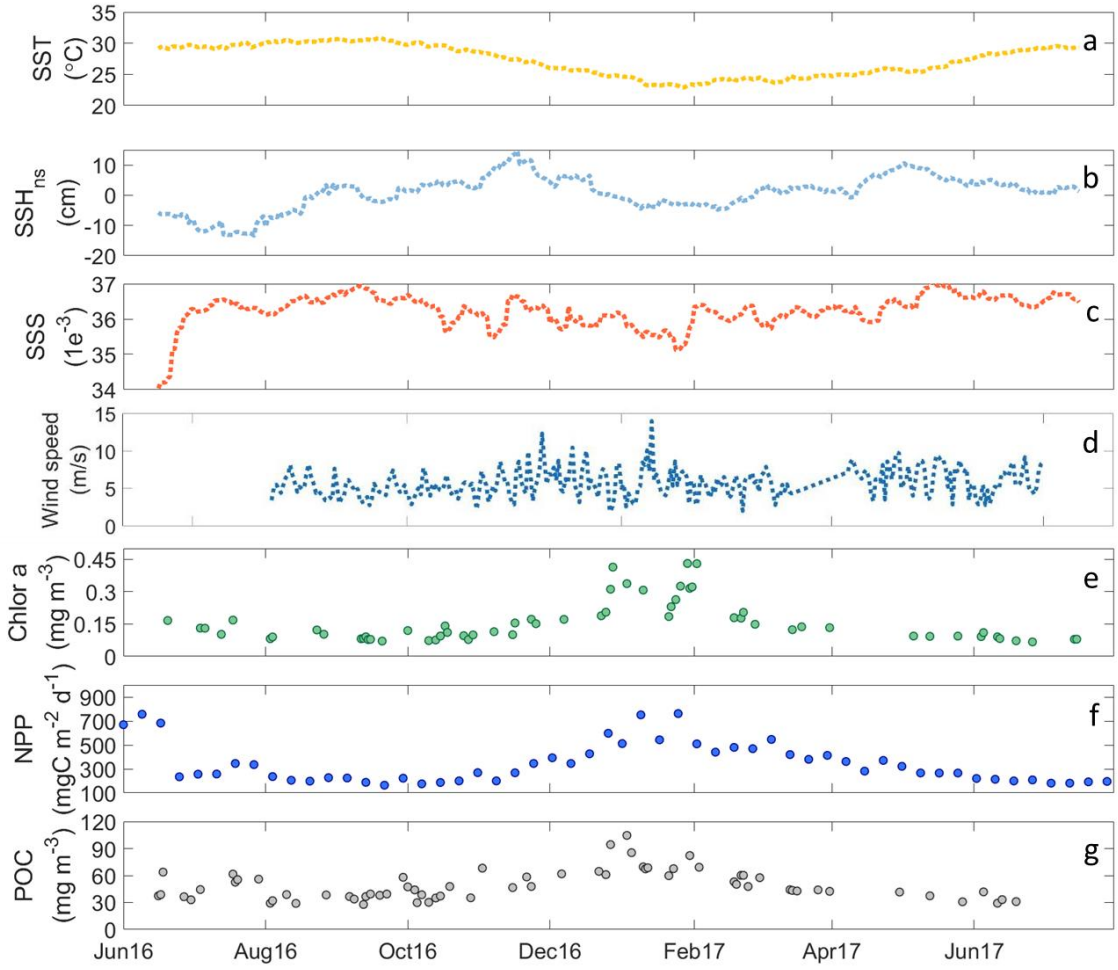

Figure 13. Time series of different variables potentially associated with the organic carbon fluxes in sediment traps within PR. Variables are presented in a top-to-bottom sequence and include sea surface temperature (SST), non-steric sea surface height (SSH_{ns}), salinity (SSS), wind speed, $Chlor_a$, net primary productivity (NPP), and satellite particulate organic carbon (POC).

Wind speed data (Figure 13d) from a buoy located near the sediment trap station is initially unavailable for the early period of the trap deployment. Nevertheless, a noticeable change in wind speed is observed

during the winter, reaching the highest speed of up to 15 m s^{-1}, a significant increase compared to the summer months in both years.

The chlorophyll-a time series (Figure 13e) showed consistently low values throughout the entire sampling period, except for the period from December to February, apparently coinciding with the change to lower SSTs and higher wind speeds. During this period, the highest chlorophyll-a values ranged between 0.3 to 0.45 mg m^{-3}, in contrast to the rest of the series, where values remained around 0.15 mg m^{-3}.

A similar variability to chlorophyll-a is observed in net primary production (Figure 13f), though with exceptionally high values in early summer showing fluctuation values around 700 mg C m^{-2} d^{-1}. Subsequently, the values decreased by half and stayed within the range of 100 to 300 mg C m^{-2} d^{-1}. Maximum values are observed in winter (~700 mg C m^{-2} d^{-1}), followed by a gradual decrease until late spring, resulting in values ranging around 200 mg C m^{-2} d^{-1}. The satellite-derived particulate organic carbon data (Figure 13g) showed values in the range of 30 to 70 mg m^{-3} during the summer months. Notably, a significant increase of ~110 mg m^{-3} was observed between December 2016 and March 2017.

We show a spatial distribution map of the period when significant pulses of chlorophyll-a concentrations were observed in PR above the trap marked with a red dot; we further plot the HYCOM-derived geostrophic flows shown with black arrows in Figure 14. These visualizations result from averaging data over an 18-day period, corresponding to the duration of particle collection in the sediment trap cups. The Chl_a images suggest a possible offshore transport of chlorophyll-a from the continental shelf to the sediment trap location (Figure 14). The left panel in the middle (Figure 14c) indicates higher chlorophyll-a concentrations near our study area, and while not entirely distinct, this observation aligns with the flow data, as it falls just beyond the Q3 percentile (Figure 12a) but remains lower than the other two observed pulses. In the middle right panel (Figure 14d) a plume of elevated chlorophyll-a concentration is observed in the surface waters near the trap, coinciding with increased organic carbon fluxes of ~20 mg m^{-2} d^{-1} in February 2017.

3.3.2 Coatzacoalcos region

The Coatzacoalcos region's organic carbon fluxes showed two pulses: one during the summer and the other in the winter (Figure 15a). The median value for the organic carbon fluxes is recorded at 7.36 mg m^{-2} d^{-1}.

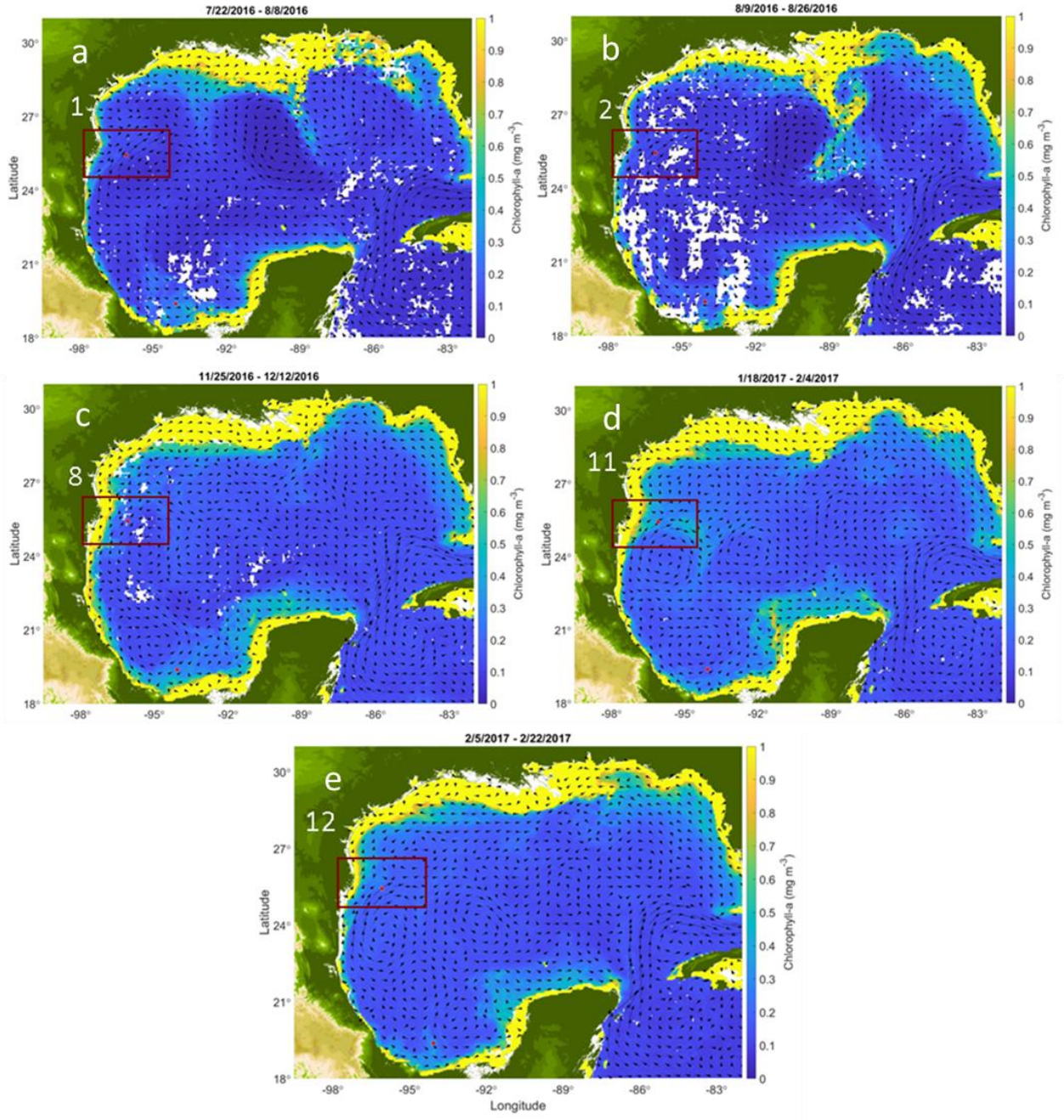

Figure 14. Spatial distribution of chlorophyll-a and currents (black arrows) corresponding to organic carbon flux peaks. Numbers indicate cup samples within the Perdido region (red rectangle).

The $\delta^{13}C$ isotopic composition (Figure 15b) presented a median value of approximately -23.79‰. However, during the winter season, there is a shift towards slightly heavier values, with measurements nearly reaching -23‰. Subsequently, a consistent decrease in its isotopic composition is observed throughout most of the sampling period, except for the final two samples, where values once again exhibit a shift towards a heavier isotopic signature.

The C: N ratio, as shown in the lower right panel (Figure 15d), had a central median value of 8, and most of the data points cluster closely around this median throughout most of the time series. However, a deviation from this pattern is observed in late spring when the ratio drops to ~4.5. Additionally, an increased dispersion during the winter suggests a higher variance in C: N ratios during this period.

The $\delta^{15}N$ isotopic composition (Figure 15c) maintained a relatively stable median value of ~3.32‰ throughout almost the entire sampling period, with a change of values shifting towards a heavier isotopic in late spring.

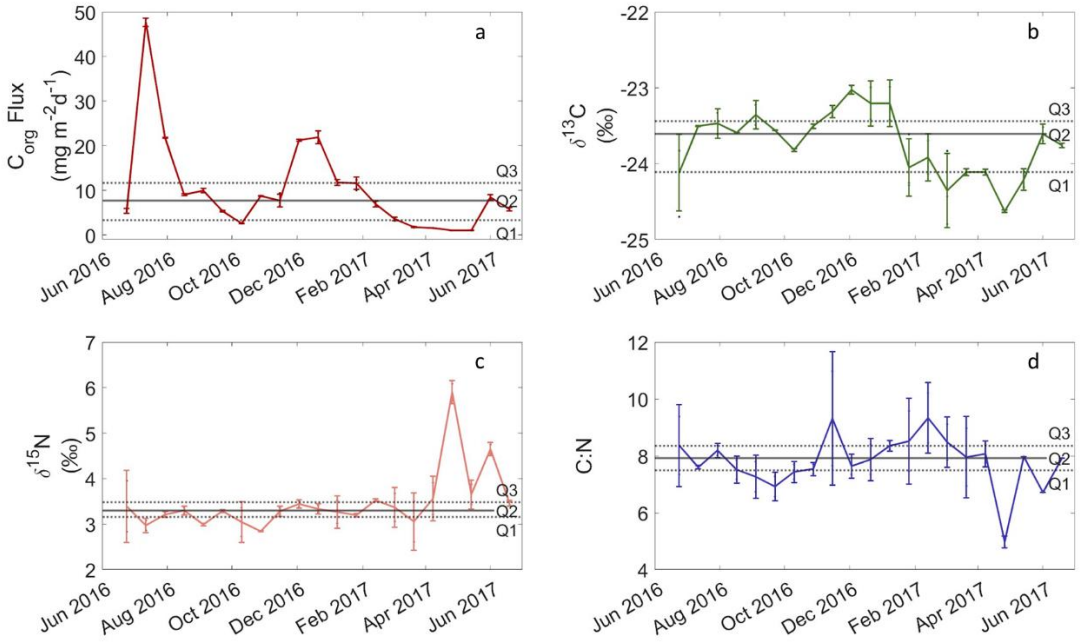

Figure 15. Time series of organic carbon and nitrogen-related parameters for Coatzacoalcos during the period from June 2016 to June 2017. The top-left panel depicts a time series of organic carbon fluxes, and the top-right panel showcases the isotopic organic carbon composition($\delta^{13}C‰_{PDB}$). The lower-right panel presents the carbon-to-nitrogen ratio, while the bottom-left panel illustrates the isotopic nitrogen composition ($\delta^{15}N‰_{AIR}$). In each panel, the Q2 line represents the median value, serving as a measure of central tendency. To assess the variability of these medians, we've added dashed lines, Q1 and Q3, which correspond to the lower and upper interquartile ranges, encompassing 25% of the observations each and aiding in identifying data points that fall outside the typical range.

The SST in the Coatzacoalcos region (Figure 16a) showed seasonality, with values spanning 25-30°C over the sampling year. The SSH_{ns} data (Figure 16b) showed values ranging from approximately -20 cm to 10 cm.

Negative values observed during the summer of 2016 likely indicate the presence of the semi-permanent Campeche gyre. In winter, we observed greater variability, probably influenced by the cyclonic gyre and temperature changes.

Salinity (Figure 16c) consistently ranges from 35 to 37 units throughout the year. Brief dips to around 35 units occurred in October and December 2016. Despite the rainy season in the summer months, which would typically lead to a higher influx of freshwater from the Grijalva-Usumacinta River complex, no significant salinity change is observed.

The wind speed data (Figure 16d) was collected from a buoy located at a moderate distance from the sampling station. Nevertheless, it demonstrated relative constancy throughout the year, with an increase during the winter season.

Chlorophyll-a concentrations (Figure 16e) exhibited significant variability, especially during the summer of 2016, with a concentration of ~0.35 mg m^{-3}. This was followed by a decline in late summer and autumn, stabilizing around 0.10 mg m^{-3}. A second peak occurred, reaching roughly 0.45 mg m^{-3}, and persisted until February 2017. Afterward, chlorophyll-a concentrations decline, oscillating around 0.15 mg m^{-3} for the remainder of the time series.

The behavior of NPP (Figure 16f) closely mirrors the fluctuations in chlorophyll-a concentration, with values ranging from 300 mg C m^{-2} d^{-1} to a peak of ~800 mg C m^{-2} d^{-1} during winter. Satellite-derived POC (Figure 16g) showed a pattern similar to chlorophyll-a and NPP, with lower concentrations in late winter of ~30 mg m^{-3}. The highest values were observed in August 2016 and winter 2017, reaching ~110 mg m^{-3} during both periods.

Figure 17 shows chlorophyll-a concentration and current patterns for Coatzacoalcos, highlighting the two largest fluxes. In the left pair of images (Figure 17a and Figure 17c) showed the first peak in organic carbon at nearly 50 mg $m^{-2}d^{-1}$, and a significant increase in chlorophyll-a concentration is observed in the region.

The currents, though not entirely clear, seem to flow east-to-west across the continental shelf, dispersing chlorophyll-a offshore near our study area, indicating the current's important role in chlorophyll-a distribution and thereby in the particulate organic carbon fluxes.

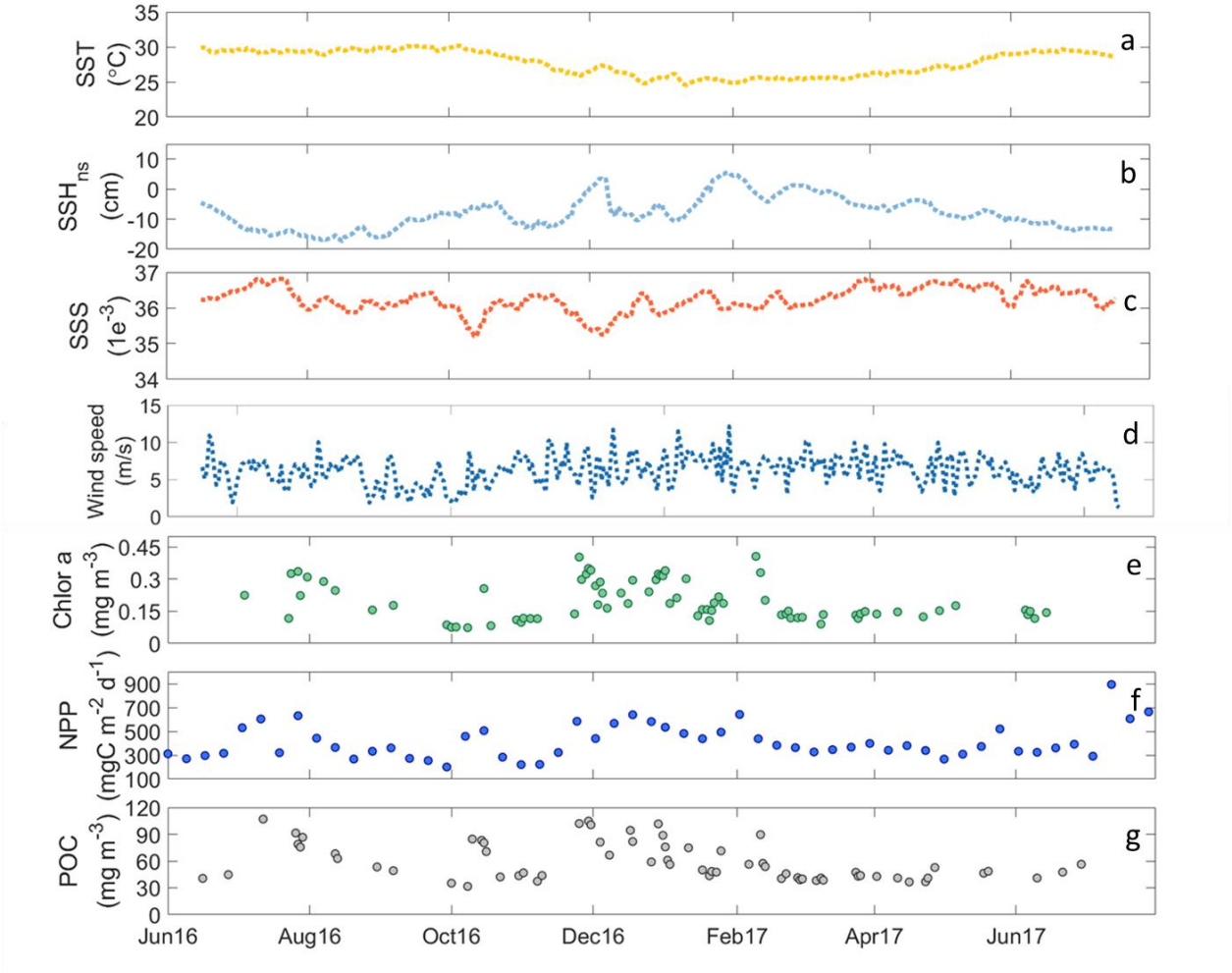

Figure 16. Time series of different variables potentially associated with the organic carbon fluxes in the sediment traps. The variables presented on a top-to-bottom include SST, SSH_{ns}, SSS, wind speed, $Chlor_a$, NPP and POC from Coatzacoalcos.

During the second pulse episode observed in winter (Figures b and 17d), with particulate organic fluxes ~25 mg m^{-2} d^{-1}, we could observe the formation of the semi-permanent Campeche cyclone. The cyclone's outer periphery redistributed chlorophyll-a near the continental shelf, transporting it offshore, just above the trap.

However, it is discernible that the eddy has undergone a modification, indicating a potential decrease in its intensity, leading to less chlorophyll-a being swept away and a reduced flow toward the sediment trap.

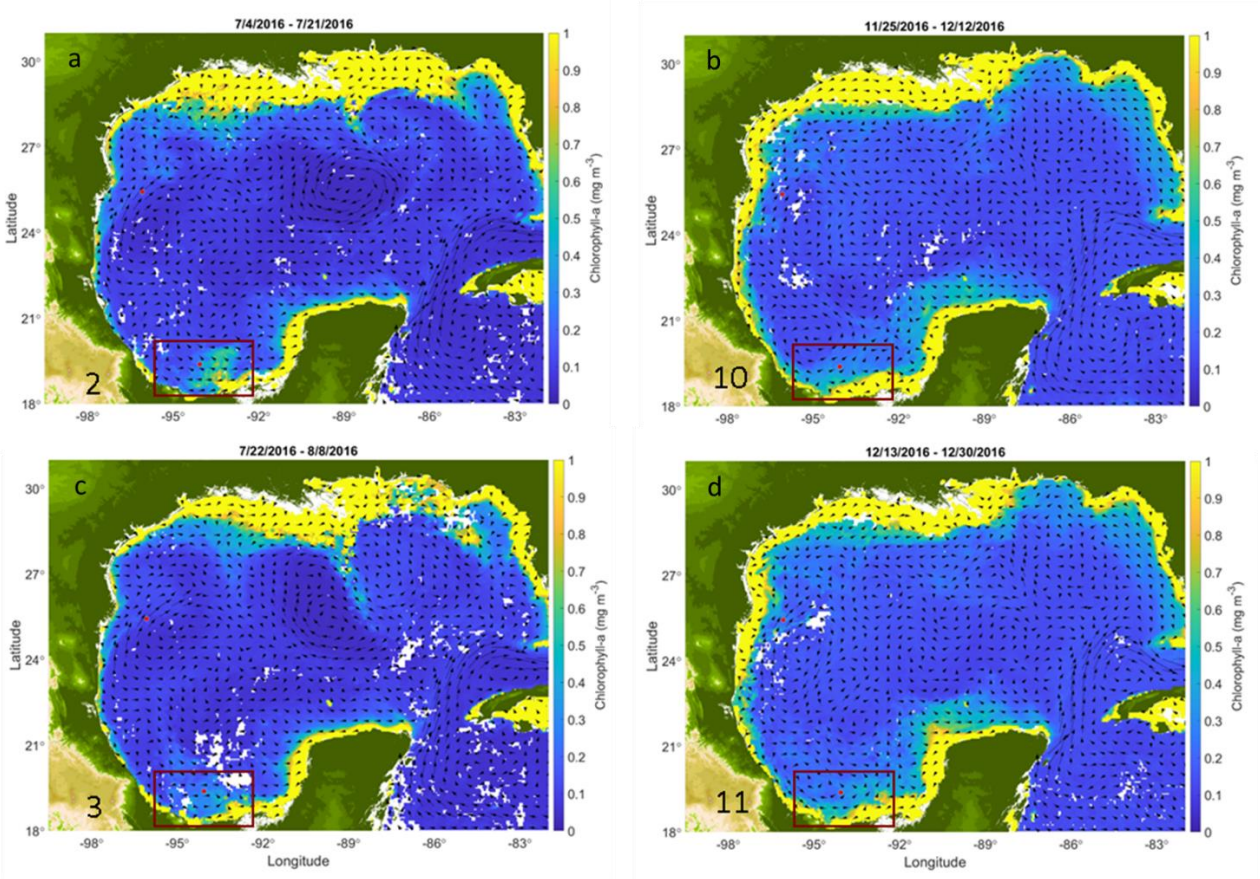

Figure 17. Spatial distribution of chlorophyll-a and currents (black arrows) corresponding to organic carbon flux peaks. Numbers indicate cup samples within the Coatzacoalcos (red rectangle).

3.4 Discussion

Organic carbon fluxes in the Perdido region and Coatzacoalcos showed temporal variability, though with distinct patterns and magnitudes. In the Perdido region, notable peaks occur during September-October 2016 and March-April 2017 (Figure 12). In Coatzacoalcos, two prominent pulses were observed in summer and winter (Figure 15).

In the oligotrophic subtropical gyres, low flux values are attributed to strongly stratified, nutrient-depleted upper waters, resulting in low primary production rates. Contributing factors include organic matter degradation, variations in the ocean's mixed layer depth, and the impacts of physical mixing, such as surface wind stress and eddies. In the GoM, we similarly observed consistently lower organic carbon fluxes during late summer in the Perdido region and Coatzacoalcos (Figure 12 and Figure 15), suggesting that these low fluxes could be influenced by similar low primary production in the surface waters.

The POC isotopic composition in the Perdido region revealed distinct low values during the first pulse in the summer of 2016 and the third pulse in February 2017, averaging -24.24‰ and -24.37‰, respectively. These values suggest contributions from specific sources, as rivers typically range from ~-24‰ to -28‰ (Kendall et al., 2001), and hydrocarbons are often around -25‰ or lighter (Silverman & Epstein, 1958 and Freeman et al., 1990). The observed isotopic composition is lighter than the expected open sea range of ~-21‰ to ~-23‰ (Goericke & Fry, 1994), indicating that other local sources, likely influence the region's isotopic signature. Further studies are needed to quantify their relative contributions

The median total value from the sediment trap was -23.67‰, indicating a consistent phenomenon that deviates from open sea conditions. These relatively lower values could be interpreted as the imprint of the Suess effect that lowers the $\delta^{13}C$ of the surface DIC through the dissolution of atmospheric CO_2 in surface waters, although we cannot rule out the influence of continental sources of carbon on the Perdido region's surface waters carbon isotopic composition.

Notably, the particulate organic carbon isotopic compositions observed during these pulse events exhibit higher dispersion, likely due to the inherent variability of the sources and drivers of organic carbon in this region. This variability results in fluctuations among individual samples, particularly noticeable when values deviate significantly towards lighter isotopic signatures implying a stronger continental source of variability.

In the Perdido region during the initial organic carbon pulse, most likely remnants of the anticyclone that flowed over the continental platform swept nutrients and chlorophyll-a offshore from the continental shelf, advecting these nutrient and chlorophyll-rich waters to the study area (Figure 14). The proximity between the first and second points suggests a delay in the fluxes of organic carbon. In December 2016, the interaction between the anticyclonic gyre and the continental shelf drove the advection of the chlorophyll-rich plume offshore and over our sediment trap.

The lower SSTs observed regionally in February 2017 played a significant role in increasing the organic carbon flux observed during this period. This suggests that temperature and, most likely, the deepening of the mixed layer, along with other factors, contributed to this phenomenon. However, the effectiveness of this transport was notably reduced in January 2017.

During the last three sampling periods in the Coatzacoalcos trap, carbon isotopic compositions showed anomalously heavy values (-22.54‰ to -22.81‰) with low organic carbon fluxes during late summer,

resembling open ocean stable isotopic composition values, implying minimal continental influence during low organic carbon flow periods.

The C: N ratios also displayed regional differences. In Perdido, the C: N ratios varied from 5 to 11, with a median of 8, showing elevated values during the organic carbon flux peaks and the lowest values in the summer of 2017. Coatzacoalcos, on the other hand, had a more stable C: N ratio with a median of 8 but with increased variability during winter and a significant drop in late spring.

In the Perdido region, the C: N ratio reached relatively high values of 9.79 and 9.23 during the first and third episodes, respectively, suggesting continental influence or refractory carbon. In Coatzacoalcos, the median C: N ratio was also around 8, within the interquartile range for both episodes. Notably, during periods of lowest flux, its behavior resembled that observed in the Perdido region.

Regarding the $\delta^{15}N$ values in PR had a median of 3.65‰ and showed significant fluctuations, particularly in the summer of 2017, reaching values as high as 6‰ before declining. In Coatzacoalcos, the $\delta^{15}N$ values were more stable with a median of 3.32‰, with a notable shift towards heavier values in late spring.

During periods of elevated organic carbon flux in the PR, nitrogen isotopic values consistently fluctuated within the interquartile range, ranging from 3.51‰ to 3.95‰. Values slightly below the first quartile indicated a lighter isotopic composition. Surface water nitrogen isotope values in the GoM typically fall between ~3.5‰ and ~5‰ (Howe et al., 2020). The values reported from both regions fall mostly within these broad boundary values. While in the Coatzacoalcos region, the variability is low, except for the last values in the PR, the variability is slightly higher around the median, probably influenced by inputs from agricultural fertilizers and other continental sources (Sigman & Fripiat, 2019). Synthetic fertilizers have a narrow $\delta^{15}N$ range of around 0‰, with most values between -2‰ and 2‰ (Bateman & Kelly, 2007). While these values suggest a continental influence, other processes like N fixation by nitrogen fixers in the surface ocean may play a small contribution, with typical values between 0.0‰ and 2.0‰ (Sigman & Fripiat, 2019).

Similar patterns were observed in Coatzacoalcos, where nitrogen isotopic values cluster around the median during both high-organic carbon periods, showing slight decreases in the first period. Overall, the data series exhibited stable variability except for the final periods, with the PR showing a fast alternation with distinctly higher and very low values and, in Coatzacoalcos, significantly heavier values at the end of the sampling period. The heavier values could result from the depletion of N in the surface ocean,

highlighted by the very low C_{org} values, and the return to light values at the end of the time series may imply a brief period of nitrogen fixation in the Perdido region.

Environmental variables, such as the SST, SSH_{ns}, salinity, wind speed, chlorophyll-a, NPP, and POC, further showed the similarities and differences between the two regions. In the case of the SSTs both regions showed maximum during summer months, implying a highly stratified surface ocean briefly stirred by mesoscales eddies associated with low PP values and low POC export fluxes. Cooling during winter months promotes a deeper mixed layer, which eventually is stirred by the northern winds "Nortes", leading to the injection of nutrients and higher primary productivity and, consequently, higher POC export fluxes in both regions. The lowest POC fluxes to the traps are consistently observed in both regions during the transition from spring into summer, probably implying the complete utilization of nutrients after the winter bloom period. However, there are two prominent organic carbon pulses happening during late summer, which cannot be readily explained by the seasonality of SSTs or the wind regime.

SSH_{ns} track mesoscale circulation, and the spatial distribution of surface chlorophyll highlights the importance of mesoscale oceanographic processes in both regions, influencing the distribution and flux of organic carbon. In the Perdido region, the interaction of an anticyclonic eddy with the continental platform during August redistributed chlorophyll-a and organic carbon over the shelf and probably nutrients, sweeping them from the shelf environments offshore, generating as could be seen from the circulation features showing a strong offshore flow during July and August. In the Coatzacoalcos region, the SSH_{ns} and current flow in July showed a strong flow over the Tabasco shelf, sweeping surface chlorophyll-a offshore over the trap location, further reflected in the high organic carbon fluxes during that month in the trap samples (Figure 14 and Figure **17**).

The comparison between the Perdido region and Coatzacoalcos highlights the complexity and variability of organic carbon fluxes in the GoM. Fluxes of organic carbon to the traps in both regions are partially controlled by the SSTs, and wind seasonality is on top of the interaction between the mesoscale eddies with the continental shelf rich in chlorophyll and nutrients sweeping them offshore for hundreds of km.

In Table 8, we show data from sediment traps reported by Honjo et al., 2008 near 1000 m depth across various study areas highlighting the variability and insights into biogeochemical processes. Organic carbon flux values range from the high value of 6.132 g m^{-2} yr^{-1} at Greenland Sea (Trap ID: I-3) to 0.204 g m^{-2} yr^{-1} at the low-productivity mid-gyre region in Hawaii (Trap ID: P-42). In the current study, the PR showed median values around 3.114 g m^{-2} yr^{-1} and slightly higher for Coatzacoalcos, 3.878 g m^{-2} yr^{-1}. These values

are relatively high compared to other regions, particularly Coatzacoalcos. These median values were clearly influenced by high organic carbon pulses observed during mid to late summer in both regions, suggesting the relevance of the geographic location of the traps, which are relatively close to eutrophic shelf environments coupled with the mesoscale circulation features that transfer organic carbon and nutrients from shelf environments offshore. These data can refine carbon export models and improve understanding of how ocean processes like mesoscale eddies control carbon transfer from the surface coastal to the deep ocean.

The elevated export of particulate organic carbon in the Perdido region and Coatzacoalcos reflects regional variability in carbon fluxes. Mesoscale processes and the interaction with continental shelf drive the offshore transport of nutrients and Chl_a to slope and deep-water regions, generating pulses that set the GoM apart from other oligotrophic regions (Table 8). Mesoscale processes, such as eddies and the continental platform, play a crucial role in redistributing nutrients from the continental shelf to deeper waters, influencing primary production, and thereby affecting the export of organic carbon to the deep ocean (Williams & Follows, 2003). This effect was observed in Figure 14 and Figure **17**.

Based on the POC differences observed between 1000 and 2000 m depths in the data from Honjo et al. (2008), it was determined that approximately 55% of the organic carbon present at 1000 m reaches 2000 m. Assuming this same fraction applies to our measurements, we calculated the theoretical organic carbon fluxes at 2000 m based on the values recorded at 1000 m in our sediment traps. The resulting fluxes were 1.71 g m^2 yr^{-1} in the Perdido region and 2.13 g m^2 yr^{-1} in Coatzacoalcos, which are consistent with the average values reported by Rixen et al., (2019) (Figure 18).

Although the fluxes have been evaluated as average according to the levels proposed by Rixen et al., (2019), if the pulse-induced fluxes (marked with * in Table X) are excluded, the adjusted values are 0.77 g m^2 yr^{-1} for the Perdido region and 1.02 g m^2 yr^{-1} for Coatzacoalcos. Despite the significant decrease in flux values when these pulses are removed, the results still fall within the average range. This may be attributed to the relative proximity of the sediment traps to the continental platform and the influence of continental shelf nutrient input in both regions.

Table 8. Organic carbon fluxes comparison with global data and other oligotrophic regions.

Trap ID	Location		FCorg ($g\ m^{-2}\ yr^{-1}$)	Depth (m)	References
	Latitude	Longitude			
PR	25.431	96.072	*3.114*	*1000*	(this study)
Coatz	19.386	94.059	*3.878*	*1000*	(this study)
A-5	70	0	1.812	1000	Von Bodungen et al., (1995)
A-6	70	0	1.728	1000	Von Bodungen et al., (1995)
A-7	70	0	3.06	1000	Von Bodungen et al., (1995)
A-15	-12.8	93	3.372	1020	Scholten et al., (2001) and Antia et al., (2001)
A-20	47.8	-19.8	0.84	1030	Kuss & Kremling, (1999) and (Scholten et al., (2001)
A-25	47.7	-20.9	1.548	1018	Honjo et al., (1992, 1993)
A-28	33.8	-21	0.936	1070	Honjo et al., (1992, 1993)
A-31	33	-22	0.516	1050	Scholten et al., (2001)
A-36	29.1	-15.4	0.444	1021	Scholten et al., (2001) and Neuer et al., (1997)
A-45	1.8	-11.3	2.796	953	Fischer & Wefer, (1996) and Wefer & Fischer, (1993)
A-46	-2.2	-10.1	1.2	1068	Fischer & Wefer, (1996) and Wefer & Fischer, (1993)
P-5	53	149	1.488	1061	Honjo (1996)
P-10	50	-145	4.824	1000	Wong et al., (1999)
P-11	50	-145	2.952	1000	Wong et al., (1999)
P-12	50	-145	1.656	1000	Wong et al., (1999)
P-13	50	-145	1.74	1000	Wong et al., (1999)
P-14	50	-145	2.4	1000	Wong et al., (1999)
P-27	40	165	1.536	953	Honda, 2001
P-28	40	165	2.196	950	Honda, 2001
P-42	15.4	-151.5	0.204	978	Honjo, (1982)
S-5	-56.9	-170.2	1.692	982	Honjo et al., (2000)
S-6	-60.3	-170.1	2.34	1003	Honjo et al., (2000)
S-7	-62	73	0.924	1000	Pilskaln, 2004
S-11	-63.1	-169.9	2.484	1031	Honjo et al., (2000)
S-13	-66.2	-168.7	1.944	937	Honjo et al., (2000)
I-1	17.7	57.9	4.14	998	Honjo et al., (1999)
I-3	17.4	58.8	6.132	903	Honjo et al., (1999)

Table 9. Organic carbon fluxes in Coatzacoalcos and Perdido region

		Coatzacoalcos			Perdido region		
Start date	End date	Bottle ID	FCorg	FCorg (55%)	Bottle ID	FCorg	FCorg (55%)
(mm/dd/yyyy)			(mgCorg/m^2 * 18 days)			(mgCorg/m^2 * 18 days)	
6/16/2016	7/3/2016	C1	97.19	53.45	-	-	-
7/4/2016	7/21/2016	C2*	859.11*	472.51*	-	-	-
7/22/2016	8/8/2016	C3*	392.31*	215.77*	P2*	312.70*	171.99*
8/9/2016	8/26/2016	C4	163.31	89.82	P3*	390.46*	214.75*
8/27/2016	9/13/2016	C5	179.37	98.65	P4	140.02	77.01
9/14/2016	10/1/2016	C6	96.92	53.31	P5	147.17	80.95
10/2/2016	10/19/2016	C7	47.08	25.90	P6	107.04	58.87
10/20/2016	11/6/2016	C8	157.79	86.79	P7	160.34	88.19
11/7/2016	11/24/2016	C9	139.43	76.69	P8	130.47	71.76
11/25/2016	12/12/2016	C10*	383.28*	210.8*	P9*	229.44*	126.19*
12/13/2016	12/30/2016	C11*	394.29*	216.86*	P10	113.26	62.29
12/31/2016	1/17/2017	C12	212.52	116.88	P11	136.74	75.20
1/18/2017	2/4/2017	C13	209.27	115.10	P12*	301.62*	165.89*
2/5/2017	2/22/2017	C14	125.64	69.10	P13*	328.49*	180.67*
2/23/2017	3/12/2017	C15	64.84	35.66	P14	190.09	104.55
3/13/2017	3/30/2017	C16	32.33	17.78	P15	54.70	30.08
3/31/2017	4/17/2017	C17	28.60	15.73	P16	36.04	19.82
4/18/2017	5/5/2017	C18	19.21	10.57	P17	36.54	20.10
5/6/2017	5/23/2017	C19	19.28	10.61	P18	37.72	20.75
5/24/2017	6/10/2017	C20	152.55	83.90	P19	57.65	31.71
6/11/2017	6/28/2017	C21	104.10	57.25	P20	20.61	11.33
6/29/2017	7/16/2017	-	-	-	P21	34.35	18.90

*Pulses of organic carbon fluxes in the sediment traps.

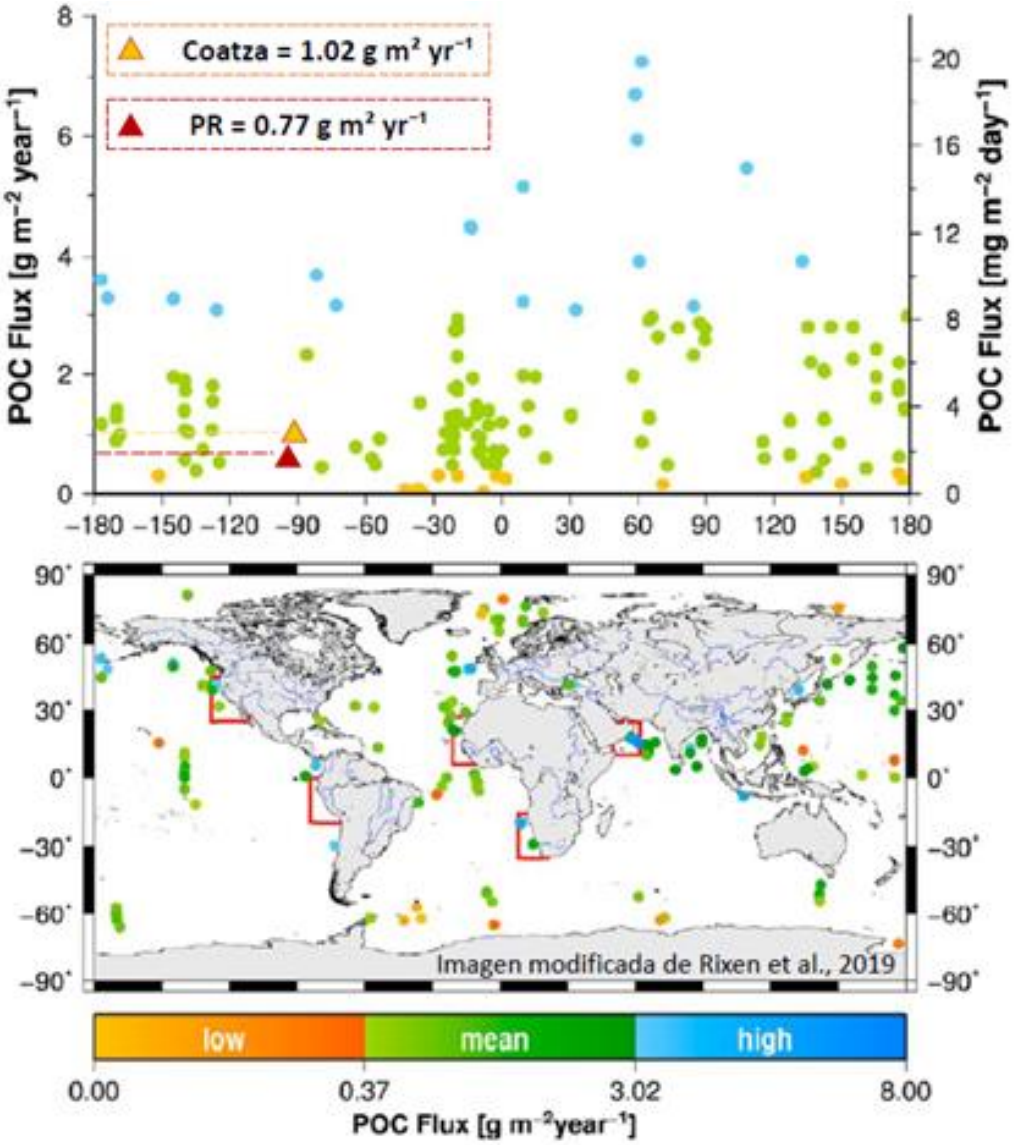

Figure 18. Annual mean organic carbon fluxes adjusted to a water depth of 2000m versus latitude (upper panel) at the trap locations depicted in the lower panel. Color coding is arbitrary and highlights high carbon fluxes in the Arabian Sea. The data are from (Honjo et al., 2008) and include also records discussed here. The red lines on the map indicate major coastal upwelling systems. Yellow and red triangles indicate organic carbon fluxes at the Perdido and Coatzacoalcos sediment trap in the GoM (Image modified from Rixen et al., 2019).

These values may be classified as average due to the influence of pulses in both regions, generated by mesoscale processes or continental input. The calculations were based on the global compilations, with a comparison between sediment traps at 1000 m and 2000 m depths (Honjo et al., 2008).

To determine the linear relationship between variables and relate them with the particulate organic carbon fluxes in the trap, we performed a multiple linear regression, considering SST and chlorophyll-a as independent variables for each region.

For the PR, the analysis provided the following model for particulate organic carbon fluxes (Equation 2):

$$CorgFluxPR = -0.0828 * SST - 287.554 * Chl_a + 12.0277 * (SST * Chl_a) \quad (2)$$

The coefficient of determination (R^2) for this model is 0.8705, indicating that approximately 87.05% of the variability in the particulate organic carbon fluxes can be explained by the SST with a 30-day lag and Chl_a with a 7-day lag. The model's p-value <0.05, shows that the regression is statistically significant.

Normality, homoscedasticity, and the absence of autocorrelation represent fundamental assumptions in regression models. Normality underpins the validity of parametric tests and the reliability of confidence intervals, while homoscedasticity ensures that the variance of residuals remains consistent across different levels of the independent variables, thereby reinforcing the model's stability (Khaled et al., 2019; Paul & Zhang, 2010). Moreover, the absence of autocorrelation confirms the independence of residuals, which is imperative for obtaining unbiased parameter estimates (Harris, 2019). Understanding these parameters is essential because they validate the underlying assumptions of statistical models, ensuring that the conclusions drawn are reliable and robust.

To check for multicollinearity, we calculated the Pearson correlation coefficient between the independent variables SST and Chl_a, which was -0.4317. This value suggests a moderate negative correlation between the predictors.

The normality of the residuals was assessed using the Shapiro-Wilk test, which yielded a W statistic of 0.9174 and a p-value of 0.1012. This result indicates that the residuals are approximately normally distributed, as the p-value is greater than 0.05.

The Durbin-Watson test (DW) was used to check for autocorrelation among the residuals. The DW statistic was 1.7933 with a p-value of 0.356. Since the DW statistics are close to 2, there is little to no autocorrelation in the residuals.

Homoscedasticity was evaluated using the Breusch-Pagan test (BP), which resulted in a BP value of 1.5725 and a p-value of 0.4556. This indicates that the variance of the residuals is constant across levels of the independent variables, as the p-value is well above 0.05.

The multiple linear regression analysis for the Coatzacoalcos region produced the following model for particulate organic carbon fluxes (Equation 3):

$$CorgFluxC = -0.3157SST - 269.7562 * Chl_a + 13.4977 * (SST * Chl_a) \quad (3)$$

The R^2 for this model is 0.8836, and the p-value <0.05, showed a strong statistical significance. To assess multicollinearity, we calculated the Pearson correlation coefficient between SST with 30-day lag and Chl_a, which was 0.0375, suggesting a very weak positive correlation between the independent variables.

The normality of the residuals (W) is 0.9709, with a p-value of 0.7742. This indicates that the residuals are normally distributed, as the p-value is greater than 0.05. The DW test is 2.1839 with a p-value of 1, suggesting there is no autocorrelation in the residuals. Homoscedasticity was evaluated with the BP test, resulting in 6.2509 and a p-value of 0.0439, indicating a slight presence of heteroscedasticity, as the p-value is just below the 0.05 threshold.

The models for both regions demonstrated a strong relationship between particulate organic carbon fluxes and the independent variables (SST and Chl_a). The coefficients for SST and Chl_a in both regions indicate their respective impacts on particulate organic carbon fluxes. Notably, the interaction term is positive and significant in both models, suggesting that the combined effect of SST and Chl_a are important in predicting organic carbon fluxes.

These results indicate that SST and Chl_a significantly influence particulate organic carbon fluxes in our study areas, though their effects vary between regions. The high R^2 values for both models confirm that SST and Chl_a are key controlling variables, accounting for much of the observed variability.

In the Perdido region, the negative correlation between SST and Chl_a suggests an inverse relationship, where lower SSTs coincide with higher chlorophyll concentrations. This pattern likely reflects enhanced primary productivity in cooler waters, most likely with a deeper mixed layer and input nutrients to the photic zone, where phytoplankton growth is favored, leading to increased organic carbon production and export to deeper waters.

While in Coatzacoalcos, the correlation between SST and Chl_a is weaker, suggesting a more complex interaction. Here, each variable appears to influence carbon fluxes independently rather than through a direct inverse relationship. This may indicate that additional factors, such as mesoscale eddies' dynamic forcing and their interactions with nutrient-rich shelf waters and offshore transport processes, increase nutrient availability in the deeper GoM waters and play a more prominent role in regulating biological productivity and carbon export.

The contrast between these regions highlights the influence of local oceanographic conditions on carbon flux dynamics. While SST and Chl_a are consistently important, their specific interactions with organic carbon fluxes appear to be region-dependent. The Perdido region shows higher amplitude seasonal SST, and deeper mixed layer depth cycles where the interaction with mesoscale eddies plays a lesser role, in contrast to the Coatzacoalcos region where a dampened seasonal SST cycle allows for an increased importance of mesoscale and offshore transport processes, pointing to the need for further investigation into other underlying processes shaping these patterns.

In conclusion, this chapter highlights the temporal variability of organic carbon fluxes in the Perdido and Coatzacoalcos regions, marked by significant pulses during two distinct periods. The analysis suggests that both regions experience organic carbon flux influenced by mesoscale eddies, temperature changes, and possibly continental sources.

Chapter 4. Spatial and temporal variability of the accumulation of organic carbon in the sediments

4.1 Introduction

The accumulation of organic carbon in marine sediments plays a crucial role in the global carbon cycle, acting as a long-term sink for atmospheric carbon dioxide and influencing the overall health of marine ecosystems (Hedges & Keil, 1995). In the Gulf of Mexico, the spatial and temporal variation in organic carbon accumulation is influenced by a complex interplay of biological, carbon primary productivity, water column dynamics, export productivity, utilization during the water column transfer, sedimentation rates, and hydrodynamic conditions (Müller-Karger et al., 2015). Quantifying the accumulation of organic carbon in deep-sea sediments is key to understanding its role as a sink of the global carbon cycle and its potential change in magnitude and direction due to global climate warming and anthropogenic activities. Marine sediments are an important reservoir of carbon regulating climate change by effectively sequestering organic carbon on millennial to million years' time scales (Berner, 2003; Burdige, 2007). Recent studies emphasize the need to quantify carbon sinks and understand the influence of natural and emerging anthropogenic processes across different time scales (Middelburg, 2018).

Spatially, the distribution of organic carbon in sediments is highly heterogeneous in the GoM, with higher concentrations typically found in areas of high primary productivity and low-energy environments where fine particles can settle (Bianchi et al., 2002). Regions near river mouths and coastal areas usually exhibit a high accumulation of organic carbon due to terrestrial inputs and greater availability of nutrients (Goñi et al., 2003).

Seasonal to interannual variability SSTs, light availability, and nutrient fluxes control primary productivity patterns, and, consequently, the export of organic matter to depth until the organic matter reaches the sea floor (Lohrenz et al., 1999). Episodic events such as storms, hurricanes, and mesoscale eddies can further influence the deposition and resuspension of organic carbon in sediments (Allison et al., 2012).

In the abyssal region of the Gulf of Mexico, these processes are compounded by the complex interplay of deep-water currents and topographical features, which can create localized areas of enhanced or reduced sediment accumulation (Ward, 2017). Understanding the patterns and drivers of organic carbon

accumulation in this region is essential for predicting how these deep-sea environments respond to natural and anthropogenic changes. The objective of this chapter is to characterize the organic carbon accumulation in the deep-sea sediment in the GoM.

4.2 Materials and methods

4.2.1 Sampling

The sediment samples in Figure 19 were collected using a Soutar-type box core and a multicore, each of the cores having an average length of 35 cm. These corers penetrate the sediments by gravity, aided by weights positioned at both sides of the box corer, or on the structural top of the multicorer. As the winch on the ship pulls up these corers, a blade closes the box corer from beneath, and the upper lid closes at the same time to ensure it does not leak out during ascent to the surface, in the multicorer; a top and bottom lids close each of the cylindrical acrylic tubes during the retrieval. In both cases, the penetration into the sediments and the subsequent closure mechanisms are designed to ensure an optimal preservation of the sediment-water interface.

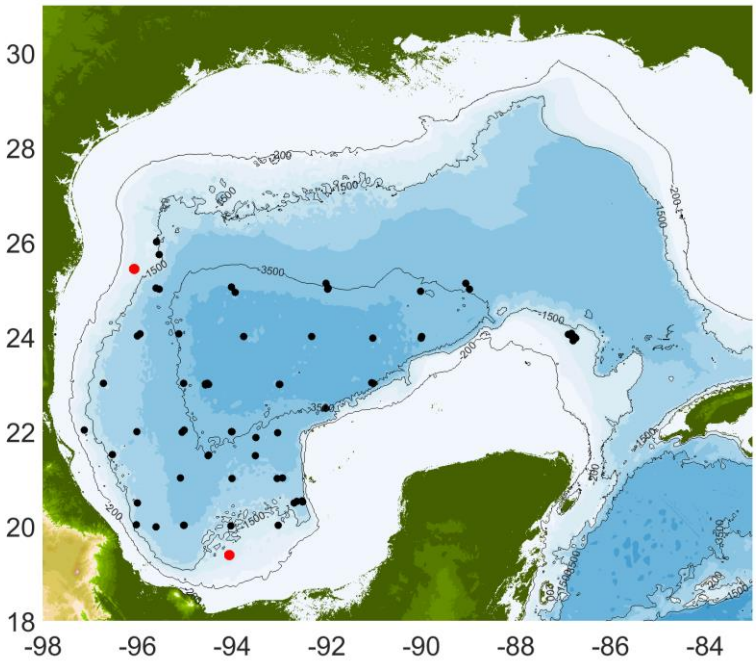

Figure 19. Map showing sediment sample stations collected during XIXIMI's cruises in black dots, with sediment trap locations indicated by red dots.

4.2.2 Sampling, processing, and chemical analysis

During the seven XIXIMI cruises from 2010 until 2019, we were able to collect a total of 66 sediment cores from 41 stations. All these stations are represented in Figure 19, where the red-filled dots mark the location of the sediment traps of the Perdido region in the northwestern GoM and Coatzacoalcos to the south.

On board the ship, sediment cores were sectioned at intervals of 1 cm intervals for the upper 5 to 6 cm and the rest of the core usually was sampled at 2 cm resolution. The samples were stored and frozen during the cruise and were kept frozen until they arrived in the refrigerated facilities at CICESE. Once in the lab, these samples were weighed, freeze-dried, and weighed again to derive the water content and the dry weight. The sediment slices were then subsampled, manually grounded into fine powder in Agatha mortar, and from the ~150 mg, an aliquot was encapsulated for subsequent elemental analysis of organic carbon and nitrogen and the stable isotopic determinations of carbon and nitrogen in an elemental analyzer coupled to a continuous flow mass spectrometer.

For the determinations of organic carbon concentrations and their isotopic signatures, aliquots were first treated with a 1N HCl solution to dissolve calcium carbonate ($CaCO_3$). Deionized water was used to rinse the residue, followed by centrifugation to eliminate the supernatant. The remaining sediments were dried in an oven at 25°C and then encapsulated in tin capsules for further analysis in the Stable Isotope Laboratory at CICESE.

4.2.2.1 Measurement of organic carbon and its isotopic composition

Organic carbon concentrations, along with their isotopic compositions ($\delta^{13}C$), were determined on a Costech® CHN analyzer coupled to a Thermo Scientific DeltaV plus Advantage® isotope ratio mass spectrometer at the Stable Isotope Laboratory at CICESE. Organic carbon concentrations are reported as µg and isotope ratios were expressed in standard δ-notation relative to Pee Dee Belemnite (v PDB) for the $\delta^{13}C$ via laboratory standards calibrated to international certified reference standards, USGS40, and Sucrose. The average precision from certified values over the period of the analysis was ±0.06‰ for $\delta^{13}C$. The organic carbon concentrations were corrected for the carbonate removal to report the organic carbon as a percent of total sediment.

4.2.2.2 Sediment dating (AMS ^{14}C)

To calculate the sedimentation rates, we used planktic foraminifera for AMS ^{14}C dating purposes. Approximately 1500 specimens were picked from selected levels at the Paleoceanography Lab in CICESE, yielding 1-2 mg of carbon suitable for dating. For cores obtained during XIXIMI cruises 1, 2, and 3, AMS ^{14}C dating was conducted at the University of Arizona AMS Laboratory. Cores from XIXIMI cruises 4, 5, 6, and 7 were dated at the Keck Carbon Cycle AMS Facility at the University of California, Irvine (Díaz-Asencio et al., 2019).

4.2.3 Data analysis

The accumulation of organic carbon is derived from sedimentation rates (Sm), the physical parameters of the sediments, and the relative concentration of organic carbon in the sediments (Calvert, 1987).

The organic carbon accumulation rates (OCAR) in the sediments are derived from the product of organic carbon percentage with the mass accumulation rates for a quantitative understanding of organic carbon accumulation in the sediment and indirectly on the utilization of organic carbon by the benthos on the sea floor at different times and space scales. The mass accumulation rates are multiplied by organic carbon concentration to obtain the organic carbon accumulation in the sediment.

We used the following equation to derive the carbon accumulation rates:

$$OCAR_{Sed} = MAR_{Sed} \times OC_{Sed} \quad (1)$$

Where $OCAR_{Sed}$ is the organic carbon accumulation rate of sediments (g $m^{-2}yr^{-1}$), MAR_{Sed} is the mass accumulation rate (g $m^{-2}yr^{-1}$) of deep-sea sediment fluxes. The MAR_{Sed} is calculated from the dry bulk density (DBD_{Sed}) and the mean sedimentation rates (MSR_{Sed}) (Equation 5):

$$MAR_{Sed} = DBD_{Sed} \times MSR_{Sed} \quad (2)$$

Where the units of the DBD_{Sed} are calculated as the dry mass of each sediment subsample divided by its bulk volume in the sampling cylinder, expressed in grams per cubic centimeter. The MSR_{Sed} units are in cm kyr^{-1}. To estimate it, the sediment age is determined by the slope derived from the relationship between

^{14}C and the sediment depth. The OC_{Sed} is the organic carbon concentration in sediments (%) and is determined with the methodology previously explained.

4.3 Results

4.3.1 Spatial distribution maps

The dry bulk density was calculated as the dry mass of each sediment subsample divided by its bulk volume in the sampling cylinder, expressed in grams per cubic centimeter (Brooks et al., 2015). DBD data from Díaz-Asencio et al. (2020 and 2023) are used in this study, to which we have added a few more cores (

Table 10).

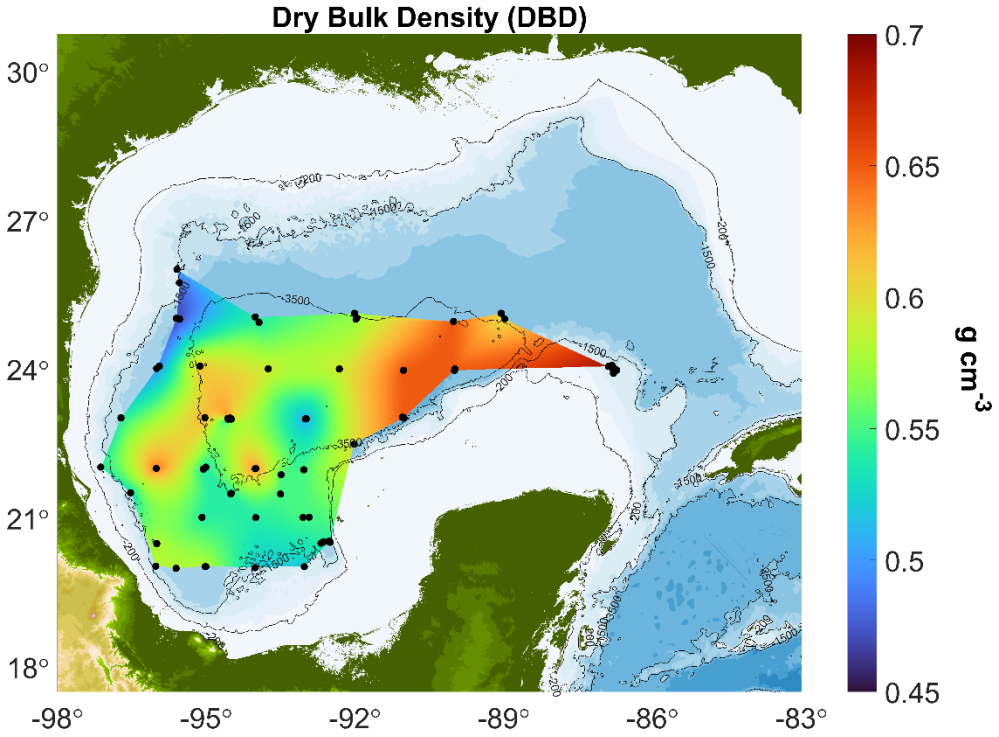

Figure 20. Mean dry bulk density from the abyssal region, black dots represent the sediment stations.

The black dots in Figure 20 represent the sediment stations and show the distribution of DBD in the abyssal region. Warm colors indicate areas with the highest DBD, whereas stations near the continental slopes exhibit the lowest DBD values.

Table 10. Sediment core's locations, characteristics, and organic carbon accumulation rates.

Core id.	Long.	Lat.	Bott. Depth	DBD	Depth	OC		Sm		MAR		OCAR	
(cruise-St)	(east)	(north)	(m)	(g cm^{-3})	(cm)	(%)		(cm kyr^{-1})		(g $m^{-2}yr^{-1}$)		(g $m^{-2}yr^{-1}$)	
						Ave.	u	Ave.	u	Ave.	u	Ave.	u
XI5-A3	-94.013	25.050	3685	0.54	0-1	0.647	0.001	5.5	0.1	31	0.1	0.201	0.006
XI5-A5	-92.010	25.124	3513	0.57	0-1	0.454	0.000	6.9	0.1	41	0.1	0.186	0.005
XI5-A8	-89.053	25.124	3477	0.6	0-1	0.673	0.001	7.1	0.3	41	0.2	0.276	0.013
XI3-A8a	-88.983	25.010	3488	0.6	0-1	0.862	0.001	7.5	0.7	46	0.4	0.396	0.034
XI6-B12	-95.123	24.060	3508	0.61	0-1	0.539	0.001	7.5	0.7	48	0.2	0.259	0.011
XI2-B13	-93.749	24.006	3739	0.59	0-1	0.753	0.001	5.8	0.8	36	0.5	0.271	0.038
XI4-B14	-92.317	24.004	3734	0.59	0-1	0.556	0.001	8.8	0.5	52	0.6	0.289	0.033
XI1-B16	-89.986	24.006	3727	0.65	0-1	0.631	0.001	6	0.7	40	0.4	0.252	0.025
XI5-C22	-94.557	22.988	3717	0.53	0-1	0.433	0.000	6.6	1.6	42	0.9	0.182	0.039
XI6-C22	-94.519	23.015	3727	0.65	0-1	0.478	0.000	6.5	0.2	44	0.2	0.211	0.010
XI7-C22	-94.495	22.993	3729	0.58	0-1	0.600	0.001	7.2	2.1	45	0.4	0.270	0.024
XI1-C22a	-95.028	23.021	3547	0.62	0-1	0.599	0.001	5	0.3	32	0.2	0.192	0.012
XI3-C23	-92.985	22.998	3741	0.51	0-1	0.607	0.001	6.5	1.8	35	1	0.212	0.061
XI7-C23	-93.003	22.998	3739	0.51	0-1	0.661	0.001	8.6	0.7	45	0.2	0.298	0.013
XI3-C24	-92.018	22.489	3551	0.6	0-1	0.954	0.001	5.4	0.4	34	0.3	0.324	0.029
XI1-C25	-91.015	23.018	3801	0.65	0-1	0.727	0.001	7.3	0.8	49	0.5	0.356	0.036
XI5-D28	-95.060	21.984	3721	0.54	0-1	0.756	0.001	6.8	0.6	38	0.4	0.287	0.030
XI3-D29	-94.004	21.997	3559	0.63	0-1	0.888	0.001	5.7	2.3	38	1.5	0.338	0.133
XI7-D29	-94.012	21.992	3564	0.63	0-1	0.705	0.001	6.5	2.7	43	1.8	0.303	0.127
XI3-D30a	-93.491	21.872	2960	0.55	0-1	0.770	0.001	6.7	0.1	38	0.1	0.293	0.008
XI1-D30	-93.033	21.972	3546	0.55	0-1	0.936	0.001	7.2	0.2	41	0.1	0.384	0.009
XI6-E33	-94.509	21.484	3431	0.54	0-1	0.787	0.001	8.8	0.1	55	0.4	0.433	0.031
XI7-E33	-94.498	21.497	3435	0.54	0-1	0.833	0.001	11	0.1	62	0.4	0.517	0.033

Table 11. Continued

Core id.	Long.	Lat.	Bott. Depth	DBD	Depth	OC		Sm		MAR		OCAR	
(cruise-St)	(east)	(north)	(m)	(g cm^{-3})	(cm)	(%)		(cm kyr^{-1})		(g $m^{-2}yr^{-1}$)		(g $m^{-2}yr^{-1}$)	
						Ave.	u	Ave.	u	Ave.	u	Ave.	u
XI5-TS1	-95.541	25.741	1355	0.48	0-1	0.675	0.001	6.8	0.3	34	0.1	0.230	0.007
XI7-TS1a	-95.591	26.010	2417	0.5	0-1	1.030	0.001	12.8	4.1	66	1.7	0.680	0.175
XI7-B11	-96.001	24.014	2400	0.5	0-1	1.065	0.001	11.1	0.6	61	0.1	0.649	0.011
XI1-B18	-86.752	23.999	1234	0.69	0-1	0.881	0.001	4.2	0.5	29	0.4	0.256	0.035
XI5-B18	-86.727	23.977	1242	0.69	0-1	0.717	0.001	4.5	0.1	32	0.1	0.229	0.007
XI6-B18	-86.892	24.054	1150	0.69	0-1	0.795	0.001	4.2	0.5	29	0.5	0.231	0.040
XI7-B18	-86.806	24.004	1182	0.7	0-1	0.897	0.001	3.8	0.7	29	0.4	0.260	0.036
XI2-C20	-96.720	23.019	1782	0.54	0-1	0.779	0.001	8.1	0.7	46	0.4	0.358	0.031
XI4-E31	-96.527	21.508	1549	0.53	0-1	0.777	0.001	10.4	0.2	49	0.3	0.381	0.023
XI7-F38	-94.003	21.008	2822	0.54	0-1	1.124	0.001	12.1	1.2	70	1	0.787	0.112
XI1-F39	-92.927	21.017	2873	0.55	0-1	0.889	0.001	10.3	0.1	58	0.1	0.516	0.009
XI4-G40	-95.998	20.485	1930	0.58	0-1	0.768	0.001	9.8	1.1	57	1	0.438	0.077
XI3-H44	-96.018	20.029	1739	0.58	0-1	0.865	0.001	7.2	1.5	4	0.9	0.381	0.078
XI1-H46	-95.010	20.022	2784	0.58	0-1	0.910	0.001	10.3	0.8	62	0.5	0.564	0.046
XI1-A1	-95.603	25.023	2130	0.47	0-1	1.193	0.001	18.1	1.8	87	0.9	1.038	0.107
XI6-D26	-97.127	22.025	966	0.54	0-1	0.783	0.001	22.8	1.4	126	0.8	0.987	0.063
XI6-D27	-96.006	22.000	2722	0.64	0-1	0.679	0.001	17	4	110	4.3	0.747	0.292
XI4-E34	-93.503	21.484	3146	0.55	0-1	1.195	0.001	23.6	3.7	131	3	1.566	0.359
XI1-G44	-92.689	20.492	2240	0.54	0-1	1.374	0.001	14.3	1.6	79	0.7	1.085	0.096
XI1-A5	-91.981	25.007	3480	0.57	0-1	0.731	0.001	6.4	0.9	38	0.5	0.277	0.039
XI2-C22a	-94.552	23.000	3711	0.62	0-1	0.585	0.001	5	0.3	32	0.2	0.190	0.011
XI2-D28	-95.008	22.024	3383	0.54	0-1	0.664	0.001	7.7	3.8	43	2.1	0.286	0.141
XI2-A3	-93.937	24.943	3684	0.54	0-1	1.012	0.001	5.5	0.1	31	0.1	0.314	0.006

Table 12. Continued

Core id.	Long.	Lat.	Bott. Depth	DBD	Depth	OC		Sm		MAR		OCAR	
(cruise-St)	(east)	(north)	(m)	(g cm^{-3})	(cm)	(%)		(cm kyr^{-1})		(g $m^{-2}yr^{-1}$)		(g $m^{-2}yr^{-1}$)	
						Ave.	u	Ave.	u	Ave.	u	Ave.	u
XI4-C22	-94.564	23.008	3721	0.59	0-1	0.954	0.001	6.76	1.3	41	0.8	0.394	0.076
XI4-G44	-92.631	20.525	2470	0.54	0-1	1.275	0.001	14.3	1.6	79	0.9	1.008	0.113
XI4-H47	-94.018	20.000	1342	0.52	0-1	0.965	0.001	25	3.5	132	1.9	1.277	0.179
XI4-H45	-95.609	19.987	2159	0.58	0-1	0.911	0.001	19.9	10.3	118	6.1	1.071	0.554
XI4-A1	-95.539	25.009	2429	0.47	0-1	1.055	0.001	18.1	1.8	87	0.9	0.917	0.091
XI4-A5	-92.010	25.124	3528	0.57	0-1	0.684	0.001	6.9	0.1	41	0.1	0.279	0.004
XI5-B11	-95.946	24.058	2298	0.5	0-1	0.751	0.001	11.1	0.6	57	0.3	0.429	0.023
XI5-G44	-92.517	20.536	2353	0.54	0-1	1.197	0.001	17.3	1.6	95	0.9	1.141	0.106
XI6-G44	-92.503	20.512	2384	0.54	0-1	1.266	0.001	16.1	1.6	89	0.9	1.125	0.112
XI6-H48	-93.023	20.020	1201	0.52	0-1	1.344	0.001	21.4	3.5	113	1.9	1.523	0.249

The MAR, derived from the DBD and MSR, many of them reported by Diaz-Asencio et al. (2020 and 2023) and complemented by additional data in this study are depicted in Figure 21 and Table 10. Generally, mean MARs are relatively low in the central abyssal plain. However, anomalously high values are observed in three regions, predominantly to the north of the Yucatan platform and the Campeche escarpment; in the southeastern region on the Campeche Knolls slope characteristic of its rough and irregular topography; and at the exit of an intricate mesh of submarine canyons. The abrupt topographic features on the Campeche Knolls are mostly controlled by the emerging diapiric structures on that slope generating abrupt topographies and relatively small and intricate canyons that control the highly variable sedimentation rates observed.

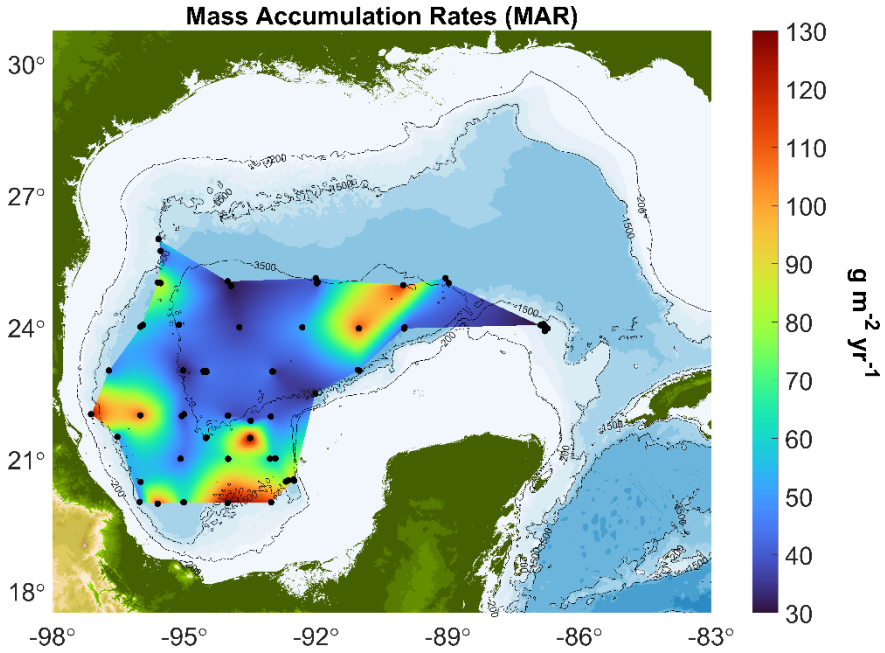

Figure 21. Mass accumulation rates in the abyssal region of the GoM, black dots represent the locations of the sediment stations where average values were calculated.

In Figure 22, we present the relative content of organic carbon in surface sediments. The data indicates elevated concentrations in stations located near the exit of large submarine canyons on the western continental slopes, and in the southern region on the foot of the Campeche Knolls and close to the Campeche Canyon.

The OCAR in sediments, derived from the organic carbon percentage and mass accumulation rates, shows the organic carbon accumulation patterns on the surface sediments of the slopes and abyssal plain environments in the GoM.

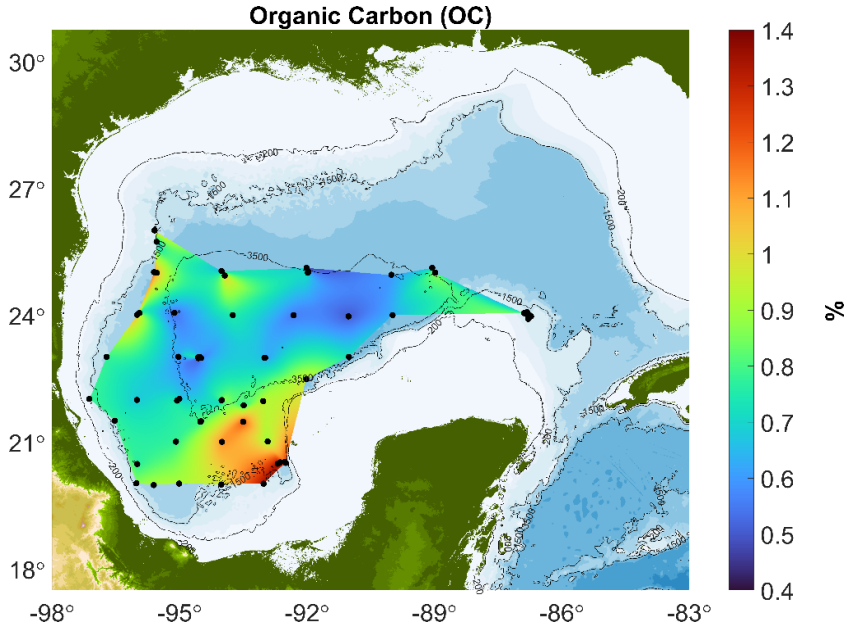

Figure 22. Patterns of organic carbon relative content in surface sediment of the GoM. Black dots indicate sediment stations.

The results represented in Figure 23, show the highest values to the south in the Campeche Knolls escarpment, with rates as high as 1.3 g $m^{-2}yr^{-1}$, and at the exit of the large canyon systems in the western slopes with values between 1 and 0.8 3 g $m^{-2}yr^{-1}$, while the rest of the GoM exhibits values below 1 g $m^{-2}yr^{-1}$.

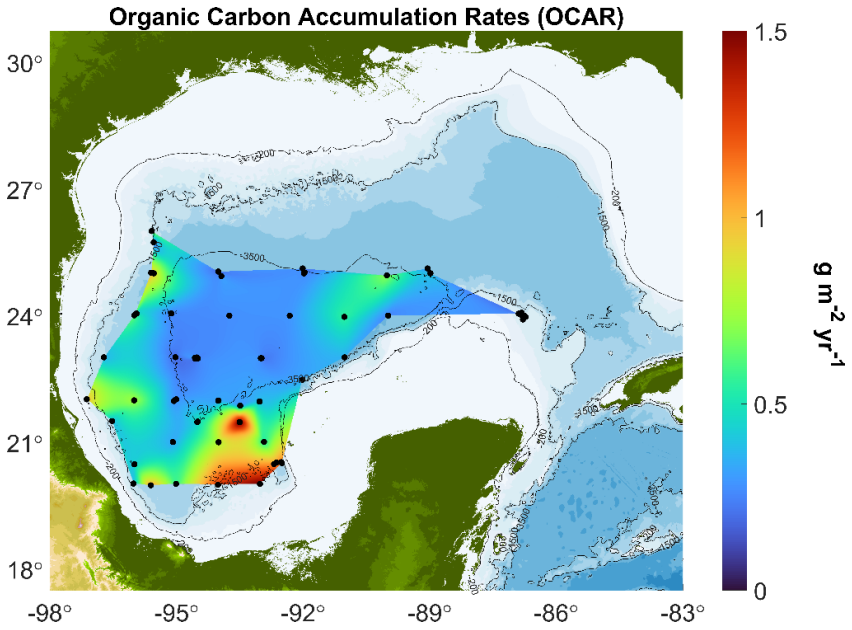

Figure 23. Organic carbon accumulation rates in the deep-sea sediment of the GoM.

4.3.1.1 Quantifying organic carbon storage in abyssal sediments

The profiles of relative organic carbon content consistently showed decreasing concentrations with depth, particularly in the first 2-7 cm of the sediment's column. This behavior implies the consumption of organic carbon by the benthic organisms in the upper core tops. For this analysis, we disregard bacterial consumption in the deeper sediment layers. By analyzing these sediment profiles, we can estimate the amount of organic carbon utilized in the uppermost sediment layer and distinguish it from the carbon preserved or buried in the geological record (Figure 24).

To characterize carbon storage in the deep-sea sediments of the GoM, we chose the depth at which the OCAR profile reaches constant values. To achieve this more precisely, we employed the first derivative (Equation 6) to characterize the most labile and reactive organic carbon (y) with respect to depth (x) in the upper cm of each core.

$$y' = \frac{dy}{dx} = \frac{\Delta OCAR}{\Delta Depth} = \frac{OCAR_{n+1} - OCAR_n}{Depth_{n+1} - Depth_n} \quad (6)$$

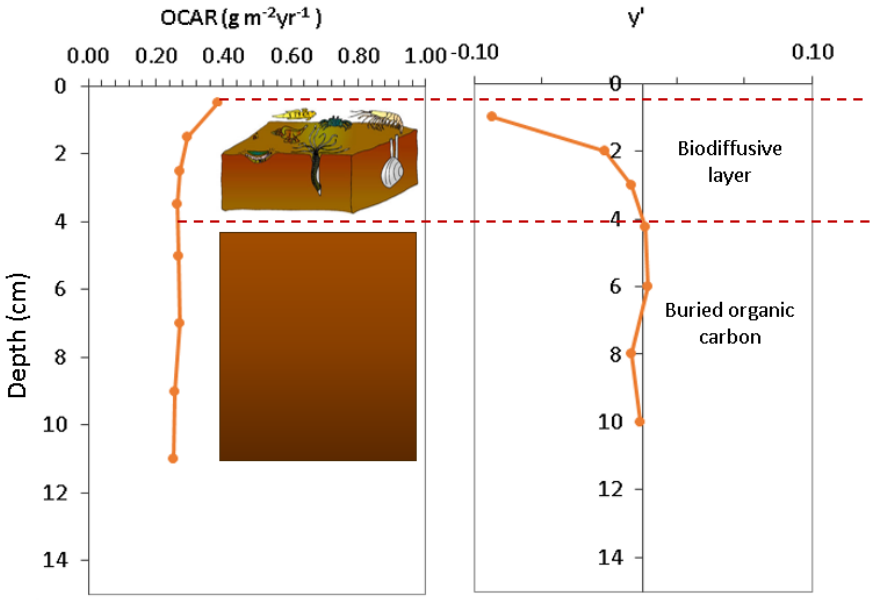

Figure 24. Conceptual model of the buried organic carbon and the biodiffusive layer in the sediments.

As illustrated in Figure 25, the shallowest depths of stabilization were typically observed in sediments on the southern abyssal plain and the deepest on the continental slopes. The accompanying histogram reveals that the most frequent depths were 3.5 cm, followed by 4.5 cm (Figure 26).

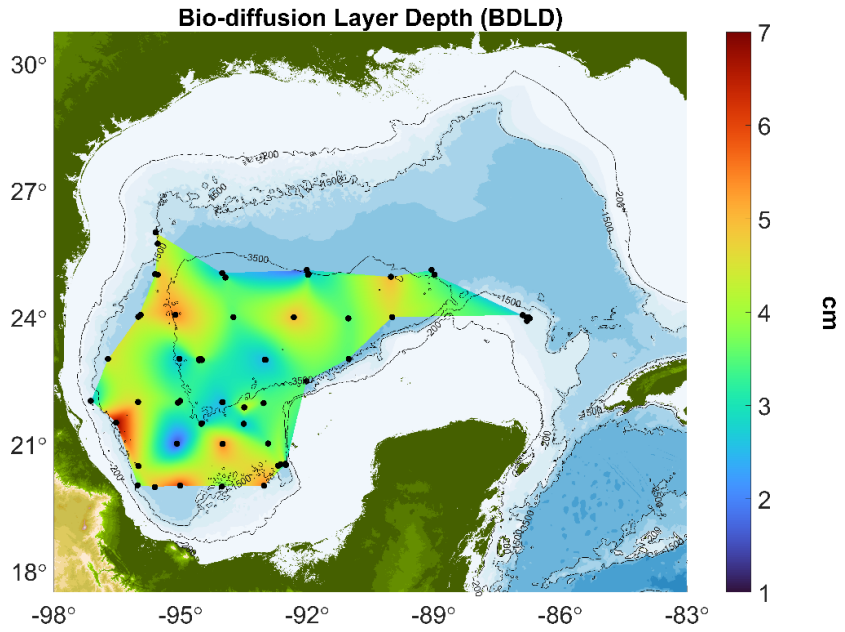

Figure 25. Sediment mixed layer depth in cm or biodiffusion layer in the deep-sea sediments of the GoM.

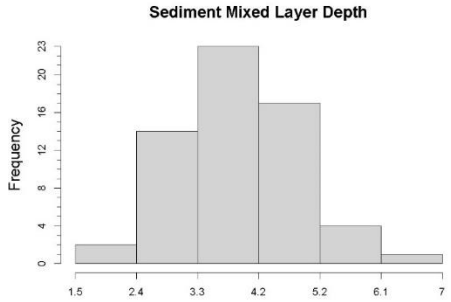

Figure 26. Histogram of the mixed layer depth or sediment biodifussive layer depths from the GoM.

The mixing layer depth reported by Díaz-Asencio et al., (2019) ranges from 2.4 to 24.3 cm, with an average of 13.0 cm in the abyssal region. These values are comparable to those observed in the equatorial Pacific but higher than in other abyssal regions.

Mixing is shallower on the continental slope. Bioturbation and deep circulation influence the mixing layer, while high turbulence decreases net sedimentation from the surface to the deep-sea sediments.

In comparison, the results from this study show similar spatial patterns but differ in magnitude in

comparison with the results from Díaz-Asencio et al., (2019). Mixing is most active in the central region and western margin in both works.

However, Díaz-Asencio et al., (2019) reported a significantly deeper mixing layer, with distinct maxima in the west, while this work shows a shallower, more gradual depth transition, suggesting a more homogeneous biodiffusion process. This may indicate that diffusion accounts for only a fraction of the total mixing.

These differences are likely due to varying controlling factors. While bioturbation plays a significant role in both layers, it has a stronger influence on this work, as it directly depends on benthic activity. In contrast, the findings of Díaz-Asencio et al., (2019) are also influenced by physical processes such as deep currents and resuspension events, explaining the greater depth and spatial heterogeneity.

Figure 27 displays the OCAR at the depths where the sediment core profile showed constant values with depth. The pattern observed in the OCAR of surface sediments in Figure 23 is very similar to that in Figure 27, where the OCAR values represent carbon effectively sequestered in the sediments. The highest values cluster around the exit of large canyons to the abyssal plain, and in the southern part, the Campeche Knolls complex and Campeche Canyon to the east.

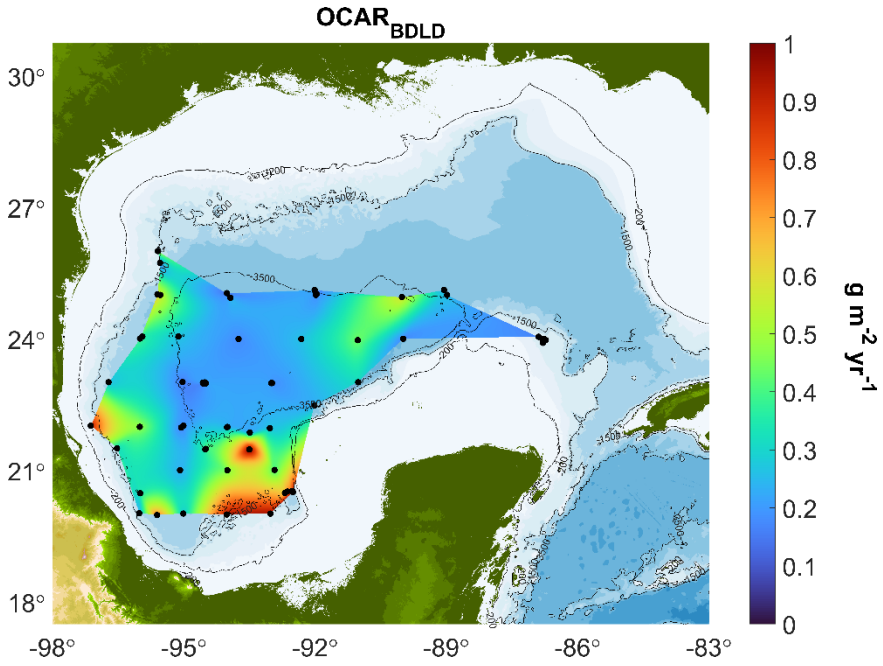

Figure 27. Organic carbon accumulation rates below the biodiffusion layer in sediments of the GoM.

4.4 Discussion

4.4.1 Comparative analysis of organic matter between surface deep-sea Sediments and the water column

The deployment over a year period of two sediment traps on the western and southern slopes of the GoM allows for a comparison between the water column and deep-sea sediment fluxes of organic carbon in these two regions. This comparative approach seeks to detect recent changes from the past few centuries in organic carbon flux variability as recorded in the sediment trap and the sediment core tops.

4.4.2 Organic carbon storage in deep-sea sediments in the GoM

Organic carbon consumption can be attributed to various processes (Figure 24), including use, bioturbation, and remineralization reactions driven mainly by the microbiota living in the sediments. Abyssal benthic communities in the GM rely on the export of biogenic carbon and inhabit soft sediment on the deep-sea floor characterized by sediments with a high biogenic component, composed of coccoliths and mostly planktic foraminifera with a minor addition by benthic foraminifera. The main macrofaunal components of these benthic epi and infaunal communities are polychaetes and pericaridean crustaceans; and the primary meiofaunal components are nematodes, harpacticoid copepods and benthic foraminifera(Escobar-Briones et al., 1999; Lalli & Parsons, 2006; Talley, 2011; Ward, 2017).

Megafauna is scarce and more widely dispersed than smaller organisms. There is significant variability at depths greater than 3,000 meters, suggesting that organisms inhabiting soft abyssal floors are patchily distributed(Escobar-Briones et al., 1999).

Organic carbon consumption was determined by subtracting the OCAR at the surface from the OCAR at the biodiffusion layer, as illustrated in Figure 28. The analysis showed a clear association between consumption rates and OCAR values, with higher consumption observed in Campeche knolls and in the canyon, with a relation with some canyons existing in the north, too; these regions exhibit elevated OCAR values. In contrast, OC consumption in the abyssal region was found to be extremely low.

These estimates could be further used as a low-limit predictor of the benthic biomass living in the upper few cm of the sediments, showing a higher standing stock in the southern region, Campeche Knolls, Campeche Canyon, and the exit of some large canyons in the northwest region.

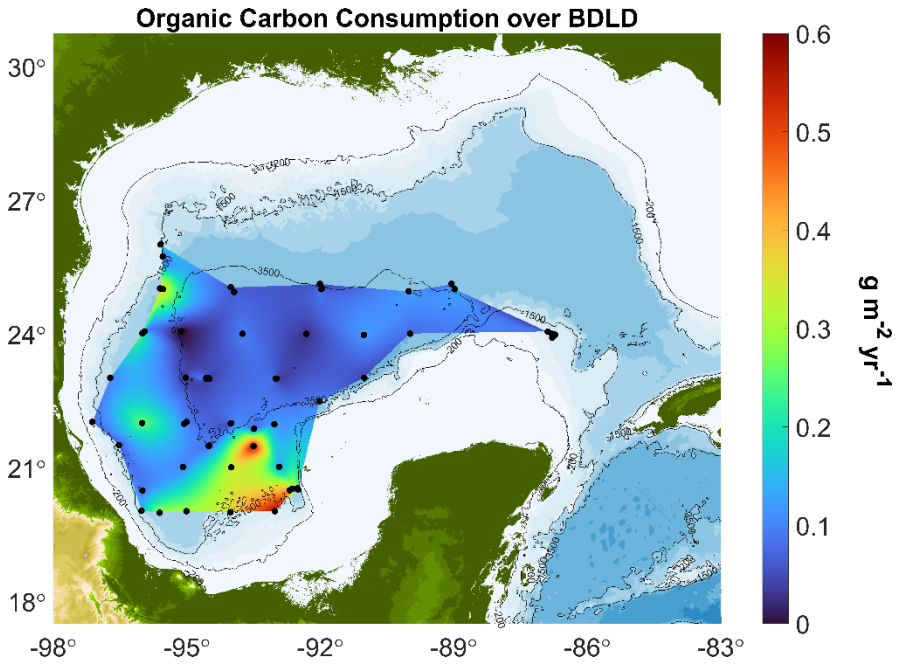

Figure 28. Organic carbon consumption within the biodiffusive layer of GoM sediments.

We further estimate the organic carbon storage in the deep-sea sediments of the total area of the GoM. The total area of the GoM is close to $16.2X10^{11}$ m^2, and the polygon enclosing all the stations where the sediment cores were retrieved has an extension of $3.43X10^{11}m^2$. This polygon represents about 21% of the total area of the GoM. This approach allowed for a first-order assessment of organic carbon distribution within this geographical area.

The product of the surface average OCAR (0.494 g m^{-2} yr^{-1}) and the polygon area give us an estimation of the total flux of organic carbon arriving at the surface sediments in this area of 0.1695 Pg C yr^{-1} and carbon storage of 0.122 Pg C yr^{-1}, considering the OCAR average from the diffusive layer of 0.356 g m^{-2} yr^{-1}. However, these calculations using the mean values may be an overestimate.

A better representation would be the median of the OCAR values (Figure 29), obtaining an OCAR of 0.115 Pg C yr^{-1} in the surface and 0.088 Pg C yr^{-1} below the diffusive layer, an estimate that may be close to the organic carbon sequestered in the polygon of our study.

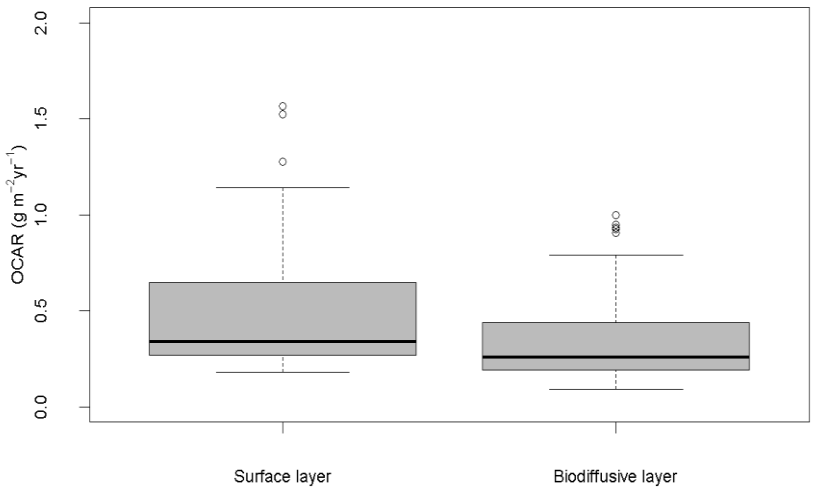

Figure 29. Organic carbon accumulation rates in surface sediments on the left and the biodiffusive layer on the right, shown through box plot analysis.

Extrapolating the median value to the entire GoM, the organic carbon arriving at the slope and abyssal at the sediment would be 0.545 Pg C yr^{-1}, and the storage of organic carbon in the biodiffusive layer would be 0.417 Pg C yr^{-1}.

For comparison, Mexico's annual carbon emissions averaged 0.646 Pg C yr^{-1} between 2000 and 2019 and increased to 0.763 Pg C yr^{-1} by 2023 (Lara & Li, 2024). Our results show that the organic carbon stored in the sediments of the GoM represents approximately one-sixth of Mexico's current annual carbon emissions.

This comparison emphasizes the critical need for mitigation strategies, improving their integration into broader carbon budgets and climate policies to address increasing greenhouse gas emissions in Mexico, and highlights the role of marine sediments as significant, though insufficient, carbon sinks relative to human-induced emissions.

To further explore this, we compare the OCAR in surface sediments with the organic carbon fluxes in the sediment traps, focusing on the stations nearest to the traps. In the Coatzacoalcos region (southern GoM), select stations H46, H47, and H48, as depicted on the Figure 30.

In the Perdido region (Figure 31), we compare OCAR between stations A1 and TS1 from two different research cruises and the sediment trap fluxes.

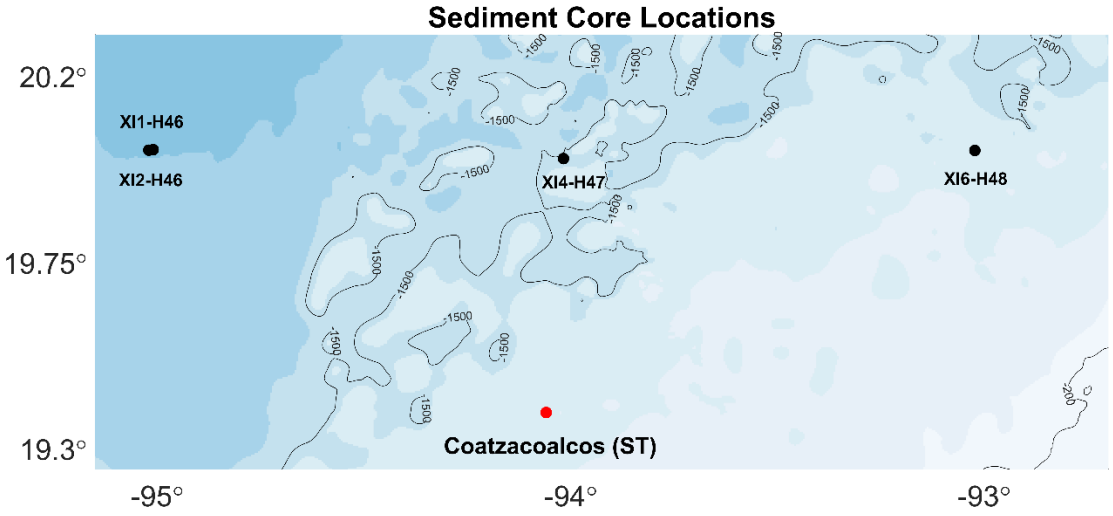

Figure 30. Coatzacoalcos sediment trap location is indicated by the red dot, along with the nearest sediment core station in black dots.

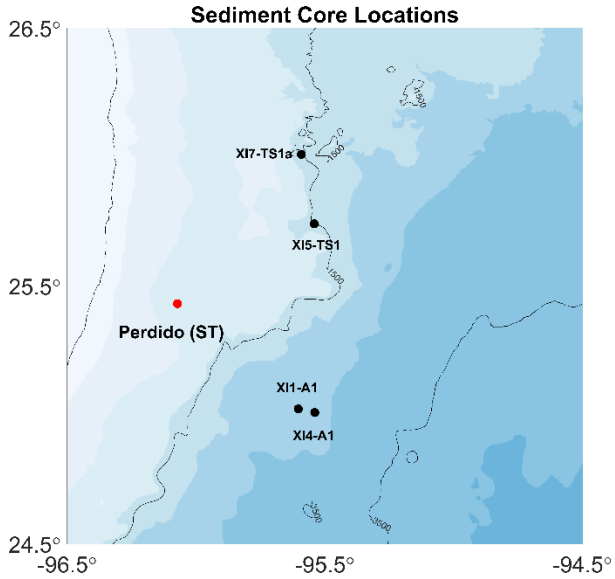

Figure 31. The Perdido region sediment trap location is indicated by the red dot, along with the nearest sediment core station in black dots.

Fluxes of OCAR in the Coatzacoalcos sediment trap are higher by a factor of 2 to 3 than the estimated OCAR in the sediments, with the lowest value recorded at station H46, likely due to its greater depth. In the Perdido region, the fluxes of OCAR in the trap are higher by a factor of 2 to 3 than the ones estimated in the sediments. The variance in the OCAR values in the traps surpasses those in the sediments. The variance in OCAR at station TS1 between cruises XI 5 and XI 7 could be attributed to depth variations.

The accumulation of organic carbon in the deep-sea sediments of the GoM is a dynamic and complex process influenced by multiple spatial, geological, and temporal factors.

Table 13. Organic carbon accumulation rates comparison between sediments and sediment traps.

Location	OCAR (g $m^{-2}yr^{-1}$)	Depth (m)
Coatzacoalcos (ST)	**3.878**	**1045**
XI1 H46	0.569	2784
XI4 H47	1.277	1342
XI6 H48	1.523	1201
Perdido region (ST)	**2.965**	**1075**
XI1 A1	1.038	2391
XI4 A1	0.917	2417
XI5 TS1	0.229	1355
XI7 TS1a	0.679	2417

The results highlight significant spatial variability in the organic carbon accumulation rates, with higher rates observed in regions influenced by specific hydrodynamic conditions and sedimentation processes, such as those near the Campeche Knolls. These findings demonstrated the importance of understanding localized variations in organic carbon accumulation to predict how these deep-sea environments may respond to natural and anthropogenic changes.

Climate change introduces additional complexities by altering physical and biogeochemical processes that regulate organic carbon fluxes. Rising temperatures significantly affect the mixed layer dynamics, enhancing ocean stratification during warmer months. This stratification limits nutrient injections into the surface waters, reducing primary productivity (Dobashi et al., 2022; Velásquez-Aristizábal et al., 2022) and subsequent carbon fluxes and accumulation. In contrast, winter mixing processes, driven mainly by cold fronts (“northers”), may require intensification to overcome stratification, further impacting nutrient mixing, surface productivity, and carbon accumulation dynamics.

Furthermore, the dynamics of eddies released by the Loop Current have also been linked to ocean warming. Studies suggest that the frequency of eddy shedding has decreased since the 1990s, a trend associated with rising temperatures (Müller-Karger et al., 2015; Sturges & Leben, 2000). If the frequency of eddy shedding continues to decrease, fewer eddies will interact with the continental shelf, limiting nutrient transport to deeper waters and subsequently reducing organic carbon fluxes and sequestration.

Under a continued warming scenario, the GoM will lower carbon fluxes and reduce sequestration accumulation, potentially, reaching numbers similar to its deep-water regions from about 0.6 g m^{-2} yr^{-1} to 0.1 g m^{-2} yr^{-1}.

Another potential source of change is the anthropogenic nutrient input from urban centers and industrial activities, especially in the southern GoM, where most of the hydrocarbon industry is concentrated, and with little known data to quantify these inputs onto the shelf and much less on its offshore transport by the interaction of coastal currents and eddies and its enrichment in nutrients especially on the surface waters over the continental slopes bordering these regions.

Chapter 5. Conclusions

The concentrations and distribution of POC in the GoM are primarily regulated by a combination of seasonal changes, riverine inputs, and mesoscale oceanographic processes. Riverine sources such as the Mississippi-Atchafalaya and Grijalva-Usumacinta systems introduce terrestrial organic carbon and nutrients into coastal and shelf waters, while mesoscale eddies, particularly cyclonic and anticyclonic ones, play a crucial role in the open ocean. Cyclonic eddies, with their upwelling effect at its center, bring nutrients closer to the euphotic layer, favoring primary productivity and enhancing POC concentrations. In contrast, anticyclonic eddies promote nutrient-poor conditions at their core due to the sinking of nutrient-poor water masses, which reduces POC levels. Spatial variability in POC concentrations reflects the balance between nutrient availability, organic matter input, and physical mixing processes, underscoring the oligotrophic nature of the deepwater region in the GoM.

The Perdido and Coatzacoalcos regions exhibit marked seasonal pulses in organic carbon fluxes, which are closely linked to regional oceanographic conditions, temperature changes, and exchanges between continental and marine sources. The interaction between mesoscale eddies and the continental shelf, transport circulation promotes the transport of nutrients and chlorophyll-rich waters offshore, enhancing organic carbon fluxes in the open ocean waters of the GoM.

Sediment core analysis throughout the GoM shows considerable spatial variability in organic carbon accumulation rates, particularly in regions such as the Campeche knolls and submarine canyons, where geomorphological features create localized conditions for increased organic carbon burial. Sediment organic carbon uptake varies, with higher rates observed in areas with greater organic carbon flux, suggesting that benthic communities and bioturbation play a role in modulating carbon storage at these depths. Overall, deepwater sediments in the GoM act as an organic carbon reservoir, with distinct differences based on biological primary productivity patterns enhanced by offshore transport of nutrients, sediment composition, benthic activity, and sea bottom morphology.

Studies in these three reservoirs highlight the interconnected nature of organic carbon dynamics in the GoM, where organic carbon distribution, fluxes, and storage are influenced by a combination of mesoscale eddies, riverine inputs, and geomorphological features. This work further emphasizes the need to monitor the interaction between physical, biogeochemical, and climatic processes in this critical region for carbon sequestration and the changes and trends that may modify the relative importance of this large sink of

organic carbon either through a further stratification of its surface waters by upper ocean warming, through changes in the circulation and mesoscale dynamics and by anthropogenic inputs from its urban centers.

Bibliography

Abram, N. J., McGregor, H. V., Tierney, J. E., Evans, M. N., McKay, N. P., & Kaufman, D. S. (2016). Early onset of industrial-era warming across the oceans and continents. *Nature*, *536*(7617), 411–418. https://doi.org/10.1038/nature19082

Allison, M. A., Demas, C. R., Ebersole, B. A., Kleiss, B. A., Little, C. D., Meselhe, E. A., Powell, N. J., Pratt, T. C., & Vosburg, B. M. (2012). A water and sediment budget for the lower Mississippi–Atchafalaya River in flood years 2008–2010: Implications for sediment discharge to the oceans and coastal restoration in Louisiana. *Journal of Hydrology*, *432–433*, 84–97. https://doi.org/10.1016/j.jhydrol.2012.02.020

Antia, A. N., Koeve, W., Fischer, G., Blanz, T., Schulz-Bull, D., Schölten, J., Neuer, S., Kremling, K., Kuss, J., Peinert, R., Hebbeln, D., Bathmann, U., Conte, M., Fehner, U., & Zeitzschel, B. (2001). Basin-wide particulate carbon flux in the Atlantic Ocean: Regional export patterns and potential for atmospheric CO_2 sequestration. *Global Biogeochemical Cycles*, *15*(4), 845–862. https://doi.org/10.1029/2000GB001376

Anwar, M. N., Fayyaz, A., Sohail, N. F., Khokhar, M. F., Baqar, M., Khan, W. D., Rasool, K., Rehan, M., & Nizami, A. S. (2018). CO2 capture and storage: A way forward for a sustainable environment. *Journal of Environmental Management*, *226*, 131–144. https://doi.org/10.1016/j.jenvman.2018.08.009

Armstrong, R. A., Lee, C., Hedges, J. I., Honjo, S., & Wakeham, S. G. (2001). A new, mechanistic model for organic carbon fluxes in the ocean based on the quantitative association of POC with ballast minerals. *Deep Sea Research Part II: Topical Studies in Oceanography*, *49*(1–3), 219–236. https://doi.org/10.1016/S0967-0645(01)00101-1

Arndt, S., Jørgensen, B. B., LaRowe, D. E., Middelburg, J. J., Pancost, R. D., & Regnier, P. (2013). Quantifying the degradation of organic matter in marine sediments: A review and synthesis. *Earth-Science Reviews*, *123*, 53–86. https://doi.org/10.1016/j.earscirev.2013.02.008

Aviso+ Altimetry. (2022). Mesoscale Eddy Trajectory Atlas Product. *Handbook, Ramonville-Saint-Agne*.

Bakun, A. (2006). Fronts and eddies as key structures in the habitat of marine fish larvae: Opportunity, adaptive response and competitive advantage. *Scientia Marina*, *70*(S2), 105–122. https://doi.org/10.3989/scimar.2006.70s2105

Balch, W. M., Bowler, B. C., Drapeau, D. T., Lubelczyk, L. C., & Lyczkowski, E. (2018). Vertical Distributions of Coccolithophores, PIC, POC, Biogenic Silica, and Chlorophyll *a* Throughout the Global Ocean. *Global Biogeochemical Cycles*, *32*(1), 2–17. https://doi.org/10.1002/2016GB005614

Bateman, A. S., & Kelly, S. D. (2007). Fertilizer nitrogen isotope signatures. *Isotopes in Environmental and Health Studies*, *43*(3), 237–247. https://doi.org/10.1080/10256010701550732

Beaugrand, G., McQuatters-Gollop, A., Edwards, M., & Goberville, E. (2013). Long-term responses of North Atlantic calcifying plankton to climate change. *Nature Climate Change*, *3*(3), 263–267. https://doi.org/10.1038/nclimate1753

Berner, R. A. (2003). The long-term carbon cycle, fossil fuels and atmospheric composition. *Nature*, *426*(6964), 323–326. https://doi.org/10.1038/nature02131

Bianchi, T. S., Lambert, C. D., Santschi, P. H., & Guo, L. (1997). Sources and transport of land-derived particulate and dissolved organic matter in the Gulf of Mexico (Texas shelf/slope): The use of ligninphenols and loliolides as biomarkers. *Organic Geochemistry*, *27*(1–2), 65–78. https://doi.org/10.1016/S0146-6380(97)00040-5

Bianchi, T. S., Mitra, S., & McKee, B. A. (2002). Sources of terrestrially-derived organic carbon in lower Mississippi River and Louisiana shelf sediments: Implications for differential sedimentation and transport at the coastal margin. *Marine Chemistry*, *77*(2–3), 211–223. https://doi.org/10.1016/S0304-4203(01)00088-3

Bidigare, R. R., Benitez-Nelson, C., Leonard, C. L., Quay, P. D., Parsons, M. L., Foley, D. G., & Seki, M. P. (2003). Influence of a cyclonic eddy on microheterotroph biomass and carbon export in the lee of Hawaii. *Geophysical Research Letters*, *30*(6), 2002GL016393. https://doi.org/10.1029/2002GL016393

Boyd, P. W., Claustre, H., Levy, M., Siegel, D. A., & Weber, T. (2019). Multi-faceted particle pumps drive carbon sequestration in the ocean. *Nature*, *568*(7752), 327–335. https://doi.org/10.1038/s41586-019-1098-2

Brooks, G. R., Larson, R. A., Schwing, P. T., Romero, I., Moore, C., Reichart, G.-J., Jilbert, T., Chanton, J. P., Hastings, D. W., Overholt, W. A., Marks, K. P., Kostka, J. E., Holmes, C. W., & Hollander, D. (2015). Sedimentation Pulse in the NE Gulf of Mexico following the 2010 DWH Blowout. *PLOS ONE*, *10*(7), e0132341. https://doi.org/10.1371/journal.pone.0132341

Buesseler, K. O., Antia, A. N., Chen, M., Fowler, S. W., Gardner, W. D., Gustafsson, O., Harada, K., Michaels, A. F., Rutgers Van Der Loeff, M., Sarin, M., Steinberg, D. K., & Trull, T. (2007). An assessment of the use of sediment traps for estimating upper ocean particle fluxes. *Journal of Marine Research*, *65*(3), 345–416. https://doi.org/10.1357/002224007781567621

Buesseler, K. O., & Boyd, P. W. (2009). Shedding light on processes that control particle export and flux attenuation in the twilight zone of the open ocean. *Limnology and Oceanography*, *54*(4), 1210–1232. https://doi.org/10.4319/lo.2009.54.4.1210

Burdige, D. J. (2007). Preservation of Organic Matter in Marine Sediments: Controls, Mechanisms, and an Imbalance in Sediment Organic Carbon Budgets? *Chemical Reviews*, *107*(2), 467–485. https://doi.org/10.1021/cr050347q

Burkhardt, S., Riebesell, U., & Zondervan, I. (1999). Effects of growth rate, CO2 concentration, and cell size on the stable carbon isotope fractionation in marine phytoplankton. *Geochimica et Cosmochimica Acta*, *63*(22), 3729–3741. https://doi.org/10.1016/S0016-7037(99)00217-3

Calvert, S. E. (1987). Oceanographic controls on the accumulation of organic matter in marine sediments. *Geological Society, London, Special Publications*, *26*(1), 137–151. https://doi.org/10.1144/GSL.SP.1987.026.01.08

Canfield, D. E. (1993). Organic Matter Oxidation in Marine Sediments. In R. Wollast, F. T. Mackenzie, & L. Chou (Eds.), *Interactions of C, N, P and S Biogeochemical Cycles and Global Change* (pp. 333–363). Springer Berlin Heidelberg. https://doi.org/10.1007/978-3-642-76064-8_14

Cervantes-Díaz, G. Y., Hernández-Ayón, J. M., Zirino, A., Herzka, S. Z., Camacho-Ibar, V., Norzagaray, O., Barbero, L., Montes, I., Sudre, J., & Delgado, J. A. (2022). Understanding upper water mass dynamics in the Gulf of Mexico by linking physical and biogeochemical features. *Journal of Marine Systems*, *225*, 103647. https://doi.org/10.1016/j.jmarsys.2021.103647

Contreras-Pacheco, Y. V., Herzka, S. Z., Vallejo-Espinosa, G., & Herguera, J. C. (2023). Particulate organic carbon in the deep-water region of the Gulf of Mexico. *Frontiers in Marine Science*, *10*, 1095212. https://doi.org/10.3389/fmars.2023.1095212

Cuevas-Lara, D., Alcocer, J., Cortés-Guzmán, D., Soria-Reinoso, I. F., García-Oliva, F., Sánchez-Carrillo, S., & Oseguera, L. A. (2021). Particulate Organic Carbon in the Tropical Usumacinta River, Southeast Mexico: Concentration, Flux, and Sources. *Water*, *13*(11), 1561. https://doi.org/10.3390/w13111561

Daly, K. L., Passow, U., Chanton, J., & Hollander, D. (2016). Assessing the impacts of oil-associated marine snow formation and sedimentation during and after the Deepwater Horizon oil spill. *Anthropocene*, *13*, 18–33. https://doi.org/10.1016/j.ancene.2016.01.006

Damien, P., Pasqueron De Fommervault, O., Sheinbaum, J., Jouanno, J., Camacho-Ibar, V. F., & Duteil, O. (2018). Partitioning of the Open Waters of the Gulf of Mexico Based on the Seasonal and Interannual Variability of Chlorophyll Concentration. *Journal of Geophysical Research: Oceans*, *123*(4), 2592–2614. https://doi.org/10.1002/2017JC013456

Damien, P., Sheinbaum, J., Pasqueron De Fommervault, O., Jouanno, J., Linacre, L., & Duteil, O. (2021). Do Loop Current eddies stimulate productivity in the Gulf of Mexico? *Biogeosciences*, *18*(14), 4281–4303. https://doi.org/10.5194/bg-18-4281-2021

Dawson, H. R. S., Strutton, P. G., & Gaube, P. (2018). The Unusual Surface Chlorophyll Signatures of Southern Ocean Eddies. *Journal of Geophysical Research: Oceans*, *123*(9), 6053–6069. https://doi.org/10.1029/2017JC013628

De La Rocha, C. L., & Passow, U. (2007). Factors influencing the sinking of POC and the efficiency of the biological carbon pump. *Deep Sea Research Part II: Topical Studies in Oceanography*, *54*(5–7), 639–658. https://doi.org/10.1016/j.dsr2.2007.01.004

Degens, E. T., Guillard, R. R. L., Sackett, W. M., & Hellebust, J. A. (1968). Metabolic fractionation of carbon isotopes in marine plankton—I. Temperature and respiration experiments. *Deep Sea Research and Oceanographic Abstracts*, *15*(1), 1–9. https://doi.org/10.1016/0011-7471(68)90024-7

Delgado, J. A., Sudre, J., Tanahara, S., Montes, I., Hernandez-Ayon, J. M., & Zirino, A. (2019). *Effect of Caribbean Water Incursion into the Gulf of Mexico derived from Absolute Dynamic Topography, Satellite Data, and Remotely – sensed Chlorophyll-<i>a</i>* [Preprint]. Remote Sensing/Current Field/Surface/Caribbean. https://doi.org/10.5194/os-2019-58

Denman, K. L. (2007). *Chapter 7: Couplings Between Changes in the Climate System and Biogeochemistry—AR4 WGI*. https://archive.ipcc.ch/publications_and_data/ar4/wg1/en/ch7.html

Díaz-Asencio, M., Bartrina, V. F., & Herguera, J. C. (2019). Sediment accumulation patterns on the slopes and abyssal plain of the southern Gulf of Mexico. *Deep Sea Research Part I: Oceanographic Research Papers*, *146*, 11–23. https://doi.org/10.1016/j.dsr.2019.01.003

Díaz-Asencio, M., Herguera, J. C., Romero, F. G., & Rafter, P. (2023). Sediment accumulation rates and carbonate fluxes of deep-sea sediments in the southern Gulf of Mexico. *Marine Geology*, *464*, 107131. https://doi.org/10.1016/j.margeo.2023.107131

Díaz-Asencio, M., Herguera, J. C., Schwing, P. T., Larson, R. A., Brooks, G. R., Southon, J., & Rafter, P. (2020). Sediment accumulation rates and vertical mixing of deep-sea sediments derived from 14C and 210Pb in the southern Gulf of Mexico. *Marine Geology*, *429*, 106288. https://doi.org/10.1016/j.margeo.2020.106288

Dobashi, R., Ueno, H., Matsudera, N., Fujita, I., Fujiki, T., Honda, M. C., & Harada, N. (2022). Impact of mesoscale eddies on particulate organic carbon flux in the western subarctic North Pacific. *Journal of Oceanography*, *78*(1), 1–14. https://doi.org/10.1007/s10872-021-00620-7

Domínguez-Guadarrama, A., & Pérez-Brunius, P. (2017). Protocolo de procesamiento de datos de altimetría para la obtención de derivados: nivel del mar, vorticidad y energía cinética. Versión 1.0. Informe técnico 22576, Dpto. Oceanografía Física, CICESE, 11p.

Ducklow, H. W., Steinberg, D. K., & Buesseler, K. O. (2001). Upper ocean carbon export and the biological pump. *Oceanography*, *14*(4), 50–58. https://la-dwh.com/wp-content/uploads/2018/02/9.2.7.18_Ducklow.pdf

Duforêt-Gaurier, L., Loisel, H., Dessailly, D., Nordkvist, K., & Alvain, S. (2010). Estimates of particulate organic carbon over the euphotic depth from in situ measurements. Application to satellite data over the global ocean. *Deep Sea Research Part I: Oceanographic Research Papers*, *57*(3), 351–367. https://doi.org/10.1016/j.dsr.2009.12.007

Eglinton, T.I., & Repeta, D. J. (2004). Organic matter in the contemporary ocean. *Treatise on Geochemistry*, *6*, 145–180. https://doi.org/10.1016/B0-08-043751-6/06155-7

Emerson, S., Fischer, K., Reimers, C., & Heggie, D. (1985). Organic carbon dynamics and preservation in deep-sea sediments. *Deep Sea Research Part A. Oceanographic Research Papers*, *32*(1), 1–21. https://doi.org/10.1016/0198-0149(85)90014-7

Eppley, R. W., & Peterson, B. J. (1979). Particulate organic matter flux and planktonic new production in the deep ocean. *Nature*, *282*(5740), 677–680. https://doi.org/10.1038/282677a0

Escobar-Briones, E., Signoret, M., & Hernández, D. (1999). Variation of the macrobenthic infaunal density in a bathymetric gradient: Western gulf of mexico. *Ciencias Marinas*, *25*(2), 193–212. https://doi.org/10.7773/cm.v25i2.667

Faghmous, J. H., Frenger, I., Yao, Y., Warmka, R., Lindell, A., & Kumar, V. (2015). A daily global mesoscale ocean eddy dataset from satellite altimetry. *Scientific Data*, *2*(1), 150028. https://doi.org/10.1038/sdata.2015.28

Falkowski, P. G., Barber, R. T., & Smetacek, V. (1998). Biogeochemical Controls and Feedbacks on Ocean Primary Production. *Science*, *281*(5374), 200–206. https://doi.org/10.1126/science.281.5374.200

Falkowski, P. G., Greene, R. M., & Geider, R. J. (1992). Physiological Limitations on Phytoplankton Productivity in the Ocean. *Oceanography*, *5*(2), 84–91. http://www.jstor.org/stable/43924603

Falkowski, P., Scholes, R. J., Boyle, E., Canadell, J., Canfield, D., Elser, J., Gruber, N., Hibbard, K., Högberg, P., Linder, S., Mackenzie, F. T., Moore Iii, B., Pedersen, T., Rosenthal, Y., Seitzinger, S., Smetacek, V., & Steffen, W. (2000). The Global Carbon Cycle: A Test of Our Knowledge of Earth as a System. *Science*, *290*(5490), 291–296. https://doi.org/10.1126/science.290.5490.291

Fiedler, B., Grundle, D. S., Schütte, F., Karstensen, J., Löscher, C. R., Hauss, H., Wagner, H., Loginova, A., Kiko, R., Silva, P., Tanhua, T., & Körtzinger, A. (2016). Oxygen utilization and downward carbon flux in an oxygen-depleted eddy in the eastern tropical North Atlantic. *Biogeosciences*, *13*(19), 5633–5647. https://doi.org/10.5194/bg-13-5633-2016

Field, D. B., Baumgartner, T. R., Charles, C. D., Ferreira-Bartrina, V., & Ohman, M. D. (2006). Planktonic Foraminifera of the California Current Reflect 20th-Century Warming. *Science*, *311*(5757), 63–66. https://doi.org/10.1126/science.1116220

Fischer, G., & Wefer, G. (1996). Long-term Observation of Particle Fluxes in the Eastern Atlantic: Seasonality, Changes of Flux with Depth and Comparison with the Sediment Record. In G. Wefer, W. H. Berger, G. Siedler, & D. J. Webb, *The South Atlantic* (pp. 325–344). Springer Berlin Heidelberg. https://doi.org/10.1007/978-3-642-80353-6_18

Freeman, K. H., Hayes, J. M., Trendel, J.-M., & Albrecht, P. (1990). Evidence from carbon isotope measurements for diverse origins of sedimentary hydrocarbons. *Nature*, *343*(6255), 254–256. https://doi.org/10.1038/343254a0

Frenger, I., Bianchi, D., Stührenberg, C., Oschlies, A., Dunne, J., Deutsch, C., Galbraith, E., & Schütte, F. (2018). Biogeochemical Role of Subsurface Coherent Eddies in the Ocean: Tracer Cannonballs, Hypoxic Storms, and Microbial Stewpots? *Global Biogeochemical Cycles*, *32*(2), 226–249. https://doi.org/10.1002/2017GB005743

Fritsch, F., & Carlson, R. (1980). Monotone Piecewise Cubic Interpolation. *SIAM Journal on Numerical Analysis*, *17*, 238–246.

Fry, B. (2008). *Stable isotope ecology* (Corrected as of 3rd printing). New York: Springer. https://link.springer.com/content/pdf/10.1007/0-387-33745-8.pdf

Gardner, W. D., Gundersen, J. S., Richardson, M. J., & Walsh, I. D. (1999). The role of seasonal and diel changes in mixed-layer depth on carbon and chlorophyll distributions in the Arabian Sea. *Deep Sea Research Part II: Topical Studies in Oceanography*, *46*(8–9), 1833–1858. https://doi.org/10.1016/S0967-0645(99)00046-6

Gaube, P., J. McGillicuddy, D., & Moulin, A. J. (2019). Mesoscale Eddies Modulate Mixed Layer Depth Globally. *Geophysical Research Letters*, *46*(3), 1505–1512. https://doi.org/10.1029/2018GL080006

Gaube, P., McGillicuddy, D. J., Chelton, D. B., Behrenfeld, M. J., & Strutton, P. G. (2014). Regional variations in the influence of mesoscale eddies on near-surface chlorophyll. *Journal of Geophysical Research: Oceans*, *119*(12), 8195–8220. https://doi.org/10.1002/2014JC010111

Giering, S. L. C., Yan, B., Sweet, J., Asper, V., Diercks, A., Chanton, J. P., Pitiranggon, M., & Passow, U. (2018). The ecosystem baseline for particle flux in the Northern Gulf of Mexico. *Elementa: Science of the Anthropocene*, *6*, 6. https://doi.org/10.1525/elementa.264

Goericke, R., & Fry, B. (1994). Variations of marine plankton δ ^{13} C with latitude, temperature, and dissolved CO_2 in the world ocean. *Global Biogeochemical Cycles*, *8*(1), 85–90. https://doi.org/10.1029/93GB03272

Goñi, M. A., Ruttenberg, K. C., & Eglinton, T. I. (1997). Sources and contribution of terrigenous organic carbon to surface sediments in the Gulf of Mexico. *Nature*, *389*(6648), 275–278. https://doi.org/10.1038/38477

Goñi, M. A., Teixeira, M. J., & Perkey, D. W. (2003). Sources and distribution of organic matter in a river-dominated estuary (Winyah Bay, SC, USA). *Estuarine, Coastal and Shelf Science*, *57*(5–6), 1023–1048. https://doi.org/10.1016/S0272-7714(03)00008-8

Graff, J. R., Westberry, T. K., Milligan, A. J., Brown, M. B., Dall'Olmo, G., Dongen-Vogels, V. V., Reifel, K. M., & Behrenfeld, M. J. (2015). Analytical phytoplankton carbon measurements spanning diverse ecosystems. *Deep Sea Research Part I: Oceanographic Research Papers*, *102*, 16–25. https://doi.org/10.1016/j.dsr.2015.04.006

Gruber, N., Lachkar, Z., Frenzel, H., Marchesiello, P., Münnich, M., McWilliams, J. C., Nagai, T., & Plattner, G.-K. (2011). Eddy-induced reduction of biological production in eastern boundary upwelling systems. *Nature Geoscience*, *4*(11), 787–792. https://doi.org/10.1038/ngeo1273

Guidi, L., Stemmann, L., Jackson, G. A., Ibanez, F., Claustre, H., Legendre, L., Picheral, M., & Gorskya, G. (2009). Effects of phytoplankton community on production, size, and export of large aggregates: A world-ocean analysis. *Limnology and Oceanography*, *54*(6), 1951–1963. https://doi.org/10.4319/lo.2009.54.6.1951

Hansell, D. A., & Carlson, C. A. (1998). Deep-ocean gradients in the concentration of dissolved organic carbon. *Nature*, *395*(6699), 263–266. https://doi.org/10.1038/26200

Harris, P. (2019). A Simulation Study on Specifying a Regression Model for Spatial Data: Choosing between Autocorrelation and Heterogeneity Effects. *Geographical Analysis*, *51*(2), 151–181. https://doi.org/10.1111/gean.12163

Hedges, J. I. (1992). Global biogeochemical cycles: Progress and problems. *Marine Chemistry*, *39*(1–3), 67–93. https://doi.org/10.1016/0304-4203(92)90096-S

Hedges, J. I., Eglinton, G., Hatcher, P. G., Kirchman, D. L., Arnosti, C., Derenne, S., Evershed, R. P., Kögel-Knabner, I., De Leeuw, J. W., Littke, R., Michaelis, W., & Rullkötter, J. (2000). The molecularly-uncharacterized component of nonliving organic matter in natural environments. *Organic Geochemistry*, *31*(10), 945–958. https://doi.org/10.1016/S0146-6380(00)00096-6

Hedges, J. I., & Keil, R. G. (1995). Sedimentary organic matter preservation: An assessment and speculative synthesis. *Marine Chemistry*, *49*(2–3), 81–115. https://doi.org/10.1016/0304-4203(95)00008-F

Heinze, C., Maier-Reimer, E., & Winn, K. (1991). Glacial pCO_2 Reduction by the World Ocean: Experiments With the Hamburg Carbon Cycle Model. *Paleoceanography*, *6*(4), 395–430. https://doi.org/10.1029/91PA00489

Henson, S., Le Moigne, F., & Giering, S. (2019). Drivers of Carbon Export Efficiency in the Global Ocean. *Global Biogeochemical Cycles*, *33*(7), 891–903. https://doi.org/10.1029/2018GB006158

Hillebrand, H., Blasius, B., Borer, E. T., Chase, J. M., Downing, J. A., Eriksson, B. K., Filstrup, C. T., Harpole, W. S., Hodapp, D., Larsen, S., Lewandowska, A. M., Seabloom, E. W., Van De Waal, D. B., & Ryabov, A. B. (2018). Biodiversity change is uncoupled from species richness trends: Consequences for conservation and monitoring. *Journal of Applied Ecology*, *55*(1), 169–184. https://doi.org/10.1111/1365-2664.12959

Hillebrand, H., Donohue, I., Harpole, W. S., Hodapp, D., Kucera, M., Lewandowska, A. M., Merder, J., Montoya, J. M., & Freund, J. A. (2020). Thresholds for ecological responses to global change do not emerge from empirical data. *Nature Ecology & Evolution*, *4*(11), 1502–1509. https://doi.org/10.1038/s41559-020-1256-9

Hoegh-Guldberg, O. (2010). Dangerous shifts in ocean ecosystem function? *The ISME Journal*, *4*(9), 1090–1092. https://doi.org/10.1038/ismej.2010.107

Honda, M. (2001). *Sediment trap experiments and a study of carbon cycle in the North Western Pacific Ocean*. Department of Earth Environment Studies, Hokkaido University.

Honda, M. C., Sasai, Y., Siswanto, E., Kuwano-Yoshida, A., Aiki, H., & Cronin, M. F. (2018). Impact of cyclonic eddies and typhoons on biogeochemistry in the oligotrophic ocean based on biogeochemical/physical/meteorological time-series at station KEO. *Progress in Earth and Planetary Science*, *5*(1), 42. https://doi.org/10.1186/s40645-018-0196-3

Honjo, S. (1982). Seasonality and Interaction of Biogenic and Lithogenic Particulate Flux at the Panama Basin. *Science*, *218*(4575), 883–884. https://doi.org/10.1126/science.218.4575.883

Honjo, S., Dymond, J., Prell, W., & Ittekkot, V. (1999). Monsoon-controlled export fluxes to the interior of the Arabian Sea. *Deep Sea Research Part II: Topical Studies in Oceanography*, *46*(8–9), 1859–1902. https://doi.org/10.1016/S0967-0645(99)00047-8

Honjo, S., Francois, R., Manganini, S., Dymond, J., & Collier, R. (2000). Particle fluxes to the interior of the Southern Ocean in the Western Pacific sector along 170°W. *Deep Sea Research Part II: Topical Studies in Oceanography*, *47*(15–16), 3521–3548. https://doi.org/10.1016/S0967-0645(00)00077-1

Honjo, S., Manganini, S. J., Krishfield, R. A., & Francois, R. (2008). Particulate organic carbon fluxes to the ocean interior and factors controlling the biological pump: A synthesis of global sediment trap programs since 1983. *Progress in Oceanography*, *76*(3), 217–285. https://doi.org/10.1016/j.pocean.2007.11.003

Honjo, S., Spencer, D. W., & Gardner, W. D. (1992). A sediment trap intercomparison experiment in the Panama Basin, 1979. *Deep Sea Research Part A. Oceanographic Research Papers*, *39*(2), 333–358. https://doi.org/10.1016/0198-0149(92)90112-7

Houghton, R. A. (2007). Balancing the Global Carbon Budget. *Annual Review of Earth and Planetary Sciences*, *35*(1), 313–347. https://doi.org/10.1146/annurev.earth.35.031306.140057

Howe, S., Miranda, C., Hayes, C. T., Letscher, R. T., & Knapp, A. N. (2020). The Dual Isotopic Composition of Nitrate in the Gulf of Mexico and Florida Straits. *Journal of Geophysical Research: Oceans*, *125*(9), e2020JC016047. https://doi.org/10.1029/2020JC016047

Hung, C.-C., Xu, C., Santschi, P. H., Zhang, S.-J., Schwehr, K. A., Quigg, A., Guo, L., Gong, G.-C., Pinckney, J. L., Long, R. A., & Wei, C.-L. (2010). Comparative evaluation of sediment trap and 234Th-derived POC fluxes from the upper oligotrophic waters of the Gulf of Mexico and the subtropical northwestern Pacific Ocean. *Marine Chemistry*, *121*(1–4), 132–144. https://doi.org/10.1016/j.marchem.2010.03.011

Iversen, M. H., & Ploug, H. (2010). Ballast minerals and the sinking carbon flux in the ocean: Carbon-specific respiration rates and sinking velocity of marine snow aggregates. *Biogeosciences*, *7*(9), 2613–2624. https://doi.org/10.5194/bg-7-2613-2010

Jouanno, J., Ochoa, J., Pallàs-Sanz, E., Sheinbaum, J., Andrade-Canto, F., Candela, J., & Molines, J.-M. (2016). Loop Current Frontal Eddies: Formation along the Campeche Bank and Impact of Coastally Trapped Waves. *Journal of Physical Oceanography*, *46*(11), 3339–3363. https://doi.org/10.1175/JPO-D-16-0052.1

Kelly, T. B., Knapp, A. N., Landry, M. R., Selph, K. E., Shropshire, T. A., Thomas, R. K., & Stukel, M. R. (2021). Lateral advection supports nitrogen export in the oligotrophic open-ocean Gulf of Mexico. *Nature Communications*, *12*(1), 3325. https://doi.org/10.1038/s41467-021-23678-9

Kemp, G., Day, J., Yáñez-Arancibia, A., & Peyronnin, N. (2016). Can Continental Shelf River Plumes in the Northern and Southern Gulf of Mexico Promote Ecological Resilience in a Time of Climate Change? *Water*, *8*(3), 83. https://doi.org/10.3390/w8030083

Kendall, C., Silva, S. R., & Kelly, V. J. (2001). Carbon and nitrogen isotopic compositions of particulate organic matter in four large river systems across the United States. *Hydrological Processes*, *15*(7), 1301–1346. https://doi.org/10.1002/hyp.216

Khaled, W., Lin, J., Han, Z., Zhao, Y., & Hao, H. (2019). Test for Heteroscedasticity in Partially Linear Regression Models. *Journal of Systems Science and Complexity*, *32*(4), 1194–1210. https://doi.org/10.1007/s11424-019-7374-2

Kharbush, J. J., Close, H. G., Van Mooy, B. A. S., Arnosti, C., Smittenberg, R. H., Le Moigne, F. A. C., Mollenhauer, G., Scholz-Böttcher, B., Obreht, I., Koch, B. P., Becker, K. W., Iversen, M. H., & Mohr, W. (2020). Particulate Organic Carbon Deconstructed: Molecular and Chemical Composition of Particulate Organic Carbon in the Ocean. *Frontiers in Marine Science*, *7*, 518. https://doi.org/10.3389/fmars.2020.00518

Klaas, C., & Archer, D. E. (2002). Association of sinking organic matter with various types of mineral ballast in the deep sea: Implications for the rain ratio. *Global Biogeochemical Cycles*, *16*(4). https://doi.org/10.1029/2001GB001765

knap, A. H., Michaels, A., Close, A. R., Ducklow, H., & Dickson, A. G. (1996). Protocols for the joint global ocean flux study (JGOFS) core measurements. In *JGOFS, Reprint of the IOC Manuals and Guides No. 29* (p. 170). UNESCO.

Knauer, G. A., Martin, J. H., & Bruland, K. W. (1979). Fluxes of particulate carbon, nitrogen, and phosphorus in the upper water column of the northeast Pacific. *Deep Sea Research Part A. Oceanographic Research Papers*, *26*(1), 97–108. https://doi.org/10.1016/0198-0149(79)90089-X

Kuss, J., & Kremling, K. (1999). Particulate trace element fluxes in the deep northeast Atlantic Ocean. *Deep Sea Research Part I: Oceanographic Research Papers*, *46*(1), 149–169. https://doi.org/10.1016/S0967-0637(98)00059-4

Lalli, C. M., & Parsons, T. R. (2006). *Biological oceanography: An introduction* (2. ed., reprinted). Elsevier Butterworth-Heinemann.

Lara, M., & Li, J. J. (2024). *México | Emisiones y fuentes de los Gases de Efecto Invernadero | BBVA Research*. Recuperado el día 18 de octubre del 2024 de https://www.bbvaresearch.com/publicaciones/mexico-emisiones-y-fuentes-de-los-gases-de-efecto-invernadero/

Laurenceau-Cornec, E. C., Mongin, M., Trull, T. W., Bressac, M., Cavan, E. L., Bach, L. T., Le Moigne, F. A. C., Planchon, F., & Boyd, P. W. (2023). Concepts Toward a Global Mechanistic Mapping of Ocean Carbon Export. *Global Biogeochemical Cycles*, *37*(9), e2023GB007742. https://doi.org/10.1029/2023GB007742

Laws, E. A., Popp, B. N., Bidigare, R. R., Kennicutt, M. C., & Macko, S. A. (1995). Dependence of phytoplankton carbon isotopic composition on growth rate and [CO2)aq: Theoretical considerations and experimental results. *Geochimica et Cosmochimica Acta*, *59*(6), 1131–1138. https://doi.org/10.1016/0016-7037(95)00030-4

Leben, R. R. (2005). Altimeter-Derived Loop Current Metrics. In W. Sturges & A. Lugo-Fernandez (Eds.), *Geophysical Monograph Series* (pp. 181–201). American Geophysical Union. https://doi.org/10.1029/161GM15

Lee-Sánchez, E., Camacho-Ibar, V. F., Velásquez-Aristizábal, J. A., Valencia-Gasti, J. A., & Samperio-Ramos, G. (2022). Impacts of mesoscale eddies on the nitrate distribution in the deep-water region of the Gulf of Mexico. *Journal of Marine Systems*, *229*, 103721. https://doi.org/10.1016/j.jmarsys.2022.103721

Libes, S. (2011). *Introduction to Marine Biogeochemistry*. Academic Press.

Linacre, L., Durazo, R., Camacho-Ibar, V. F., Selph, K. E., Lara-Lara, J. R., Mirabal-Gómez, U., Bazán-Guzmán, C., Lago-Lestón, A., Fernández-Martín, E. M., & Sidón-Ceseña, K. (2019). Picoplankton Carbon Biomass Assessments and Distribution of *Prochlorococcus* Ecotypes Linked to Loop Current Eddies During Summer in the Southern Gulf of Mexico. *Journal of Geophysical Research: Oceans*, *124*(11), 8342–8359. https://doi.org/10.1029/2019JC015103

Linacre, L., Lara-Lara, R., Camacho-Ibar, V., Herguera, J. C., Bazán-Guzmán, C., & Ferreira-Bartrina, V. (2015). Distribution pattern of picoplankton carbon biomass linked to mesoscale dynamics in the southern gulf of Mexico during winter conditions. *Deep Sea Research Part I: Oceanographic Research Papers*, *106*, 55–67. https://doi.org/10.1016/j.dsr.2015.09.009

Liu, Z., & Xue, J. (2020). The Lability and Source of Particulate Organic Matter in the Northern Gulf of Mexico Hypoxic Zone. *Journal of Geophysical Research: Biogeosciences*, *125*(9), e2020JG005653. https://doi.org/10.1029/2020JG005653

Lohrenz, S. E., Fahnenstiel, G. L., Redalje, D. G., Lang, G. A., Dagg, M. J., Whitledge, T. E., & Dortch, Q. (1999). Nutrients, irradiance, and mixing as factors regulating primary production in coastal waters

impacted by the Mississippi River plume. *Continental Shelf Research*, *19*(9), 1113–1141. https://doi.org/10.1016/S0278-4343(99)00012-6

Longhurst, A. R. (1991). Role of the marine biosphere in the global carbon cycle. *Limnology and Oceanography*, *36*(8), 1507–1526. https://doi.org/10.4319/lo.1991.36.8.1507

Longhurst, A. R., & Glen Harrison, W. (1989). The biological pump: Profiles of plankton production and consumption in the upper ocean. *Progress in Oceanography*, *22*(1), 47–123. https://doi.org/10.1016/0079-6611(89)90010-4

Lutz, M., Dunbar, R., & Caldeira, K. (2002). Regional variability in the vertical flux of particulate organic carbon in the ocean interior. *Global Biogeochemical Cycles*, *16*(3). https://doi.org/10.1029/2000GB001383

Martin, J. H., Knauer, G. A., Karl, D. M., & Broenkow, W. W. (1987). VERTEX: Carbon cycling in the northeast Pacific. *Deep Sea Research Part A. Oceanographic Research Papers*, *34*(2), 267–285. https://doi.org/10.1016/0198-0149(87)90086-0

Martínez-López, B., & Zavala-Hidalgo, J. (2009). Seasonal and interannual variability of cross-shelf transports of chlorophyll in the Gulf of Mexico. *Journal of Marine Systems*, *77*(1–2), 1–20. https://doi.org/10.1016/j.jmarsys.2008.10.002

McDougall, T. J., & Barker, P. M. (2011). *Getting started with TEOS-10 and the Gibbs Seawater (GSW) Oceanographic Toolbox*. Trevor J McDougall.

McGillicuddy, D. J. (2016). Mechanisms of Physical-Biological-Biogeochemical Interaction at the Oceanic Mesoscale. *Annual Review of Marine Science*, *8*(1), 125–159. https://doi.org/10.1146/annurev-marine-010814-015606

Meybeck, M. (1982). Carbon, nitrogen, and phosphorus transport by world rivers. *American Journal of Science*, *282*(4), 401–450. https://doi.org/10.2475/ajs.282.4.401

Middelburg, J. J. (2018). Reviews and syntheses: To the bottom of carbon processing at the seafloor. *Biogeosciences*, *15*(2), 413–427. https://doi.org/10.5194/bg-15-413-2018

Müller-Karger, F. E., Smith, J. P., Werner, S., Chen, R., Roffer, M., Liu, Y., Muhling, B., Lindo-Atichati, D., Lamkin, J., Cerdeira-Estrada, S., & Enfield, D. B. (2015). Natural variability of surface oceanographic conditions in the offshore Gulf of Mexico. *Progress in Oceanography*, *134*, 54–76. https://doi.org/10.1016/j.pocean.2014.12.007

Müller-Karger, F. E., Walsh, J. J., Evans, R. H., & Meyers, M. B. (1991). On the seasonal phytoplankton concentration and sea surface temperature cycles of the Gulf of Mexico as determined by satellites. *Journal of Geophysical Research: Oceans*, *96*(C7), 12645–12665. https://doi.org/10.1029/91JC00787

Neuer, S., Ratmeyer, V., Davenport, R., Fischer, G., & Wefer, G. (1997). Deep water particle flux in the Canary Island region: Seasonal trends in relation to long-term satellite derived pigment data and lateral sources. *Deep Sea Research Part I: Oceanographic Research Papers*, *44*(8), 1451–1466. https://doi.org/10.1016/S0967-0637(97)00034-4

Oey, L. -Y., Ezer, T., Forristall, G., Cooper, C., DiMarco, S., & Fan, S. (2005). An exercise in forecasting loop current and eddy frontal positions in the Gulf of Mexico. *Geophysical Research Letters*, *32*(12), 2005GL023253. https://doi.org/10.1029/2005GL023253

O'Leary, T. D., & Langton, S. R. (1989). Calculated bicarbonate or total carbon dioxide? *Clinical Chemistry*, *35*(8), 1697–1700. https://doi.org/10.1093/clinchem/35.8.1697

Onstad, G. D., Canfield, D. E., Quay, P. D., & Hedges, J. I. (2000). Sources of particulate organic matter in rivers from the continental usa: Lignin phenol and stable carbon isotope compositions. *Geochimica et Cosmochimica Acta*, *64*(20), 3539–3546. https://doi.org/10.1016/S0016-7037(00)00451-8

Pasqueron De Fommervault, O., Perez-Brunius, P., Damien, P., Camacho-Ibar, V. F., & Sheinbaum, J. (2017). Temporal variability of chlorophyll distribution in the Gulf of Mexico: Bio-optical data from profiling floats. *Biogeosciences*, *14*(24), 5647–5662. https://doi.org/10.5194/bg-14-5647-2017

Paul, S. R., & Zhang, X. (2010). Testing for normality in linear regression models. *Journal of Statistical Computation and Simulation*, *80*(10), 1101–1113. https://doi.org/10.1080/00949650902964275

Pegliasco, C., Busché, C., & Faugère, Y. (2022). *Mesoscale Eddy Trajectory Atlas META3.2 Delayed-Time all satellites: Version META3.2 DT allsat* (Version 3.2 DT allsat 1993-01-01/2021-08-02) [NetCDF]. CNES. https://doi.org/10.24400/527896/A01-2022.005.210802

Pérez-Brunius, P., García-Carrillo, P., Dubranna, J., Sheinbaum, J., & Candela, J. (2012). Direct observations of the upper layer circulation in the southern Gulf of Mexico. *Deep Sea Research Part II: Topical Studies in Oceanography*, *85*, 182–194. https://doi.org/10.1016/j.dsr2.2012.07.020

Pilskaln, C. H. (2004). Seasonal and interannual particle export in an African rift valley lake: A 5-yr record from Lake Malawi, southern East Africa. *Limnology and Oceanography*, *49*(4), 964–977. https://doi.org/10.4319/lo.2004.49.4.0964

Poloczanska, E. S., Brown, C. J., Sydeman, W. J., Kiessling, W., Schoeman, D. S., Moore, P. J., Brander, K., Bruno, J. F., Buckley, L. B., Burrows, M. T., Duarte, C. M., Halpern, B. S., Holding, J., Kappel, C. V., O'Connor, M. I., Pandolfi, J. M., Parmesan, C., Schwing, F., Thompson, S. A., & Richardson, A. J. (2013). Global imprint of climate change on marine life. *Nature Climate Change*, *3*(10), 919–925. https://doi.org/10.1038/nclimate1958

Rabalais, N. N., Turner, R. E., & Scavia, D. (2002). Beyond Science into Policy: Gulf of Mexico Hypoxia and the Mississippi River. *BioScience*, *52*(2), 129. https://doi.org/10.1641/0006-3568(2002)052[0129:BSIPGO]2.0.CO;2

Rau, G. H., Chavez, F. P., & Friederich, G. E. (2001). Plankton variations in Monterey Bay, California: Evidence of non-diffusive inorganic carbon uptake by phytoplankton in an upwelling environment. *Deep Sea Research Part I: Oceanographic Research Papers*, *48*(1), 79–94. https://doi.org/10.1016/S0967-0637(00)00039-X

Riley, G. A. (1963). Organic aggregates in seawater and the dynamics of their formation and utilization. *Limnology and Oceanography*, *8*(4), 372–381. https://doi.org/10.4319/lo.1963.8.4.0372

Rixen, T., Gaye, B., & Emeis, K.-C. (2019). The monsoon, carbon fluxes, and the organic carbon pump in the northern Indian Ocean. *Progress in Oceanography*, *175*, 24–39. https://doi.org/10.1016/j.pocean.2019.03.001

Roca-Martí, M., Benitez-Nelson, C. R., Umhau, B. P., Wyatt, A. M., Clevenger, S. J., Pike, S., Horner, T. J., Estapa, M. L., Resplandy, L., & Buesseler, K. O. (2021). Concentrations, ratios, and sinking fluxes of major bioelements at Ocean Station Papa. *Elementa: Science of the Anthropocene*, *9*(1), 00166. https://doi.org/10.1525/elementa.2020.00166

Rodhe, H. (1990). A Comparison of the Contribution of Various Gases to the Greenhouse Effect. *Science*, *248*(4960), 1217–1219. https://doi.org/10.1126/science.248.4960.1217

Rosenheim, B. E., Roe, K. M., Roberts, B. J., Kolker, A. S., Allison, M. A., & Johannesson, K. H. (2013). River discharge influences on particulate organic carbon age structure in the Mississippi/Atchafalaya River System. *Global Biogeochemical Cycles*, *27*(1), 154–166. https://doi.org/10.1002/gbc.20018

Rosenzweig, C., Karoly, D., Vicarelli, M., Neofotis, P., Wu, Q., Casassa, G., Menzel, A., Root, T. L., Estrella, N., Seguin, B., Tryjanowski, P., Liu, C., Rawlins, S., & Imeson, A. (2008). Attributing physical and biological impacts to anthropogenic climate change. *Nature*, *453*(7193), 353–357. https://doi.org/10.1038/nature06937

Sabine, C. L., Feely, R. A., Gruber, N., Key, R. M., Lee, K., Bullister, J. L., Wanninkhof, R., Wong, C. S., Wallace, D. W. R., Tilbrook, B., Millero, F. J., Peng, T.-H., Kozyr, A., Ono, T., & Rios, A. F. (2004). The Oceanic Sink for Anthropogenic CO_2. *Science*, *305*(5682), 367–371. https://doi.org/10.1126/science.1097403

Sarmiento, J. L. (2006). *Ocean Biogeochemical Dynamics*. Princeton University Press. https://doi.org/10.1515/9781400849079

Sarmiento, J. L., & Gruber, N. (2013). *Ocean Biogeochemical Dynamics*. Princeton University Press. https://doi.org/10.2307/j.ctt3fgxqx

Schmitz, W. J., Biggs, D. C., Lugo-Fernandez, A., Oey, L.-Y., & Sturges, W. (2013). A Synopsis of the Circulation in the Gulf of Mexico and on its Continental Margins. In W. Sturges & A. Lugo-Fernandez (Eds.), *Geophysical Monograph Series* (pp. 11–29). American Geophysical Union. https://doi.org/10.1029/161GM03

Scholten, J. C., Fietzke, J., Vogler, S., Rutgers Van Der Loeff, M. M., Mangini, A., Koeve, W., Waniek, J., Stoffers, P., Antia, A., & Kuss, J. (2001). Trapping efficiencies of sediment traps from the deep Eastern North Atlantic: *Deep Sea Research Part II: Topical Studies in Oceanography*, *48*(10), 2383–2408. https://doi.org/10.1016/S0967-0645(00)00176-4

Schwing, P. T., O'Malley, B. J., & Hollander, D. J. (2018). Resilience of benthic foraminifera in the Northern Gulf of Mexico following the Deepwater Horizon event (2011–2015). *Ecological Indicators*, *84*, 753–764. https://doi.org/10.1016/j.ecolind.2017.09.044

Seki, M. P., Polovina, J. J., Brainard, R. E., Bidigare, R. R., Leonard, C. L., & Foley, D. G. (2001). Biological enhancement at cyclonic eddies tracked with GOES Thermal Imagery in Hawaiian waters. *Geophysical Research Letters*, *28*(8), 1583–1586. https://doi.org/10.1029/2000GL012439

Sharkey, T. D., Berry, J. A., & Raschke, K. (1985). Starch and Sucrose Synthesis in *Phaseolus vulgaris* as Affected by Light, CO_2, and Abscisic Acid. *Plant Physiology*, *77*(3), 617–620. https://doi.org/10.1104/pp.77.3.617

Sharp, J. H. (1973). Total organic carbon in seawater—Comparison of measurements using persulfate oxidation and high temperature combustion. *Marine Chemistry*, *1*(3), 211–229. https://doi.org/10.1016/0304-4203(73)90005-4

Sigman, D. M., & Fripiat, F. (2019). Nitrogen Isotopes in the Ocean. In *Encyclopedia of Ocean Sciences* (pp. 263–278). Elsevier. https://doi.org/10.1016/B978-0-12-409548-9.11605-7

Silverman, & Epstein. (1958). Carbon Isotopic Compositions of Petroleums and Other Sedimentary Organic Materials. *AAPG Bulletin*, *42*. https://doi.org/10.1306/0BDA5AEC-16BD-11D7-8645000102C1865D

Stocker, T. F. (2013). The Ocean as a Component of the Climate System. In *International Geophysics* (Vol. 103, pp. 3–30). Elsevier. https://doi.org/10.1016/B978-0-12-391851-2.00001-5

Stramska, M. (2009). Particulate organic carbon in the global ocean derived from SeaWiFS ocean color. *Deep Sea Research Part I: Oceanographic Research Papers*, *56*(9), 1459–1470. https://doi.org/10.1016/j.dsr.2009.04.009

Stramski, D., Joshi, I., & Reynolds, R. A. (2022). Ocean color algorithms to estimate the concentration of particulate organic carbon in surface waters of the global ocean in support of a long-term data record from multiple satellite missions. *Remote Sensing of Environment*, *269*, 112776. https://doi.org/10.1016/j.rse.2021.112776

Stramski, D., Reynolds, R. A., Babin, M., Kaczmarek, S., Lewis, M. R., Röttgers, R., Sciandra, A., Stramska, M., Twardowski, M. S., Franz, B. A., & Claustre, H. (2008). Relationships between the surface concentration of particulate organic carbon and optical properties in the eastern South Pacific and eastern Atlantic Oceans. *Biogeosciences*, *5*(1), 171–201. https://doi.org/10.5194/bg-5-171-2008

Strubinger Sandoval, P., Dall'Olmo, G., Haines, K., Rasse, R., & Ross, J. (2022). Uncertainties of particulate organic carbon concentrations in the mesopelagic zone of the Atlantic ocean. *Open Research Europe*, *1*, 43. https://doi.org/10.12688/openreseurope.13395.3

Sturges, W., & Leben, R. (2000). Frequency of Ring Separations from the Loop Current in the Gulf of Mexico: A Revised Estimate. *Journal of Physical Oceanography*, *30*(7), 1814–1819. https://doi.org/10.1175/1520-0485(2000)030<1814:FORSFT>2.0.CO;2

Suess, E. (1980). Particulate organic carbon flux in the oceans—Surface productivity and oxygen utilization. *Nature*, *288*(5788), 260–263. https://doi.org/10.1038/288260a0

Świrgoń, M., & Stramska, M. (2015). Comparison of in situ and satellite ocean color determinations of particulate organic carbon concentration in the global ocean. *Oceanologia*, *57*(1), 25–31. https://doi.org/10.1016/j.oceano.2014.09.002

Talley, L. D. (2011). *Descriptive Physical Oceanography: An Introduction* (6th ed). Academic press. Elsevier Science & Technology.

Tcherkez, G. (2006). Viewpoint: How large is the carbon isotope fractionation of the photorespiratory enzyme glycine decarboxylase? *Functional Plant Biology*, *33*(10), 911. https://doi.org/10.1071/FP06098

Thomson, R. E., & Fine, I. V. (2003). Estimating Mixed Layer Depth from Oceanic Profile Data. *Journal of Atmospheric and Oceanic Technology*, *20*(2), 319–329. https://doi.org/10.1175/1520-0426(2003)020<0319:EMLDFO>2.0.CO;2

Trefry, J. H., Metz, S., Nelsen, T. A., Trocine, R. P., & Eadie, B. J. (1994). Transport of Particulate Organic Carbon by the Mississippi River and Its Fate in the Gulf of Mexico. *Estuaries*, *17*(4), 839. https://doi.org/10.2307/1352752

Turner, J. T. (2015). Zooplankton fecal pellets, marine snow, phytodetritus and the ocean's biological pump. *Progress in Oceanography*, *130*, 205–248. https://doi.org/10.1016/j.pocean.2014.08.005

Velásquez-Aristizábal, J. A., Camacho-Ibar, V. F., Durazo, R., Valencia-Gasti, J. A., Lee-Sánchez, E., & Trasviña-Castro, A. (2022). Nitracentric/Hydrographic Classification and Prediction of Nitrate Profiles for Oceanographic Stations Under the Influence of Mesoscale Eddies in the Gulf of Mexico. *Frontiers in Marine Science*, *9*, 827574. https://doi.org/10.3389/fmars.2022.827574

Vidal, V. M. V., Vidal, F. V., & Pérez-Molero, J. M. (1992). Collision of a loop current anticyclonic ring against the continental shelf slope of the western Gulf of Mexico. *Journal of Geophysical Research: Oceans*, *97*(C2), 2155–2172. https://doi.org/10.1029/91JC00486

Volk, T. (1989). Effect on atmospheric CO2 from seasonal variations in the high latitude ocean. *Advances in Space Research*, *9*(8), 153–157. https://doi.org/10.1016/0273-1177(89)90040-9

Volk, T., & Hoffert, M. I. (1985). Ocean Carbon Pumps: Analysis of Relative Strengths and Efficiencies in Ocean-Driven Atmospheric CO_2 Changes. In E. T. Sundquist & W. S. Broecker (Eds.), *Geophysical Monograph Series* (pp. 99–110). American Geophysical Union. https://doi.org/10.1029/GM032p0099

Von Bodungen, B., Antia, A., Bauerfeind, E., Haupt, O., Koeve, W., Machado, E., Peeken, I., Peinert, R., Reitmeier, S., Thomsen, C., Voss, M., Wunsch, M., Zeller, U., & Zeitzschel, B. (1995). Pelagic processes and vertical flux of particles: An overview of a long-term comparative study in the Norwegian Sea and Greenland Sea. *Geologische Rundschau*, *84*(1), 11–27. https://doi.org/10.1007/BF00192239

Vukovich, F. M. (2007). Climatology of Ocean Features in the Gulf of Mexico Using Satellite Remote Sensing Data. *Journal of Physical Oceanography*, *37*(3), 689–707. https://doi.org/10.1175/JPO2989.1

Vukovich, F. M. (2012). Changes in the Loop Current's Eddy Shedding in the Period 2001–2010. *International Journal of Oceanography*, *2012*, 1–18. https://doi.org/10.1155/2012/439042

Wang, X.-C., Chen, R. F., & Gardner, G. B. (2004). Sources and transport of dissolved and particulate organic carbon in the Mississippi River estuary and adjacent coastal waters of the northern Gulf of Mexico. *Marine Chemistry*, *89*(1–4), 241–256. https://doi.org/10.1016/j.marchem.2004.02.014

Ward, C. H. (Ed.). (2017). *Habitats and Biota of the Gulf of Mexico: Before the Deepwater Horizon Oil Spill: Volume 1: Water Quality, Sediments, Sediment Contaminants, Oil and Gas Seeps, Coastal Habitats, Offshore Plankton and Benthos, and Shellfish*. Springer New York. https://doi.org/10.1007/978-1-4939-3447-8

Waters, C. N., Zalasiewicz, J., Summerhayes, C., Barnosky, A. D., Poirier, C., Gałuszka, A., Cearreta, A., Edgeworth, M., Ellis, E. C., Ellis, M., Jeandel, C., Leinfelder, R., McNeill, J. R., Richter, D. deB.,

Steffen, W., Syvitski, J., Vidas, D., Wagreich, M., Williams, M., … Wolfe, A. P. (2016). The Anthropocene is functionally and stratigraphically distinct from the Holocene. *Science*, *351*(6269), aad2622. https://doi.org/10.1126/science.aad2622

Wefer, G., & Berger, W. H. (1991). Isotope paleontology: Growth and composition of extant calcareous species. *Marine Geology*, *100*(1–4), 207–248. https://doi.org/10.1016/0025-3227(91)90234-U

Wefer, G., & Fischer, G. (1993). Seasonal patterns of vertical particle flux in equatorial and coastal upwelling areas of the eastern Atlantic. *Deep Sea Research Part I: Oceanographic Research Papers*, *40*(8), 1613–1645. https://doi.org/10.1016/0967-0637(93)90019-Y

Williams, R. G., & Follows, M. J. (2003). Physical Transport of Nutrients and the Maintenance of Biological Production. In M. J. R. Fasham (Ed.), *Ocean Biogeochemistry* (pp. 19–51). Springer Berlin Heidelberg. https://doi.org/10.1007/978-3-642-55844-3_3

Wong, C. S., Whitney, F. A., Crawford, D. W., Iseki, K., Matear, R. J., Johnson, W. K., Page, J. S., & Timothy, D. (1999). Seasonal and interannual variability in particle fluxes of carbon, nitrogen and silicon from time series of sediment traps at Ocean Station P, 1982–1993: Relationship to changes in subarctic primary productivity. *Deep Sea Research Part II: Topical Studies in Oceanography*, *46*(11–12), 2735–2760. https://doi.org/10.1016/S0967-0645(99)00082-X

Yamanaka, Y., & Tajika, E. (1996). The role of the vertical fluxes of particulate organic matter and calcite in the oceanic carbon cycle: Studies using an ocean biogeochemical general circulation model. *Global Biogeochemical Cycles*, *10*(2), 361–382. https://doi.org/10.1029/96GB00634

Young, J. N., Bruggeman, J., Rickaby, R. E. M., Erez, J., & Conte, M. (2013). Evidence for changes in carbon isotopic fractionation by phytoplankton between 1960 and 2010: 50-year record of global surface ε_p. *Global Biogeochemical Cycles*, *27*(2), 505–515. https://doi.org/10.1002/gbc.20045

Zavala-Hidalgo, J., Gallegos-García, A., Martínez-López, B., Morey, S. L., & O'Brien, J. J. (2006). Seasonal upwelling on the Western and Southern Shelves of the Gulf of Mexico. *Ocean Dynamics*, *56*(3–4), 333–338. https://doi.org/10.1007/s10236-006-0072-3